7-9-2009

Stochastic methods for uncertainty quantification in radiation transport

Erin D. Fichtl

Erin Fichtl

Candidate

Chemical and Nuclear Engineering

Department

This dissertation is approved, and it is acceptable in quality
and form for publication:

Approved by the Dissertation Committee:
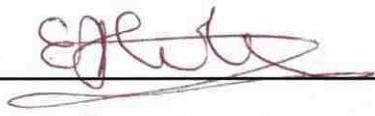
Anil Prinja , Chairperson
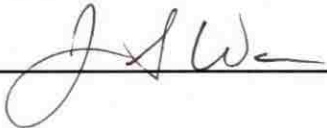
Cassiano de Oliveira

Evangelos Coutsias

James Warsa

Stochastic Methods for Uncertainty Quantification in Radiation Transport

by

Erin D. Fichtl

B.A., Physics, Hastings College, 2002

M.S., Nuclear Engineering, University of New Mexico, 2005

DISSERTATION

Submitted in Partial Fulfillment of the

Requirements for the Degree of

Doctor of Philosophy

Engineering

The University of New Mexico

Albuquerque, New Mexico

May, 2009

Acknowledgments

I would first like to thank my dissertation advisor, Anil Prinja, for his invaluable guidance through this arduous process, for sharing his insightful and boundless knowledge of transport theory with me over the past five and a half years, and for his understanding when we decided to start a family and move to Los Alamos in the middle of my dissertation work. I would also like to thank my committee members, Vageli Coutsias, Jim Warsa and Cassiano de Oliveira, for their efforts in reading this dissertation and for providing helpful and insightful comments. I would particularly like to thank Jim Warsa, who has been my advisor at LANL, and Professor Vageli Coutsias for teaching me the numerical methods necessary to complete this work. I am also grateful to Scott Turner and Jim Warsa for providing me with a workspace at LANL and taking me on when my fellowship ended. Last, but not least, I want to thank my family: My sister, Lauren, for preserving my sanity and being the best and most loving nanny imaginable, my sweet and beautiful children, Caden and Keira, whose smiles, laughs and antics brighten our lives, and my husband, Chris, for all of his love and support and a million other things that I do not have the space to list here.

Stochastic Methods for Uncertainty Quantification in Radiation Transport

by

Erin D. Fichtl

ABSTRACT OF DISSERTATION

Submitted in Partial Fulfillment of the

Requirements for the Degree of

Doctor of Philosophy

Engineering

The University of New Mexico

Albuquerque, New Mexico

May, 2009

Stochastic Methods for Uncertainty Quantification in Radiation Transport

by

Erin D. Fichtl

B.A., Physics, Hastings College, 2002

M.S., Nuclear Engineering, University of New Mexico,2005

Ph.D., Engineering, University of New Mexico, 2009

Abstract

The use of stochastic spectral expansions, specifically generalized polynomial chaos (gPC) and Karhunen-Loéve (KL) expansions, is investigated for uncertainty quantification in radiation transport. The gPC represents second-order random processes in terms of an expansion of orthogonal polynomials of random variables. The KL expansion is a Fourier-type expansion that represents a second-order random process with known covariance function in terms of a set of uncorrelated random variables and the eigenmodes of the covariance function. The flux and, in multiplying materials, the k-eigenvalue, which are the problem unknowns, are always expanded in a gPC expansion since their covariance functions are also unknown. This work assumes a single uncertain input—the total macroscopic cross section—although this does not represent a limitation of the approaches considered here. Two particular types of input parameter uncertainty are investigated: The cross section as a univariate Gaussian, log-normal, gamma or beta random variable, and the cross section

as a spatially varying Gaussian or log-normal random process. In the first case, a gPC expansion in terms of a univariate random variable suffices, while in the second, a truncated KL expansion is first necessary followed by a gPC expansion in terms of multivariate random variables. Two solution methods are examined: The Stochastic Finite Element Method (SFEM) and the Stochastic Collocation Method (SCM). The SFEM entails taking Galerkin projections onto the orthogonal basis, which yields a system of fully-coupled equations for the PC coefficients of the flux and the k-eigenvalue. This system is linear when there is no multiplication and can be solved using Richardson iteration, employing a standard operator splitting such as block Gauss-Seidel or block Jacobi, or a Krylov iterative method, which can be preconditioned using these splittings. When multiplication is present, the SFEM system is non-linear and a Newton-Krylov method is employed to solve it. The SCM utilizes a suitable quadrature rule to compute the moments or PC coefficients of the flux and k-eigenvalue, and thus involves the solution of a system of independent deterministic transport equations. The accuracy and efficiency of the two methods are compared and contrasted. Both are shown to accurately compute the PC coefficients of the unknown, and numerical proof is provided that the two methods are in fact equivalent in certain cases. The PC coefficients are used to compute the moments and probability density functions of the unknowns, which are shown to be accurate by comparing with Monte Carlo results. An analytic diffusion analysis, corroborated by numerical results, reveals that the random transport equation is well approximated by a deterministic diffusion equation when the medium is diffusive with respect to the average cross section but without constraint on the amplitude of the random fluctuations. Our work shows that stochastic spectral expansions are a viable alternative to random sampling-based uncertainty quantification techniques since both provide a complete characterization of the distribution of the flux and the k-eigenvalue. Furthermore, it is demonstrated that, unlike perturbation methods, SFEM and SCM can handle large parameter uncertainty.

Contents

Contents

Contents

Contents

List of Figures

List of Figures

List of Figures

List of Figures

List of Tables

List of Tables

Chapter 1

Introduction

The development of stochastic transport methods is necessary for the physical constructs in which materials, initial conditions or boundary conditions are, or appear to be, random. True material stochasticity can arise from fluctuations in material properties, such as densities or isotopic abundance, or from heterogeneities in the material itself. Uncertainties in material parameters, initial conditions and boundary conditions, which then translate into uncertainties in the solution itself, can also be treated using stochastic characterizations of problem inputs and unknowns. In nuclear engineering applications, the uncertainty inherent in experimentally determined cross section data, for instance, necessitates evaluation of the resulting uncertainty present in the numerical transport solution. This becomes particularly important when the system under consideration contains fission sources. Generally, the composition of stochastic media or uncertain parameters are described in a statistical sense by defining appropriate probability density functions. Solution methods are then devised to obtain the moments, particularly means and variances, and probability density functions (pdfs) of the flux and other unknowns.

The moments and pdfs may be found using sampling-based methods such as

Monte Carlo in which large numbers of realizations are generated using the statistical characterization, transport calculations are conducted for each realization, and the results are averaged over all realizations. However, the method is extremely computationally intensive because it involves the generation of thousands, possibly millions, of transport solutions. Alternately, it is possible to average the transport equation directly, thereby yielding a system of equations for the mean, and possibly higher moments, of the flux. These equations are generally not closed, however, necessitating a closure model. These models produce sets of equations that are generally not as time-consuming to solve as Monte Carlo, but they are strictly accurate only in the physical regimes for which they were constructed and are not easily generalized. One such description was derived by Levermore, Pomraning and Vanderhaegen for binary, or two-state, Markovian mixtures [1–4]. While their formalism has been widely applied [5–16], it is not exact in time-dependent and scattering regimes since it assumes that the transport process is Markovian in nature, which is true only in time-independent, purely absorbing materials. More recently, Akcasu attempted to amend the model to improve its accuracy in the presence of scattering, introducing the so-called Modified-Levermore-Pomraning model [17]. The model is exact for certain classes of problems with scattering and preserves the correct atomic mix and diffusion limits [18], but is plagued with difficulties when applied to finite slabs [19]. An exact system of closed equations for the average flux was also developed by Prinja et al. for charged particle transport assuming a continuous Gaussian distribution [20, 21] and Markovian binary statistics [22]. Selim et al. have also developed analytic solutions for the first and second moments of the flux also assuming continuous Gaussian statistics and anisotropic scattering in finite [23] and semi-infinite [24] domains. Once again, however, these methods are not broadly applicable.

Traditionally, uncertainty quantification for nuclear engineering applications has been approached using perturbation methods, particularly Gandini's generalized perturbation theory (GPT) [25], and sampling-based methods (i.e., Monte Carlo) [26].

GPT produces sensitivity coefficients that can then be used to conduct uncertainty analysis. It was developed to address bilinear functions of the real and adjoint neutron fluxes and involves solving the inhomogeneous "generalized adjoint" and "generalized forward" transport equations. An equivalent theory, dubbed the equivalent generalized perturbation theory (EGPT) [27], reduces the inhomogeneous GPT equations to homogeneous ones, thereby simplifying solution. GPT and EGPT yield sensitivity coefficients for the flux with respect to perturbed inputs that are subsequently used to quantify uncertainty. Perturbation methods are limited, however, in that they can only deal with small perturbations and cannot yield higher-order statistical moments or pdfs of the output in question. Sampling-based methods yield far more information about the uncertainty in the outputs—i.e., means, standard deviations, pdfs and cumulative density functions—as well as detailed information about the sensitivity of outputs to uncertain inputs. However, as stated before, they require prohibitively large numbers of transport solutions.

Given the limitations of commonly used methods, it is desirable to develop solution methods that possess the compactness of a closure model or perturbation method while retaining the flexibility of the Monte Carlo approach. In order to be more useful than existing methods, these new schemes must be solvable using a relatively small number of transport solutions and must be easily generalizable to a wide range of statistical characterizations. The development and investigation of such methods form the basis for this research.

As in the methods previously described, heterogeneities or uncertainties in the material are treated within a probabilistic framework. One approach is to use Karhunen-Loève (KL) or polynomial chaos (PC) expansions to represent random or uncertain properties in terms of a finite number of random variables, thereby reducing the 'random dimension' to a finite number of random variables. These expansions have been used for many years and there exists a mature body of literature

describing their properties and applications in a variety of fields to both stochastic problems and uncertainty quantification. The KL expansion, due to Loève [28], reproduces a second-order random process in an optimal expansion in terms of the eigenmodes of its covariance function. Homogeneous chaos, a subset of PC, was first conceived of by Wiener and employs Hermite polynomials in terms of normal random variables as its basis [29]. Wiener's concept was extended by Ogura to include Charlier chaos for Poisson processes [30] and more recently by Xiu and Karniadakis' generalized polynomial chaos (gPC) to include other polynomial bases belonging to the Askey scheme [31, 32]. The bases were shown to be optimal when the statistics of the random parameter corresponded to the weight function of the polynomial set. Ghanem and Spanos [33] applied the KL and homogeneous chaos expansions to the random quantities in their equation and, by taking Galerkin projections onto the polynomial basis, devised the Stochastic Finite Element Method (SFEM). SFEM employing homogeneous chaos has subsequently been applied to random interfaces in soil layers [34], fluid flow in porous media and over rough terrain [35–39], heat conduction [40], structural dynamics [41–48], acoustic scattering [49] and stochastic eigenvalue problems [50–52]. It has also been applied to problems with log-normal [40, 53] and other non-Gaussian [54, 55] statistics. SFEM has also been used in collaboration with gPC for application to fluid flow problems [56, 57], heat conduction [58], stochastic elliptic partial differential equations [59, 60] and advection-diffusion [61–63] problems, chemical reactor simulations [64] and flows in human arterial networks [65]. Recently, SFEM has been also applied to radiative transfer by Emery [66] and to neutron diffusion [67] and transport [68] by Williams et. al. In this preliminary work, KL and Legendre chaos expansions were used to model random cross sections in one-dimensional neutron diffusion and transport problems in the absence of scattering, for which the equations could be solved analytically.

More recently, the Stochastic Collocation Method (SCM) was proposed by Mathelin et al. [69] as an alternative approach to calculating the moments of the unknown

or the PC coefficients themselves. The method employs an appropriate quadrature set to directly compute the PC moments of the quantity in question. Instead of solving a coupled system, as in SFEM, the computation involves solving a sequence of uncoupled deterministic equations, therefore the method is easily incorporated into existing deterministic codes. The method has been successfully applied to elliptic partial differential equations [70, 71], various problems in mechanics [72–74] and fluid flow problems [69, 75–77]. There has also been some interest in using sparse grid or Smolyak quadratures in cases where the stochastic quantities are functions of multiple random variables [78–80], which is generally more efficient than taking tensor products of one-dimensional quadratures, particularly as the number of dimensions increases.

The application of these methods is explored in the context of one-dimensional steady-state neutron transport. Extension to multiple dimensions is straightforward since the application of SCM, SFEM or Monte Carlo to the random variable(s) is independent of the discretization of other variables in the system and is therefore left for future research. In the physical scenario, the total cross section, σ, is assumed to be an uncertain parameter and is therefore taken to be a function of the random dimension. When σ is spatially invariant, which might physically represent uncertainty in experimentally determined cross section data, it is represented as a single second-order random variable and replaced by a gPC expansion [31, 32]. When σ is spatially variant, which may physically represent density fluctuations in the material, it can be described in terms of its KL expansion, although this approach is limited since the KL expansion can only be applied when the covariance function of the process is known. Furthermore, the random variables used in the expansion are only independent if they are Gaussian, a fact which has important ramifications for the solution process. The SFEM provides a means of application to the transport equation. The PC expansion is first applied to random physical parameters as well as the problem unknown. Projecting onto the orthogonal basis then yields a system

of deterministic equations from which the expansion coefficients can be determined, much as in the deterministic finite element method. Alternately, the PC coefficients can be calculated using SCM.

The objective of this thesis is to conduct a preliminary investigation into the use of spectral expansions for uncertainty quantification in radiation transport. Chapter 2 contains a description of the transport formulation, including a discussion of transport in multiplying media and randomness encountered, either as material stochasticity or uncertainty, in physical parameters. There is also a general theoretical discussion of the KL expansion. Chapter 3 details the application of the KL expansion to the transport equation for cross sections that are normal and log-normal random processes using SCM. A study is performed on the accuracy and convergence of the KL expansion and a detailed asymptotic analysis of the diffusion limit is conducted with cross sections represented using the KL expansion. Chapter 4 contains a discussion of gPC expansions, which have as their bases sets of orthogonal polynomials. The application of SFEM and SCM to the transport equation for computing the PC expansion coefficients of the flux is described, both when the cross section is a random variable and when it is a random process represented by the KL expansion. Several different iterative schemes are proposed for solving the SFEM equations and a spectral analysis is conducted to determine their suitability. Analysis is also conducted to determine the well-posedness of the SFEM equations. Chapter 5 contains numerical results comparing the SFEM and SCM. Specifically, studies on the accuracy and convergence of the SFEM and SCM methods for cross sections that are both random variables and random processes as well as a comparison of the computational efficiency of SFEM and SCM. Chapter 6 describes the application of SFEM to multiplying media, which produces a coupled set of non-linear equations that are solved using a Newton-Krylov method. Results for a uniform random variable are compared with SCM. SCM is also applied for cross sections that are single random variables of various distributions. The SCM is further applied to a reactor problem

in which the enrichment is uncertain, varying randomly within the fuel, and is represented using a Gaussian random process. Finally, Chapter 7 contains conclusions, including an evaluation of the suitability of the method for uncertainty quantification in radiation transport, as well as a discussion of proposed future work.

Chapter 2

Transport Considerations

2.1 Deterministic Transport Formulation

The steady-state transport of mono-energetic neutrons through matter is described by the following one-dimensional form of the Boltzmann transport equation [81]

$$\mu \frac{\partial \psi(x, \mu)}{\partial x} + \sigma(x)\psi(x, \mu) = \frac{\sigma_s(x) + \nu \sigma_f(x)}{2} \phi(x) + Q(x, \mu) \tag{2.1}$$

where $\mu = \cos(\theta)$ is the direction cosine, $\sigma(x)$ is the total macroscopic cross section, $\sigma_s(x)$ is the scattering cross section, $\sigma_f(x)$ is the fission cross section, ν is the average number of neutrons produced per fission, $Q(x, \mu)$ is a volume source, $\psi(x, \mu)$ is the angular flux and

$$\phi(x) = \int_{-1}^{1} d\mu' \, \psi(x, \mu') \tag{2.2}$$

is the scalar flux. A discrete ordinates, or S$_\text{N}$, angular discretization is employed in which the angular derivative is approximated using Gauss-Legendre quadrature with weights w_n and abscissas μ_n. Eq. 2.1 can then be written

$$\mu_n \frac{\partial \psi_n(x)}{\partial x} + \sigma(x)\psi_n(x) = \frac{\sigma_s(x) + \nu \sigma_f(x)}{2} \phi(x) + Q_n(x) \tag{2.3}$$

where $\psi_n(x) = \psi(x, \mu_n)$, $Q_n(x) = Q(x, \mu_n)$ and

$$\phi(x) = \sum_{n=1}^{N} w_n \psi_n(x). \tag{2.4}$$

Spatial discretization is accomplished using a linear discontinuous (LD) finite element method, which employs linear basis functions and allows function discontinuity at cell boundaries. A uniform grid with I cells is applied to the system, linear basis expansions are assigned to the grid and material properties within individual spatial cells are assumed to be homogeneous. The basis expansions are defined in the following way. In space, for cell i

$$B_i^+(x) = \begin{cases} \frac{x - x_{i-\frac{1}{2}}}{\Delta x_i} & \text{if } x_{i-\frac{1}{2}} < x < x_{i+\frac{1}{2}} \\ 0 & \text{otherwise} \end{cases} \tag{2.5}$$

$$B_i^-(x) = \begin{cases} \frac{x_{i+\frac{1}{2}} - x}{\Delta x_i} & \text{if } x_{i-\frac{1}{2}} < x < x_{i+\frac{1}{2}} \\ 0 & \text{otherwise} \end{cases} \tag{2.6}$$

where $x_{i-\frac{1}{2}}$ and $x_{i+\frac{1}{2}}$ are the left and right cell boundaries, respectively, and Δx_i is the width of the cell (see Figure 2.1). The flux within a cell is now a discrete function
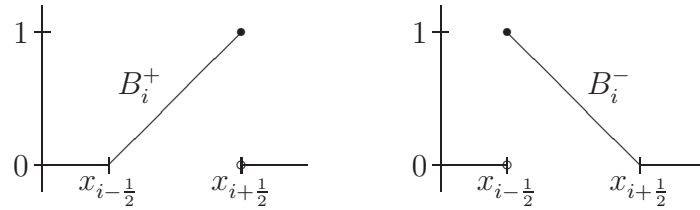
Figure 2.1: Basis Expansions

of angle and a linear function of space, and can be expressed as

$$\psi_n(x) = \psi_{n,i}^+ B_i^+(x) + \psi_{n,i}^- B_i^-(x) \tag{2.7}$$

and there are $2IN$ unknowns—a $\psi_{n,i}^+$ and a $\psi_{n,i}^-$ for each spatial cell $i = 1, 2 \ldots I$ and angular abscissa $n = 1, 2 \ldots N$.

In order to obtain the LD transport equations, the fluxes in Eq. 2.3 are replaced by the LD approximation given in Eq. 2.7. The inner product of this equation is then taken with respect to the two basis functions, $B_i^+(x)$ and $B_i^-(x)$, yielding two equations in terms of $\psi_{n,i}^+$ and $\psi_{n,i}^-$ for each angular abscissa, n, and spatial cell, i. Derivative terms must be dealt with carefully at cell boundaries since the trial functions are discontinuous at this point and the inner products are therefore dependent on the direction in which the particles are traveling. For instance, the inner product of the spatial derivative term in Eq. 2.3 with $B_i^-(x)$ for $\mu_n > 0$ is taken in the following way:

$$
\begin{aligned}
\langle B_i^- \mid \frac{\partial \psi_n(x)}{\partial x} \rangle &= \int_i dx\, B_i^-(x) \frac{\partial \psi_n(x)}{\partial x} \\
&= \left[B_i^- \psi_n \right]_i - \int_i dx\, \frac{\partial B_i^-}{\partial x} \psi_n \\
&= \left[\frac{x_{i+\frac{1}{2}} - x}{\Delta x_i} \psi_n \right]_i + \int_i dx\, \frac{1}{\Delta x_i} \psi_n \\
&= -\psi_{n,i-1}^+ + \frac{1}{2} \left(\psi_{n,i}^+ + \psi_{n,i}^- \right).
\end{aligned} \tag{2.8}
$$

First, integration by parts is applied to the integral. The definite integral term is then evaluated at the cell boundaries. Although the solution itself is allowed to be discontinuous at the boundary between cells i and $i-1$, it is important to correctly account for the passing of particles across cell boundaries. Otherwise, the scheme will not be conservative. It follows therefore that at $x_{i-\frac{1}{2}}$, given that $\mu_n > 0$ and the particles are therefore flowing from cell $i-1$ to cell i, the incoming value for cell i ($\psi_{n,i}^-$) must equal the outgoing value of cell $i-1$ ($\psi_{n,i-1}^+$). Nothing can be said about the continuity of the solution itself, however, and it is still discontinuous. Adjacent groups are therefore coupled in space wherever there is a spatial derivative term.

If there are I spatial cells and N discrete ordinates angles, the linear system for the $2IN$ unknowns is solved iteratively because direct inversion of the matrix is

prohibitively expensive. The so-called 'source iteration' takes the form

$$\mathbf{L}\vec{\psi}^{(\ell+1)} = \mathbf{M}(\mathbf{S_s} + \mathbf{S_f})\mathbf{D}\vec{\psi}^{(\ell)} + \vec{Q} \tag{2.9}$$

where ℓ is the iteration index, $\vec{\psi}$ and $\vec{Q}$ are vectors of flux unknowns and volume source terms and are arranged such that

$$\vec{\psi} = \begin{bmatrix} \vec{\psi}_1^+ & \vec{\psi}_1^- & \vec{\psi}_2^+ & \vec{\psi}_2^- & \ldots & \vec{\psi}_I^+ & \vec{\psi}_I^- \end{bmatrix}^T$$

where each vector $\vec{\psi}_i^+$ contains ψ_i^+ at each of the N discrete angles and $\vec{\psi}_i^-$ contains ψ_i^- at each of the N discrete angles

$$\vec{\psi}_i^+ = \begin{bmatrix} \vec{\psi}_{i,1}^+ & \vec{\psi}_{i,2}^+ & \ldots & \vec{\psi}_{i,N}^+ \end{bmatrix}^T \text{ and } \vec{\psi}_i^- = \begin{bmatrix} \vec{\psi}_{i,1}^- & \vec{\psi}_{i,2}^- & \ldots & \vec{\psi}_{i,N}^- \end{bmatrix}^T.$$

$\mathbf{L}$ is the streaming and removal operator, with $\mathbf{L}\psi$ respresenting the left-hand side of Eq. 2.3, and has dimension $2IN \times 2IN$. $\mathbf{S_s} = \frac{\sigma_s}{2}\mathbf{S}$ and $\mathbf{S_f} = \frac{\nu\sigma_f}{2}\mathbf{S}$ are the scattering and fission source matrices where

$$\mathbf{S} = \mathrm{I}_{2I}$$

and I_{2I} is the $2I \times 2I$ identity matrix. $\mathbf{M}$ is the moment-to-discrete operator

$$\mathbf{M} = \mathrm{I}_{2I} \otimes \begin{bmatrix} 1 \\ 1 \\ \vdots \\ 1 \end{bmatrix}$$

where the vector of ones is N elements long and $\otimes$ denotes the Kronecker product. Therefore $\mathbf{M}$ has dimension $2IN \times 2I$ and, in effect, places N copies of each scalar flux into a vector the size of the angular flux. The discrete-to-moment operator multiplies the angular flux to form a vector containing scalar flux values, $\mathbf{D}\vec{\psi} = \vec{\phi}$

$$\mathbf{D} = \mathrm{I}_{2I} \otimes \begin{bmatrix} \mu_1 & \mu_2 & \ldots & \mu_N \end{bmatrix}$$

thus $\mathbf{D}$ is of dimension $2I \times 2IN$ and

$$\vec{\phi} = \begin{bmatrix} \phi_1^+ & \phi_1^- & \phi_2^+ & \phi_2^- & \dots & \phi_I^+ & \phi_I^- \end{bmatrix}^T.$$

When a system contains fission sources (i.e., $\sigma_f > 0$), it is desirable to calculate the criticality. If a system is critical, the number of neutrons produced in the successive generations is a constant, indicating a self-sustaining, steady state chain reaction. If the system is super- or subcritical, more or fewer neutrons, respectively, are produced in successive generations and the chain reaction will grow or die out. Criticality is indicated by the multiplication eigenvalue, k:

$$k < 1 \quad \text{subcritical,}$$
$$k = 1 \quad \text{critical,}$$
$$k > 1 \quad \text{supercritical.}$$

The k-eigenvalue is explicitly incorporated into the transport equation by dividing the fission term

$$\mathbf{L}\vec{\psi} = \mathbf{M}\mathbf{S_s}\mathbf{D}\vec{\psi} + \frac{1}{k}\mathbf{M}\mathbf{S_f}\mathbf{D}\vec{\psi}. \tag{2.10}$$

It can then be calculated using the traditional power iteration [82] or a more advanced Krylov subspace method such as the Restarted or Implicitly Restarted Arnoldi Methods [83]. Rearranging Eq. 2.10 and applying $\mathbf{D}$ to both sides, the multiplication eigenvalue problem can be written as

$$k\vec{\phi} = \mathbf{A}\vec{\phi} \tag{2.11}$$

where $\mathbf{A} = (\mathbf{I} - \mathbf{D}\mathbf{L^{-1}}\mathbf{M}\mathbf{S_s})^{-1}\mathbf{D}\mathbf{L^{-1}}\mathbf{M}\mathbf{S_f}$. The power iteration proceeds as follows:

$$\vec{\phi}^{(\ell+1)} = \frac{A\vec{\phi}^{(\ell)}}{\|A\vec{\phi}^{(\ell)}\|} \tag{2.12a}$$

$$k^{(\ell+1)} = \vec{\phi}^{(\ell)}A\vec{\phi}^{(\ell)} \tag{2.12b}$$

where ℓ is the iteration index and $\vec{\phi}^{(0)}$ is initialized randomly.

2.2   Stochastic Transport Formulation

There are two types of uncertainty in nuclear systems: Aleatory and epistemic. Aleatory uncertainty refers to randomness in the behavior of the system. In a transport setting it is often encountered as variability in the material itself, e.g., the presence of more than one material in the domain. Epistemic uncertainty stems from lack of knowledge about the correct values of input parameters, for instance, experimental uncertainty in the measured values of various physical parameters, e.g., the number density, cross section, fuel enrichment, etc. While the source of the uncertainty determines how uncertain inputs are represented and affects the subsequent interpretation of output uncertainties, it does not affect the solution process itself. The focus of this work is quantifying the effect of uncertainty, whether aleatory or epistemic, in the macroscopic cross section(s), σ, on the flux. It is assumed that the probability density function (pdf) of the cross section(s), $P(\sigma)$, where $P(\sigma)d\sigma$ is the probability that the cross section lies between σ and $\sigma + d\sigma$, is known. It then remains to compute the moments and the pdf of the flux. The moments can be thought of as 'ensemble averages' in the random dimension, denoted $\langle \cdot \rangle$, or averages over all statistically possible 'realizations' of the cross section.

The randomness in the cross section, which then translates into randomness in the flux, can be incorporated mathematically into the transport equation by introducing an additional dimension—the random dimension, $\omega \in \Omega$, where Ω is the space of random events. The stochastic version of the 1-D transport equation (Eq. 2.3) can then be written as

$$\mu_n \frac{\partial \psi_n(x,\omega)}{\partial x} + \sigma(x,\omega)\psi_n(x,\omega) = \frac{\sigma_s(x,\omega) + \nu\sigma_f(x,\omega)}{2}\phi(x,\omega) + Q_n(x) \quad (2.13)$$

if all of the cross sections are to be random and spatially variant. The solution of this equation is the goal of this work, in which three different methods are employed: the sampling-based Monte Carlo method, the Stochastic Collocation Method (SCM)

and the Stochastic Finite Element Method (SFEM).

2.3   The Karhunen-Loève Expansion

The Karhunen-Loève (KL) expansion represents a second-order random process, $\sigma(x, \omega)$, in a Fourier-type expansion in terms of the eigenvalues and eigenfunctions of its covariance function, $C_\sigma(x_1, x_2)$. Given that the covariance function is known, the expansion allows the random process, which is a function of both the spatial and the random dimensions, to be represented in terms of finite number of random variables and continuous functions in space. In effect, it provides a systematic manner in which to 'discretize' the random dimension and the accuracy of the approximation is quite simply improved by retaining additional random variables in the expansion. The random process, $\sigma(x, \omega)$, is defined to be a function of $x \in X$, where X is the spatial domain, and $\omega \in \Omega$, where Ω is the space of random events. It has expectation value $E[\sigma(x)] = \langle \sigma(x) \rangle$ and, for notational clarity, a zero-mean 'random part' $\tilde{\sigma}(x, \omega) = \sigma(x, \omega) - \langle \sigma(x) \rangle$. As a second-order random process on the domain X, σ must have a finite variance

$$E\left[\tilde{\sigma}^2(x)\right] < \infty, \ x \in X \tag{2.14}$$

and covariance

$$C_\sigma(x_1, x_2) = E\left[\tilde{\sigma}(x_1)\tilde{\sigma}(x_2)\right], \ x_1, x_2 \in X. \tag{2.15}$$

While each random process has a unique covariance, a covariance may correspond to numerous random processes [28]. The process is also required to be continuous in the quadratic mean (q.m. continuous)—i.e., $\lim_{h\to 0} E\left[(\sigma(x+h) - \sigma(x))^2\right] = 0$, $x \in X$—to ensure that the covariance is also continuous on $X \times X$.

The KL expansion separates the random and spatial dimensions so that they can

be dealt with separately using a generalized Fourier series of the form

$$\sigma(x,\omega) = \sum_{k=1}^{\infty} a_k(\omega)\varphi_k(x), \tag{2.16}$$

where $\{a_k(\omega)\}$ is a set of orthogonal random variables and $\{\varphi_k(x)\}$ is a set of deterministic functions, and is convergent in the quadratic mean, i.e.,

$$\lim_{K\to\infty} E\left[\left(\sigma(x,\omega) - \sum_{k=1}^{K} a_k(\omega)\varphi_k(x)\right)^2\right] = 0, \ \text{uniformly on } X. \tag{2.17}$$

It expands a second-order random process in terms of a numerable set of orthogonal random variables, $\{\xi_k(\omega)\}$, which are in effect a discretization of the random dimension, and the orthogonal eigenfunctions and eigenvalues of the covariance function, where the eigenfunctions are functions of the spatial dimension. Since the covariance function is, by definition, bounded, symmetric and positive definite, by Mercer's theorem it has a uniformly convergent expansion [28]

$$C_\sigma(x_1, x_2) = \sum_{k=0}^{\infty} \lambda_k \varphi_k(x_1)\varphi_k(x_2) \tag{2.18}$$

where $\{\lambda_k\}$ are the eigenvalues and $\{\varphi_k(x)\}$ the eigenfunctions of the covariance kernel. They satisfy the following homogeneous Fredholm integral equation of the second kind

$$\int_X C_\sigma(x_1, x_2)\varphi_k(x_2)dx_2 = \lambda_k \varphi_k(x_1). \tag{2.19}$$

The $\{\varphi_k(x)\}$ form a complete, orthogonal set which can be normalized by forcing

$$\int_X \varphi_k(x)\varphi_\ell(x)dx = \delta_{k\ell} \tag{2.20}$$

and the eigenvalues, $\{\lambda_k\}$, form a countably infinite set of positive real numbers. These sets can be used to expand the random process, analogous to Eq. 2.16, as

$$\sigma(x,\omega) = \langle\sigma(x)\rangle + \sum_{k=1}^{\infty} \sqrt{\lambda_k}\varphi_k(x)\xi_k(\omega). \tag{2.21}$$

The $\xi_k(\omega)$ are given explicitly by

$$\xi_k(\omega) = \frac{1}{\sqrt{\lambda_k}} \int_X \tilde{\sigma}(x,\omega)\varphi_k(x)dx \tag{2.22}$$

and are uncorrelated with zero mean and unit variance [33]:

$$\langle \xi_k \rangle = 0 \tag{2.23}$$

$$\langle \xi_k \xi_l \rangle = \delta_{kl}. \tag{2.24}$$

This expansion has the following advantages:

- It is optimal in the sense that the mean-square error that results from representing $\sigma(x,\omega)$ in terms of a finite number of eigenfunctions is minimized. This is true regardless of the probabilistic structure of the process, provided that its variance is finite [28]. Any other generalized Fourier representation of $\sigma(x,\omega)$ in terms of another linear combination of functions will have larger mean-square error than the KL expansion when the same number of terms are retained [33].

- If $\sigma(x,\omega)$ is a Gaussian process, then the random variables, $\{\xi_k(\omega)\}$, form a Gaussian vector and any subset of $\{\xi_k(\omega)\}$ is jointly Gaussian [28]. Furthermore, because the variables are always uncorrelated, the fact that they are Gaussian implies that they are also independent and are given by

$$P(\xi_k) = \frac{1}{\sqrt{2\pi}} \exp\left(-\frac{\xi_k^2}{2}\right), \, \xi_k \in [-\infty, \infty]. \tag{2.25}$$

When $\sigma(x,\omega)$ is not given in terms of a Gaussian process, the $\{\xi_k(\omega)\}$ are not necessarily independent [33]. This has important implications for our solution method, as will be discussed later.

Chapter 3

The Karhunen-Loéve Expansion: Numerical Results

As discussed in the previous section, the Karhunen-Loève (KL) expansion represents a second-order random process in an expansion in terms of the eigenvalues and eigenfunctions of its covariance. In section 3.1, a covariance function is selected and its eigenmodes are derived. Section 3.2 contains a description of the numerical implementation for cross sections that are both normal and log-normal random processes. In section 3.3, the convergence of the KL expansion is examined for both the rod model, which can be compared against an analytic solution, and S_8, which is compared against a Monte Carlo solution. Results are computed using Gauss-Hermite quadrature, the convergence of which is also examined. And finally, an asymptotic analysis of the diffusion limit is conducted in section 3.4.

3.1   The Exponential Covariance Function

Use of the KL expansion relies on our ability to solve Eq. 2.19 for $\varphi_k(x)$ and λ_k, so a savvy choice of C_σ can simplify the solution process considerably. We have chosen to use the exponential kernel, which represents the first-order Markovian process, which has been used extensively in a variety of fields [33],

$$C_\sigma(x_1, x_2) = v_\sigma \exp\left(\frac{-|x_1 - x_2|}{\lambda_c}\right), \tag{3.1}$$

where v_σ is the variance and λ_c is the correlation length, which is a measure of the length over which x_1 and x_2 become independent. As $\lambda_c \to \infty$, the cross section is fully correlated throughout the domain and therefore has no spatial structure. The cross section is a univariate random variable. As $\lambda_c \to 0$, the cross section at each spatial point is completely independent of every other point in the system, though it is still random, and the cross section therefore has considerable spatial structure.

The eigenfunctions and eigenvalues we seek satisfy the following integral equation, found by substituting Eq. 3.1 into Eq. 2.19

$$v_\sigma \int_0^L \exp\left(\frac{-|x_1 - x_2|}{\lambda_c}\right) \varphi(x_2)dx_2 = \lambda\varphi(x_1), \;\; x_1, x_2 \in [0, L]. \tag{3.2}$$

This equation is easily converted into a second-order differential equation with homogeneous boundary conditions by refashioning the integral term as

$$\int_0^L \exp\left(\frac{-|x_1 - x_2|}{\lambda_c}\right) \varphi(x_2)dx_2 =$$
$$\int_0^x \exp\left(\frac{-(x_1 - x_2)}{\lambda_c}\right) \varphi(x_2)dx_2 + \int_x^L \exp\left(\frac{(x_1 - x_2)}{\lambda_c}\right) \varphi(x_2)dx_2 \tag{3.3}$$

and differentiating twice with respect to x_1 to obtain

$$\varphi''(x) + \alpha^2\varphi(x) = 0, \tag{3.4}$$

where

$$\alpha^2 = \frac{2v_\sigma - \frac{\lambda}{\lambda_c}}{\lambda_c\lambda}.$$

Chapter 3. The Karhunen-Loéve Expansion: Numerical Results

The boundary conditions are found by evaluating Eq. 3.3 and its first derivative at $x = 0$ and $x = L$ and rearranging to obtain

$$\lambda_c \varphi'(0) - \varphi(0) = 0 \qquad (3.5a)$$

$$\lambda_c \varphi'(L) + \varphi(L) = 0. \qquad (3.5b)$$

A nontrivial solution for Eq. 3.4 exists for $\alpha^2 \geq 0$, and is given by

$$\varphi(x) = a_1 \cos(\alpha x) + a_2 \sin(\alpha x). \qquad (3.6)$$

Application of the boundary conditions yields the following transcendental equation for α:

$$\tan(\alpha L) = \frac{2\alpha\lambda_c}{\lambda_c^2 \alpha^2 - 1}. \qquad (3.7)$$

This equation has numerous solutions, α_k, each of which correspond to an eigenvalue

$$\lambda_k = \frac{2v_\sigma \lambda_c}{\alpha_k^2 \lambda_c^2 + 1} \qquad (3.8)$$

and an eigenfunction

$$\varphi_k(x) = A_k \left(\sin(\alpha_k x) + \lambda_c \alpha_k \cos(\alpha_k x) \right), \qquad (3.9)$$

where A_k is chosen such that

$$\int_0^L \varphi_k^2(x)dx = 1. \qquad (3.10)$$

Fig. 3.1(a) shows the first ten eigenvalues of the covariance function, λ_k, for various values of λ_c. As can be seen, the eigenvalues decay monotonically as k increases. The larger the correlation length —i.e., the stronger the correlation between points—the faster the eigenvalues decay and the more dominant the largest eigenvalue, λ_1, becomes. Thus, when the eigenvalues decay rapidly, the first few terms in

:   :

(a) Eigenvalues   (b) Eigenfunctions ($\lambda_c = 1$ cm)
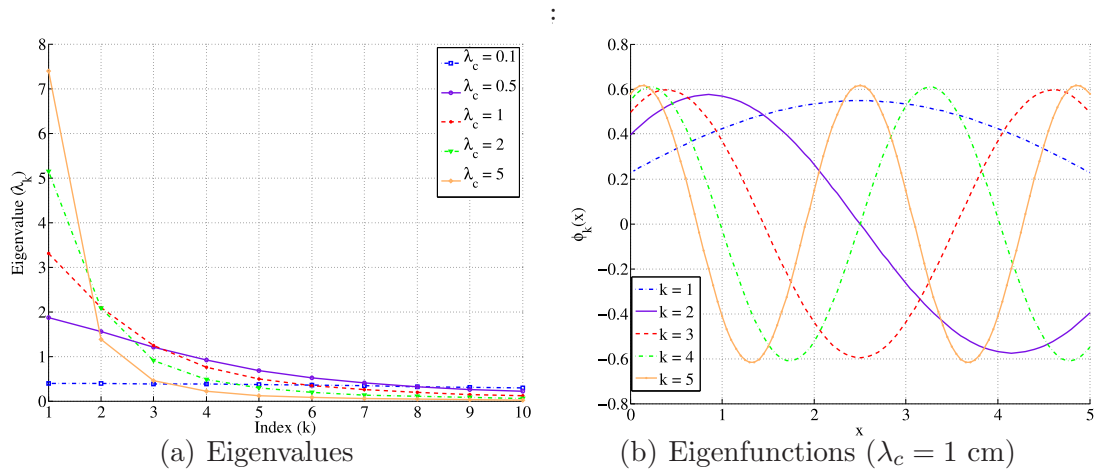
Figure 3.1: Eigenfunctions and Eigenvalues for the Exponential Covariance Function ($L = 5$ cm, $v_\sigma = 2$ cm^{-2})

the expansion (Eq. 2.21) contribute largely to the sum while later terms are less significant. Therefore it may be possible to represent $\sigma(x, \omega)$ faithfully with a relatively brief expansion. When the eigenvalues decay slowly, however, the terms are more equally weighted and many more terms must be retained. Also shown in Fig. 3.1(b) are the eigenfunctions, φ_k, as a function of x. As k increases, the functions become more oscillatory. Thus, when the larger eigenvalues dominate, we would expect that each successive term in the expansion will have little effect on the magnitude of the sum because the corresponding eigenvalues are small and will instead cause small-scale oscillations.

3.2   Numerical Implementation

We now come to the heart of the matter—solution of the random transport equation. While theoretically we could apply the KL expansion to the flux itself, we could not calculate the expansion coefficients since its covariance function is unknown. Instead, we rewrite the transport equation as a function of the random dimension, ω, and

expand the cross section as discussed previously

$$\mu\frac{\partial\psi(x,\mu,\omega)}{\partial x} + \sigma(x,\omega)\psi(x,\mu;\omega) = \frac{c\sigma(x,\omega)}{2}\int_{-1}^{1}d\mu'\psi(x,\mu';\omega) + \frac{Q(x,\mu)}{2}. \quad (3.11)$$

As can be seen, only the total cross section, $\sigma(x,\omega)$, and by extension the flux, $\psi(x,\mu;\omega)$, are random. The scattering ratio, c, is taken to be a deterministic quantity. We stress that this is not a necessary condition; rather, it allows us to focus on the implementation and effectiveness of the KL expansion.

3.2.1 Normal Random Processes

The cross section is represented using the KL expansion, truncated at order K, as

$$\sigma(x,\omega) = \langle\sigma(x)\rangle + \tilde{\sigma}(x,\omega) = \langle\sigma(x)\rangle + \sum_{n=1}^{K}\sqrt{\lambda_k}\varphi_k(x)\xi_k(\omega). \quad (3.12)$$

Since we are restricting our consideration to a Gaussian random process, the set $\{\xi_k(\omega)\}_1^K$ is made up of identical, independent random variables given by Eq. 2.22. If the KL expansion is used to represent the cross section, the flux also becomes a function of these variables, i.e., $\psi(\omega) = \psi(\xi_1(\omega), \ldots, \xi_K(\omega))$. The moments of ψ are therefore given by

$$\langle\psi^n\rangle = \int_{-\infty}^{\infty}d\xi_1\cdots\int_{-\infty}^{\infty}d\xi_K\,P(\xi_1,\ldots,\xi_K)\psi^n(\xi_1,\ldots,\xi_K)$$
$$= \int_{-\infty}^{\infty}d\xi_1 P(\xi_1)\cdots\int_{-\infty}^{\infty}d\xi_K P(\xi_K)\psi^n(\xi_1,\ldots,\xi_K) \quad (3.13)$$

where $P(\xi_1,\ldots,\xi_K) = \prod_{k=1}^{K}P(\xi_k)$ by the independence of the $\{\xi_k\}$. Each value of $\psi(\omega)$ corresponds to a unique combination of values, $\{\xi_k(\omega)\}_1^K$, which physically corresponds to a 'realization' of the material. Obviously, there are an infinite number of possible realizations, therefore is it necessary to approximate each integral in Eq. 3.13 with a finite number of terms using numerical integration. Monte Carlo is one possibility, but it would require an inordinately large number of realizations.

Alternately, the Stochastic Collocation Method (SCM) employing a tensor product of one-dimensional Gauss-Hermite quadrature rules could be used to evaluate the integral in Eq. 3.13 since the ξ_k are independent

$$\langle \psi^n \rangle = \sum_{m_1=1}^{M_1} w_{m_1} \cdots \sum_{m_K=1}^{M_K} w_{m_K} \, \psi^n(\theta_{m_1}, \ldots, \theta_{m_K}) \tag{3.14}$$

where the K is the order of the KL expansion, M_k is the quadrature order for the integration over $\xi_k(\omega)$, and the w_{m_k} and θ_{m_k} are the Gauss-Hermite quadrature weights and abscissas. Thus, evaluation of this integral requires the solution of $M_1 M_2 \ldots M_K$ uncoupled transport equations, or M^K equations if $M = M_1 = M_2 = \cdots = M_K$. It is clear that the independence of the $\{\xi_k(\omega)\}$ simplifies the solution process considerably—if they were dependent, a K-dimensional quadrature would be necessary.

In order to establish the accuracy of the solution, it is desirable to compare it with an exact solution. Such a solution was developed by Prinja and Gonzalez-Aller [21] in which they assumed Gaussian distributed density fluctuations and a semi-infinite, source-free medium. While the equation cannot generally be written in standard transport form, in the special case of the rod-model the equation simplifies to

$$\frac{\partial \langle \psi^+ \rangle}{\partial x} + [\langle \sigma \rangle - (1-c)C_0(x)] \, \langle \psi^+ \rangle \;=\; \frac{c \langle \sigma \rangle}{2} \langle \phi \rangle \tag{3.15a}$$

$$-\frac{\partial \langle \psi^- \rangle}{\partial x} + [\langle \sigma \rangle + (1-c)C_0(x)] \, \langle \psi^- \rangle \;=\; \frac{c \langle \sigma \rangle}{2} \langle \phi \rangle \tag{3.15b}$$

where $\langle \phi \rangle = \langle \psi^+ \rangle + \langle \psi^- \rangle$ and $C_0(x)$ is related to the covariance function by

$$C_0(x) = \int_0^x C_\sigma(x')dx'. \tag{3.16}$$

3.2.2 Log-Normal Random Processes

The KL expansion for Gaussian processes is given in terms of the ξ_k, which are distributed according to the normal distribution from which negative values are drawn

with equal probability as positive values. It is therefore possible, and indeed likely, that the KL expansion will yield cross sections that are negative in all or part of the domain in some instances, an unphysical result. As the variance increases with relation to the mean, the number of negative cross sections produced will increase as well. Thus, this method can only be applied to a small subset of stochastic materials for which the variance of the cross section is some small percentage of its mean. Alternately, the cross section could be taken to be a log-normal process, given by

$$\sigma(x, \omega) = e^{w(x,\omega)} \tag{3.17}$$

where $w(x, \omega)$ is a Gaussian random process with KL expansion

$$w_{KL}(x, \omega) = \langle w(x) \rangle + \sum_{k=1}^{K} \sqrt{\lambda_k} \varphi_k(x) \xi_k(\omega). \tag{3.18}$$

Thus,

$$\sigma_{KL}(x, \omega) = \exp \left(\langle w(x) \rangle + \sum_{k=1}^{K} \sqrt{\lambda_k} \varphi_k(x) \xi_k(\omega) \right). \tag{3.19}$$

Given Eq. 3.19 and the mean, $\langle \sigma \rangle$, and variance, v_σ, of the log-normal cross section, it is possible to calculate the covariance function of σ as well as $\langle w \rangle$ and v_w for use in the KL expansion of w. The mean and variance of w are given by

$$\langle w \rangle = \ln \left(\frac{\langle \sigma \rangle^2}{\sqrt{v_\sigma + \langle \sigma \rangle^2}} \right) \tag{3.20}$$

$$v_w = \ln \left(\frac{v_\sigma}{\langle \sigma \rangle^2} + 1 \right). \tag{3.21}$$

The covariance function of σ is given by

$$C_\sigma(x, x') = \langle \sigma \rangle^2 \left[\left(\frac{\langle \sigma^2 \rangle}{\langle \sigma \rangle^2} \right)^{\rho_w(x,x')} - 1 \right] \tag{3.22}$$

where $\rho_w(x, x')$ is the correlation function of w

$$\rho_w = \frac{C_w(x, x')}{v_w} = \exp \left(\frac{-|x_1 - x_2|}{\lambda_c} \right). \tag{3.23}$$

The correlation function of σ is then found to be

$$\rho_\sigma(x, x') = \frac{C_\sigma(x, x')}{v_\sigma} = \frac{\left(\frac{\langle \sigma^2 \rangle}{\langle \sigma \rangle^2}\right)^{\rho_w(x,x')} - 1}{\frac{\langle \sigma^2 \rangle}{\langle \sigma \rangle^2} - 1}. \tag{3.24}$$

Fig. 3.2 shows ρ_σ plotted vs. ρ_w for various values of $\frac{\langle \sigma^2 \rangle}{\langle \sigma \rangle^2}$. When $\frac{\langle \sigma^2 \rangle}{\langle \sigma \rangle^2} \approx 1$, the two correlation functions are virtually identical and as $\frac{\langle \sigma^2 \rangle}{\langle \sigma \rangle^2}$ gets larger, they become increasingly dissimilar with $\rho_\sigma < \rho_w$ everywhere except the endpoints where $\rho_\sigma = \rho_w = 0$ and $\rho_\sigma = \rho_w = 1$.
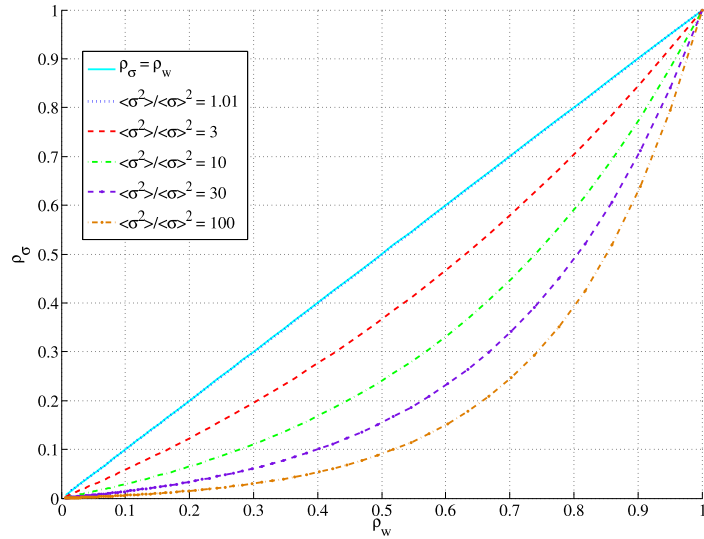
Figure 3.2: ρ_σ vs. ρ_w for various values of $\frac{\langle \sigma^2 \rangle}{\langle \sigma \rangle^2}$

3.3 Accuracy and Convergence of the KL Expansion for Gaussian and Log-Normal Random Processes

Results for the KL expansion were obtained using a linear discontinuous discretization in space. In all cases, $\langle \sigma \rangle = 5$ cm^{-1}, $v_\sigma = 2$ cm^{-2}, $L = 5$ cm, $\lambda_c = 1$ cm, $c = 0.5$ and $I = 250$ spatial cells. An isotropic incident source was placed on the left edge and vacuum boundary conditions were assumed on the right edge. The numerical KL solutions were obtained using the SCM, implemented using tensor products of the one-dimensional Gauss-Hermite quadrature rule, $\{w_m, \theta_m\}$, $m = 1, \ldots, M$. The flux was obtained by solving the discretized version of Eq. 3.11 for $\psi(\theta_{m_1}, \ldots, \theta_{m_K})$ and numerically integrating using Eq. 3.14. In order to test the accuracy of the KL expansion, results were first obtained using the rod model (i.e., an angular quadrature with two abscissas, $\mu = \pm 1$) and compared against the semi-infinite medium solution given in Eqs. 3.15a and 3.15b. Once the accuracy of the KL expansion was established, results were then obtained for an S$_8$ discrete ordinates discretization in angle for both normal and log-normal random cross sections with convergence of the quadrature determined by comparison with a Monte Carlo solution.

3.3.1 Rod Model: Comparison of SCM with an Analytic Solution

Fig. 3.3(a) shows the scalar flux for K=0 (i.e., the deterministic solution where $\sigma(x, \omega) = \langle \sigma \rangle$) as well as the semi-infinite medium and KL expansion solutions. While the semi-infinite medium solution is exact when the slab is semi-infinite, the slab in this case is clearly finite, and it is not expected that the KL solution will ever exactly duplicate the solution. However, for an optically thick slab such as the

one examined here, the results should be similar enough to confirm that the KL expansion gives a correct solution. As can be seen, the semi-infinite and KL results are similar. Fig. 3.3(b) shows the relative error in the scalar flux for the KL expansion solution as compared with the semi-infinite medium solution. The quadrature order, M, seems to have a greater effect on the accuracy of the solution than the KL order on the right-hand side of the slab whereas the opposite is true close to the incident edge. The fact that the accuracy of the solution is dominated by the order of the quadrature far from the incident edge but not close to it indicates that as the beam penetrates the slab, the flux becomes an increasingly higher-order function of the random variables. The incoming beam is deterministic, but its behavior becomes increasingly random as the beam traverses the slab due to the uncertainty inherent in the cross section. The flux appears to be converged for K = 5 and M = 6 while the standard deviation, shown in Fig. 3.5(a), requires K = 5 and M = 8. This indicates that the first moment, or mean, of the flux is in fact a lower order function of the random variables than the second moment of the flux, $\langle \phi^2 \rangle$.

As can be seen in Figs. 3.4 and 3.5(b), similar results are obtained for $c = 0.9$, with the flux requiring M = 4 for convergence while the standard deviation required M = 6. Also, for this larger scattering ratio, a smaller quadrature order is necessary to achieve convergence—for the flux, M = 4 as compared with M = 6 for $c = 0.5$, and for the standard deviation, M = 6 as compared with M = 8 for $c = 0.5$. Once again, this indicates that in diffusive materials, the moments of the flux are lower order functions of the random variables than they are in non-diffusive materials.

:

(a) Scalar Flux

:
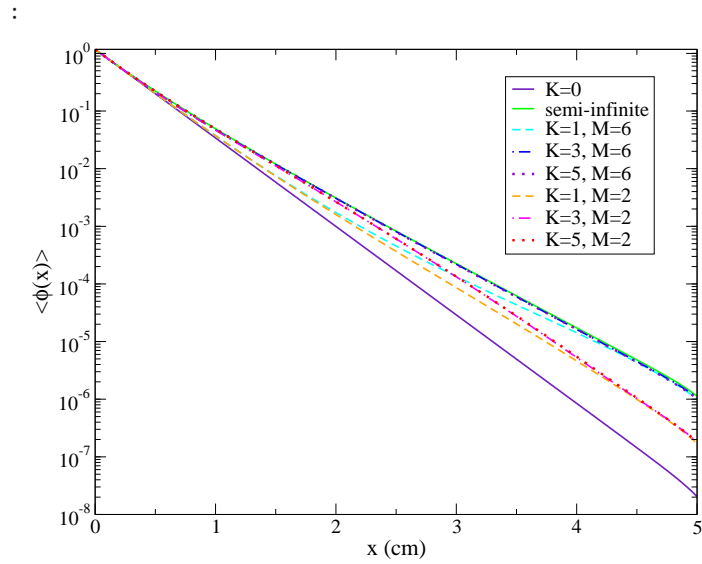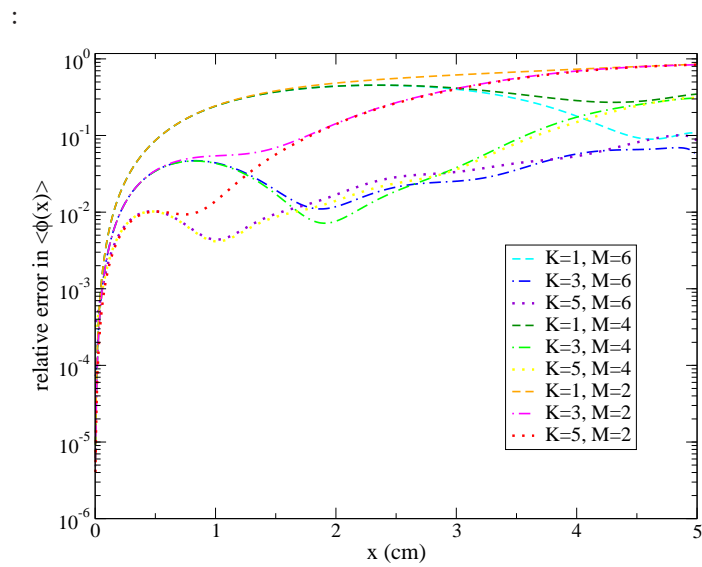
(b) Relative Error in the Scalar Flux

Figure 3.3: Scalar Flux and its Relative Error for the Rod Model ($c = 0.5$)

:

(a) Scalar Flux

:
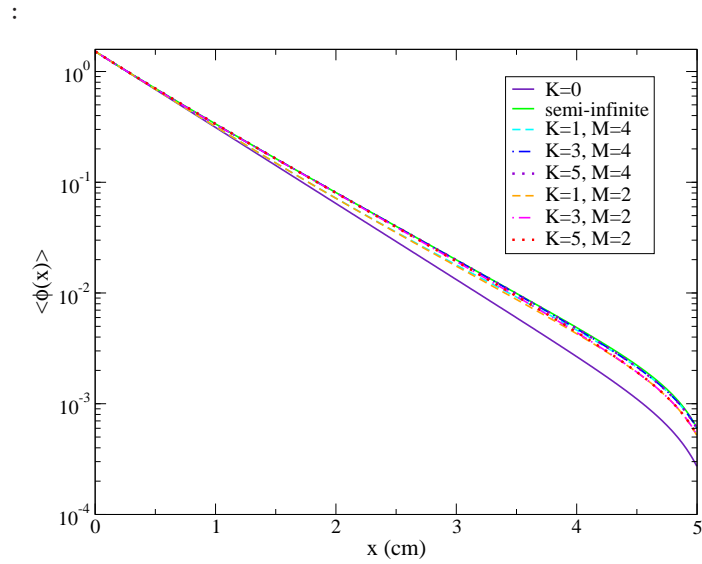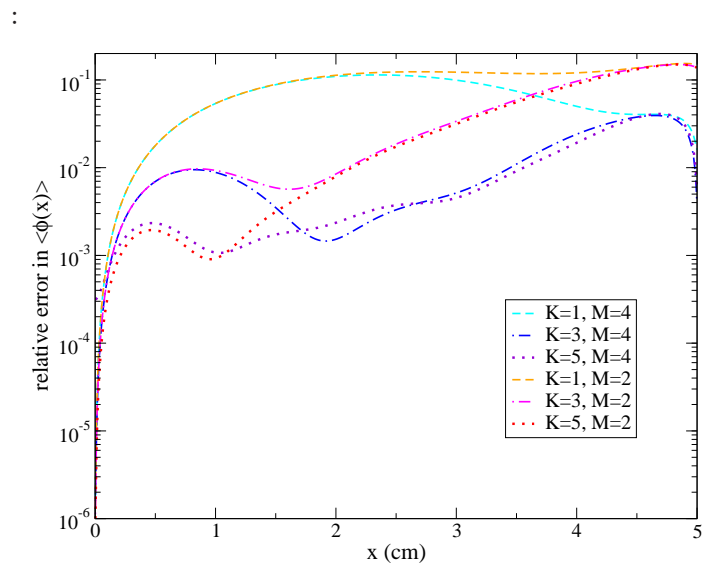
(b) Relative Error in the Scalar Flux

Figure 3.4: Scalar Flux and its Relative Error for the Rod Model ($c = 0.9$)

.
.

(a) $c = 0.5$

.
.

(b) $c = 0.9$
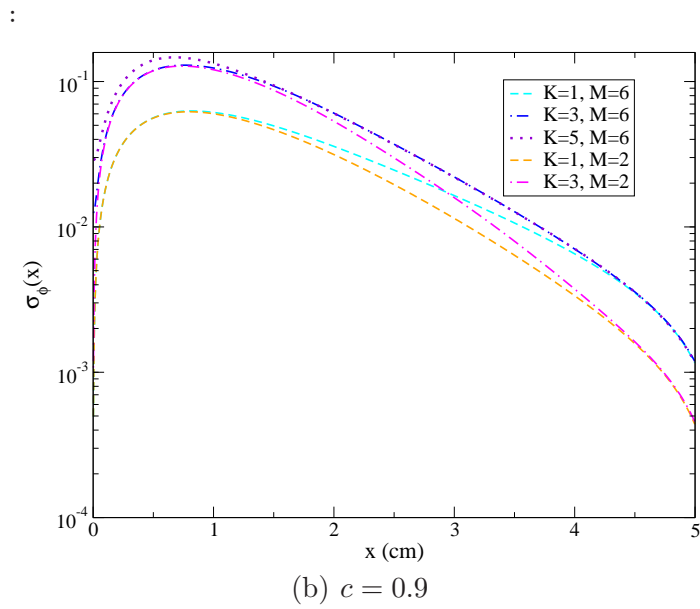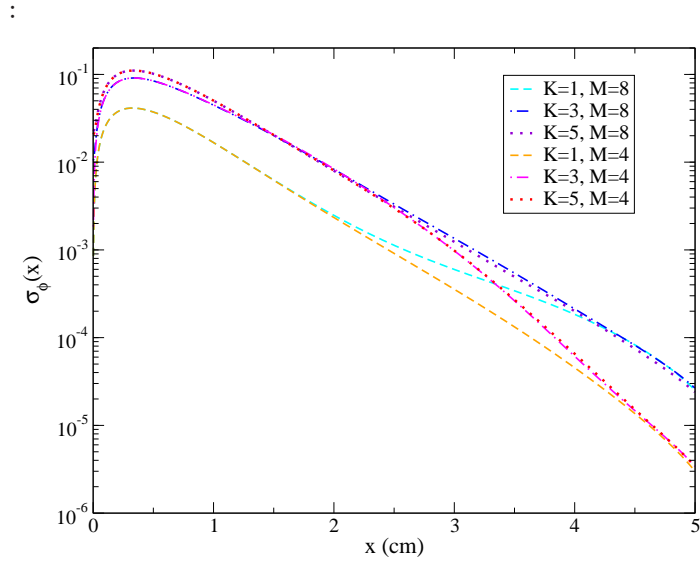
Figure 3.5: Standard Deviation in the Scalar Flux

3.3.2 S_8 Angular Discretization: Comparison of SCM with Monte Carlo

Normal Distribution

Results were also obtained for an S_8 angular quadrature order, for which the scalar flux was judged to be converged. Since there is no analytic solution in this case, the SCM results are compared against Monte Carlo results, which are denoted in the legend as $K = 5(\cdot)$. The number in parentheses denotes the number of realizations required to achieve a sample standard deviation of 10^{-2}. The flux and standard deviation for $c = 0.5$ and $c = 0.9$ are shown in Figs. 3.6 and 3.7, respectively. Results are similar to those obtained for the rod model. Particularly, it takes fewer SCM quadrature points to converge the scalar flux than the standard deviation and the larger the scattering ratio, the more rapidly the SCM quadrature converges. Also, the KL expansion order seems to have a greater effect on the accuracy of the solution at the incident edge while SCM quadrature order seems to have the greatest effect at the right side of the slab. S_8 also requires larger SCM quadrature orders than the rod model to converge the same problem.

As was mentioned in Section 3.2.2, there is the distinct possibility that some of the cross sections generated by the KL expansion will be negative for some values of x. Table 3.1 shows the number of transport equations required by the KL expansion and the number of these that must be discarded due to negative cross sections for various KL and SCM quadrature orders for $v_\sigma = 2$ cm^{-2}, $L = 5$ cm and $\lambda_c = 1$ cm. The larger the KL expansion and SCM quadrature order, the larger the percentage of equations that will be discarded. For K = 5 and M = 8, for instance, 34.47% of the equations have negative cross sections. Despite the fact that so many terms were discarded, the standard deviation in Fig. 3.6(b) shows excellent agreement with the Monte Carlo result. This is due to the shape of the normal distribution from which

:

(a) Scalar Flux

:

(b) Standard Deviation of the Scalar Flux
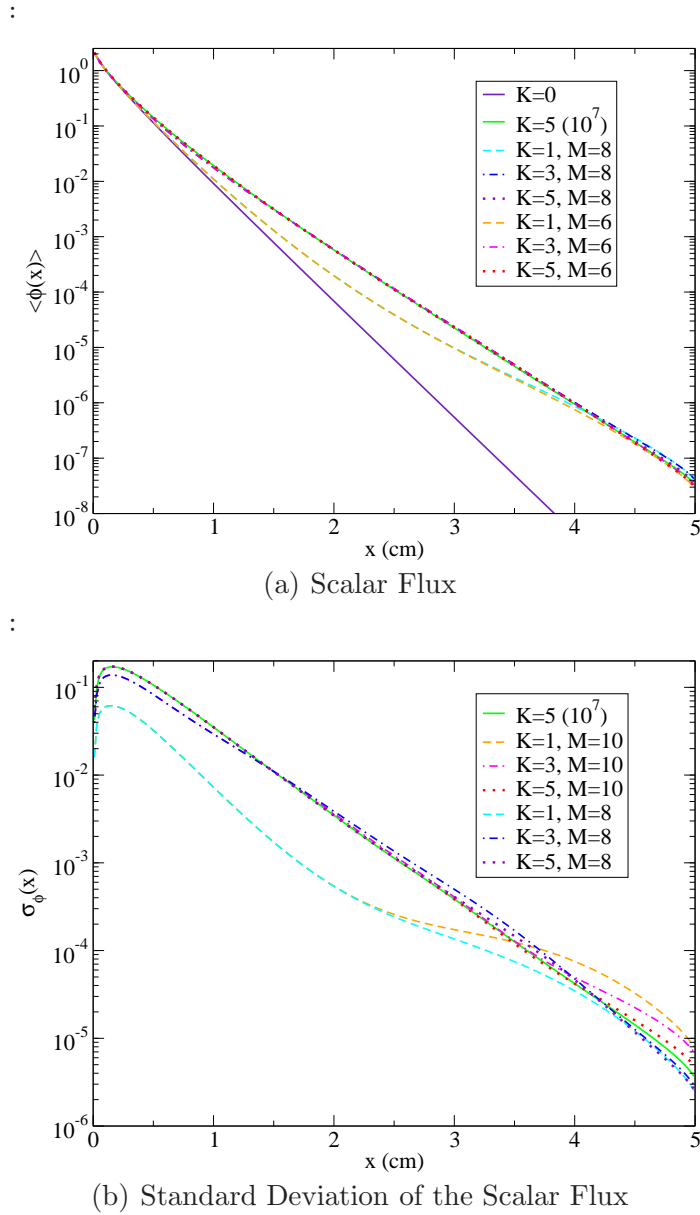
Figure 3.6: Normal Cross Section: Scalar Flux and its Relative Error for S_8 ($c = 0.5$, $v_\sigma = 2.0$ cm^{-2})

the ξ_k are sampled and the structure of Gauss-Hermite quadrature. The negative cross sections correspond to the most negative quadrature abscissas, for which the distribution, and by extension the quadrature weights, are very small. The final

:

(a) Scalar Flux

:

(b) Standard Deviation of the Scalar Flux
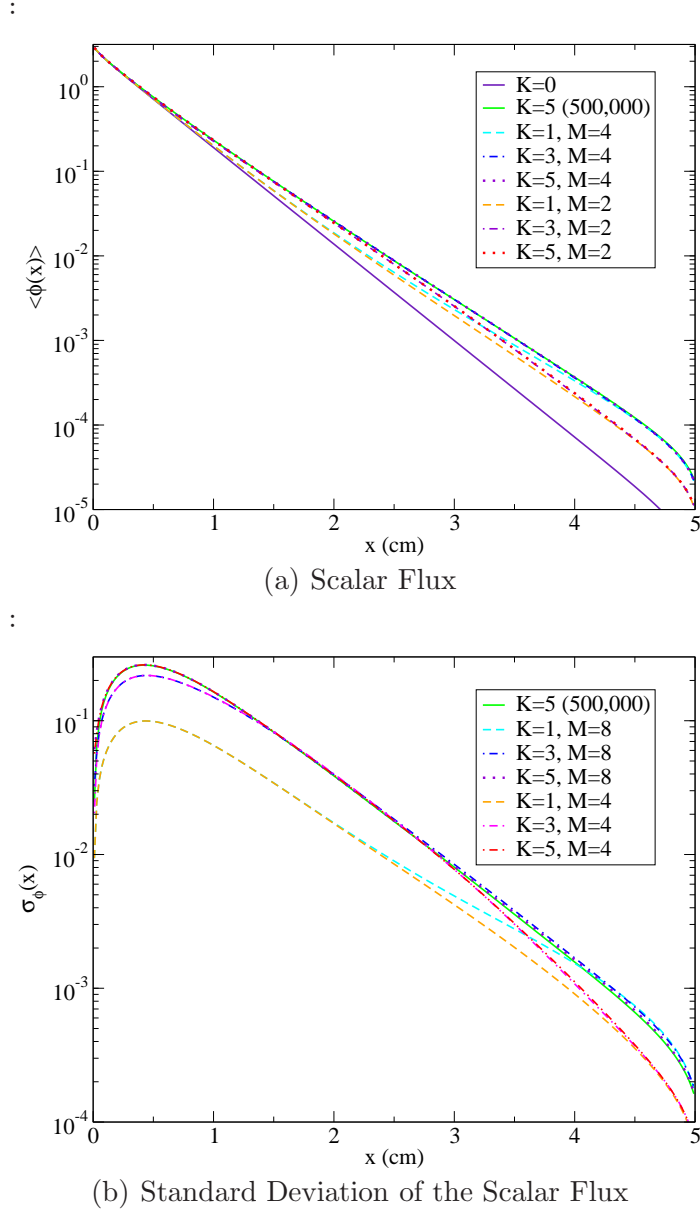
Figure 3.7: Normal Cross Section: Scalar Flux and its Relative Error for S_8 ($c = 0.9$, $v_\sigma = 2.0$ cm^{-2})

column in Table 3.1 shows the sum of the weights for those terms in which the cross section is positive throughout the domain. When all of the cross sections are positive and all terms are kept in the expansion, the weights should sum to one. As can be

seen, even when more than a third of the equations have to be discarded for K = 5 and M = 8, the weights still sum to 0.99962517, a deviation of less than 3.75×10^{-4}. Therefore, the discarded terms would have little impact on the total sum even if they could be included. Thus, while negative cross sections are not desirable and will most definitely have some impact on the accuracy of the solution, the effect appears to be negligible in these cases.

KL order	quadrature order	number of equations	equations discarded	sum of the GH weights
1	2	2	0	1.00000000
1	4	4	0	1.00000000
1	6	6	0	1.00000000
1	8	8	0	1.00000000
1	10	10	0	1.00000000
3	2	8	0	1.00000000
3	4	64	0	1.00000000
3	6	216	24	0.99993264
3	8	512	106	0.99992143
3	10	1000	288	0.99991428
5	2	32	0	1.00000000
5	4	1024	58	0.99968662
5	6	7776	1760	0.99963450
5	8	32768	11294	0.99962517
5	10	100000	42592	0.99961537

Table 3.1: Number of Equations Required for the KL Expansion ($v_\sigma = 2$ cm^{-2}, $L = 5$ cm and $\lambda_c = 1$ cm)

Log-Normal Distribution

SCM results were also obtained for the KL expansion of the log-normal cross section for $\langle \sigma \rangle = 5$ cm^{-1}, $v_\sigma = 2$ cm^{-2}, $L = 5$ cm, $\lambda_c = 1$ cm and $I = 250$, as above, and compared against Monte Carlo. In this case, the cross section always remains positive since the cross section only ranges between zero and infinity. In comparing Fig. 3.6 with Fig. 3.8 and Fig. 3.7 with Fig. 3.9 it can be seen that the SCM quadrature converges more rapidly for the log-normal distribution than the normal distribution. This is due to the fact that the log-normal cross section distribution is only semi-infinite rather than infinite in extent like the normal cross section: The lack of a long tail on the negative side of the peak combined with the fact that all of the points in the SCM quadrature integration can be included contributes to this more rapid convergence. The convergence of the KL expansion appears to be equivalent to that for the normal cross section.

Fig. 3.10 shows similar results for $v_\sigma = 25.0$ cm^{-2}. For this larger variance, it is necessary to use a KL order of 9 to get a converged solution, compared with a KL order of 5 for $v_\sigma = 2.0$.

3.4   Diffusion Analysis

3.4.1   Normal Random Processes

Also of interest is the behavior of the flux in the diffusion limit. Only results are shown in this section; for a detailed derivation of the diffusion equations listed below,

:

(a) Scalar Flux

:
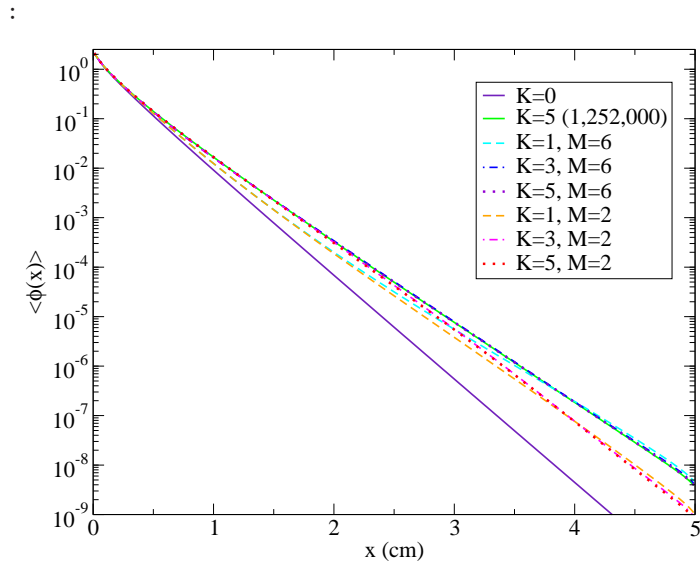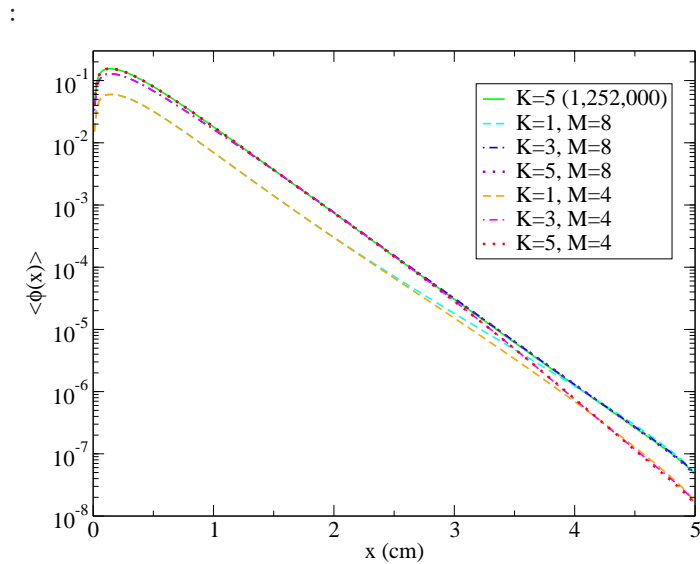
(b) Standard Deviation of the Scalar Flux

Figure 3.8: Log-Normal Cross Section: Scalar Flux and its Relative Error for S_8 ($c = 0.5$, $v_\sigma = 2.0$ cm^{-2})

35

see Appendix B. The analysis was conducted for both the semi-infinite medium and

:

(a) Scalar Flux

:
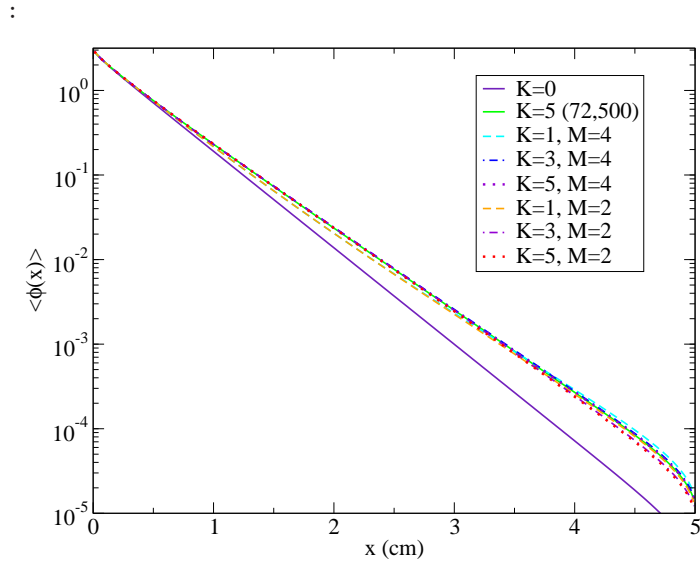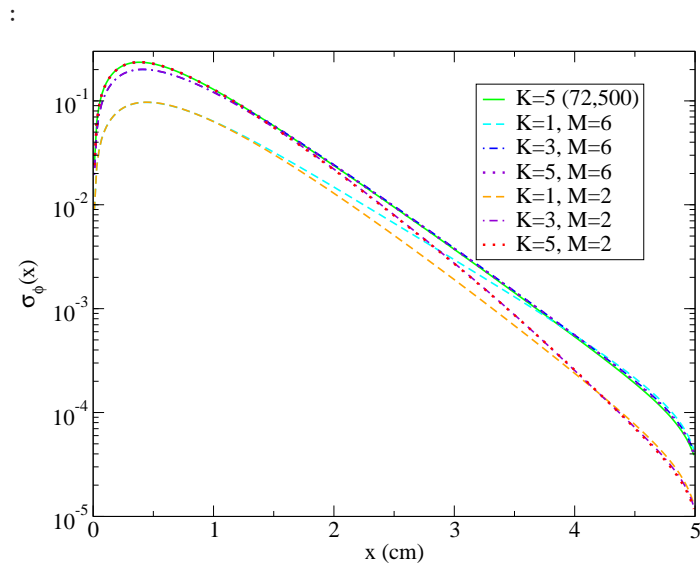
(b) Standard Deviation of the Scalar Flux

Figure 3.9: Log-Normal Cross Section: Scalar Flux and its Relative Error for S_8 ($c = 0.9$, $v_\sigma = 2.0$ cm^{-2})

the KL expansion using standard diffusion scalings:

$$\langle \sigma \rangle \sim \mathcal{O}\left(\frac{1}{\epsilon}\right), \ (1-c) \sim \mathcal{O}(\epsilon^2), \ Q \sim \mathcal{O}(\epsilon) \tag{3.25}$$

:

(a) Scalar Flux

:
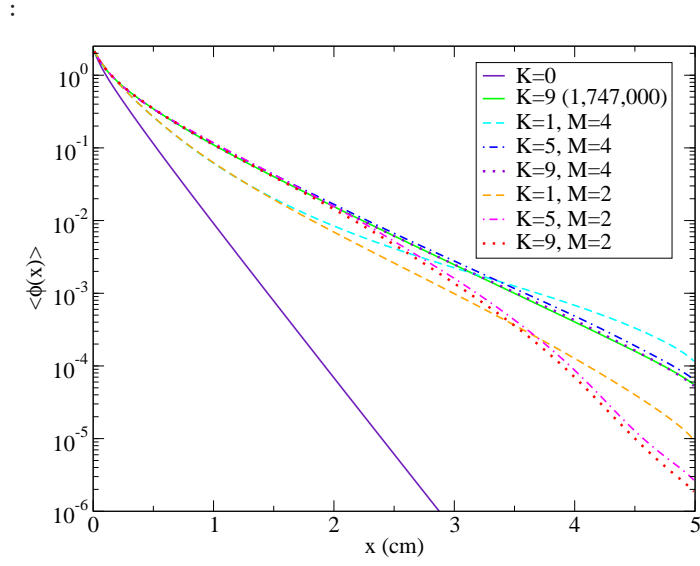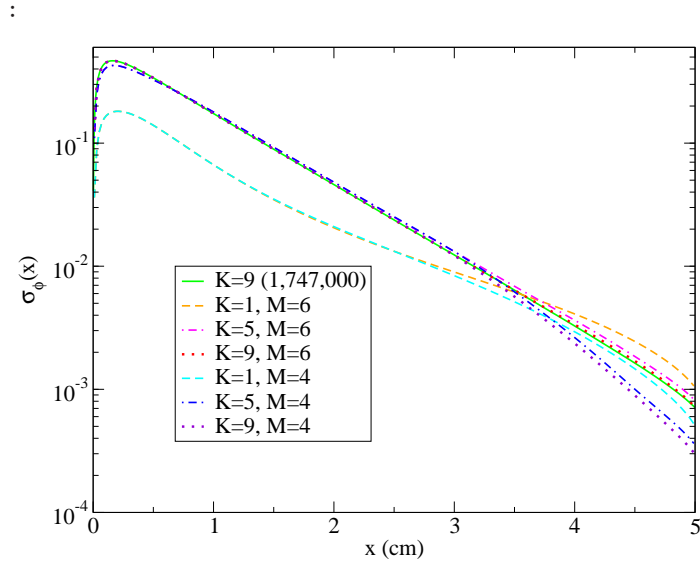
(b) Standard Deviation of the Scalar Flux

Figure 3.10: Log-Normal Cross Section: Scalar Flux and its Relative Error for S_8 ($c = 0.5$, $v_\sigma = 25.0$ cm^{-2})

for $\epsilon \ll 1$. The scaling of the variance presents an interesting dilemma. If

$$v_\sigma \sim \mathcal{O}\left(\frac{1}{\epsilon^2}\right)$$

so that the standard deviation grows in proportion to the mean, then a stochastic diffusion equation is obtained:

$$-D_{KL}(x,\omega)\frac{\partial^2 \phi(x,\omega)}{\partial x^2} + \sigma_{a,KL}(x,\omega)\phi(x,\omega) = Q(x) \tag{3.26}$$

where $D_{KL}(x,\omega) = \frac{1}{3\sigma_{KL}(x,\omega)}$ and $\sigma_{a,KL}(x,\omega) = (1-c)\sigma_{KL}(x,\omega)$. If instead the variance of the cross section is scaled in the same way as the mean,

$$v_\sigma \sim \mathcal{O}\left(\frac{1}{\epsilon}\right),$$

so that the standard deviation grows at a slower rate than the mean as ϵ becomes small, Eqs. 3.11 and 3.15a-3.15b yield the following *deterministic* diffusion equations, respectively:

$$-\frac{1}{\langle\sigma\rangle}\frac{\partial^2 \phi(x)}{\partial x^2} + \langle\sigma_a\rangle\phi(x) = 0 \tag{3.27}$$

and

$$-\langle D\rangle\frac{\partial^2 \phi(x)}{\partial x^2} + \langle\sigma_a\rangle\phi(x) = Q(x) \tag{3.28}$$

where $D = \frac{1}{3\langle\sigma\rangle}$ for S-N and $D = \frac{1}{\langle\sigma\rangle}$ for rod geometry. These equations are diffusion equations given for the mean total and absorption cross sections and are independent of the variable ω. Furthermore, they are identical to the diffusion equations obtained when the variance is taken to be $\mathcal{O}(1)$. Thus, in diffusive materials where the variance and mean of the cross section are on the same order or the variance is lower order than the mean, the flux is in fact deterministic. When the diffusion scalings are introduced to the numerical implementation, as ϵ becomes very small, each individual realization limits to a nonrandom solution which is the same for each realization and is, in fact, the diffusion solution given by Eq. 3.28.

The diffusion scalings were introduced to the numerical implementation and ϕ was plotted for 10 individual KL realizations. Four different plots are shown in Fig. 3.11(a), corresponding to $\epsilon = 2^{-n}$, $n = 0$, 5, 10, 15. Results are shown for a KL order of 5, $\langle \sigma \rangle = 5$ cm^{-1}, $v_\sigma = 2$ cm^{-2}, $\lambda_c = 1$ cm, $c = 0.5$, $L = 5$ cm, $N = 8$ and $I = 250$. As predicted by the analysis, as ϵ gets small, each individual realization limits to a nonrandom solution. This solution is the same for each realization and is, in fact, the diffusion solution given by Eq. 3.28. Although the plots are not shown here, this result appears to be independent of the number of terms in the KL expansion and S_N quadrature order.

It is also revealing to examine the norm of the relative difference between the numerical and diffusion solutions for various ϵ,

$$\delta(n) = \frac{\|\phi_{\text{diff}} - \langle \phi \rangle(n)\|_2}{\|\phi_{\text{diff}}\|_2},$$

where $\langle \phi \rangle(n)$ and ϕ_{diff} are the scaled semi-infinite medium or KL and diffusion solutions, respectively. Fig. 3.11(b) shows $\delta(n)$ plotted vs. n, where $\epsilon = 2^{-n}$, for 25 individual realizations for the same physical parameters as in Fig. 3.11(a). As can be seen, the relative difference in each individual realization scales as $\sqrt{\epsilon}$.

The same analysis was conducted on the semi-infinite medium solution, results for which are shown in Fig. 3.12 for $\langle \sigma \rangle = 5$ cm^{-1}, $v_\sigma = 2$ cm^{-2}, $\lambda_c = 1$ cm, $c = 0.5$, $L = 5$ cm and $I = 250$. In this case the relative difference scales as ϵ, which seems counter intuitive considering it scales as $\sqrt{\epsilon}$ for the KL expansion when the same scalings are used. However, while $C_0(x)$ in Eqs. 3.15a and 3.15b is scaled as $\frac{1}{\epsilon}$ since v_σ appears explicitly in its definition (see equations 3.1 and 3.16), $\tilde{\sigma}(x, \omega)$ in Eq. 3.12 (which is, in turn, substituted into Eq. 3.11) is a function of $\sqrt{v_\sigma}$ through the $\sqrt{\lambda_k}$ term (see the definition of λ_k in Eq. 3.8) and is therefore scaled as $\frac{1}{\sqrt{\epsilon}}$. Therefore, the asymptotic expansion of ϕ for the KL expansion contains half-powers of ϵ

$$\phi = \sum_{n=0}^{\infty} \epsilon^{\frac{n}{2}} \phi^{(n)} \tag{3.29}$$

while the asymptotic expansion of ϕ for the semi-infinite medium contains only integer powers of ϵ

$$\phi = \sum_{n=0}^{\infty} \epsilon^n \phi^{(n)}. \tag{3.30}$$

Thus, while in either case $\phi^{(0)}$ is the diffusion solution, the first correction term, $\phi^{(1)}$, which we would expect to be of the same order of magnitude as $\delta(n)$, is multiplied by $\sqrt{\epsilon}$ for the KL expansion and ϵ for the semi-infinite medium.
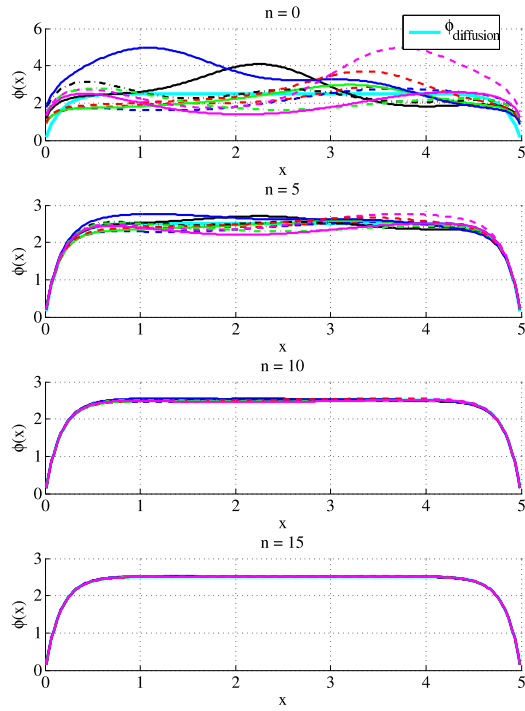
(a) Scalar Flux for 10 KL Realizations and Diffusion
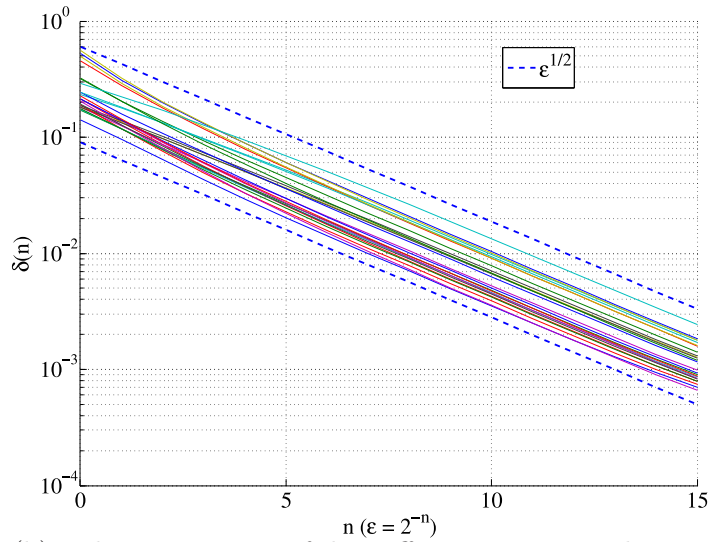
(b) Relative L_2 Norm of the Difference Between the Numerical and Diffusion Solutions for 25 KL Realizations

Figure 3.11: Diffusion Limit for a Normal Random Process
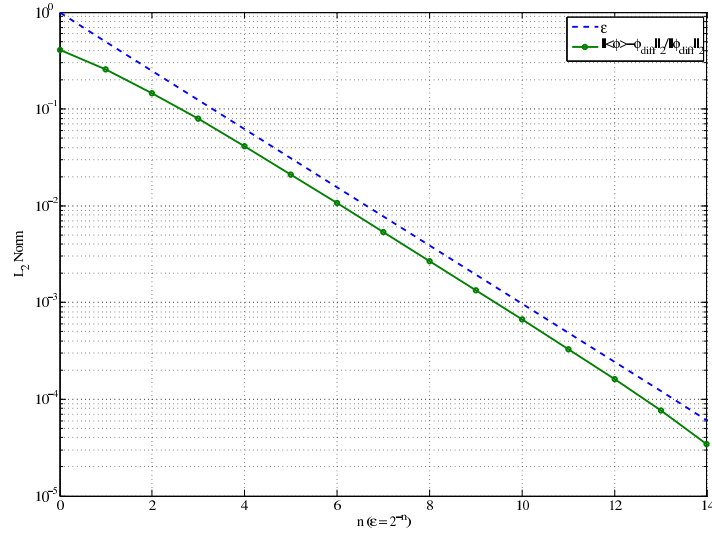
Figure 3.12: Relative L_2 Norm of the Difference Between the Numerical and Diffusion Solutions for a Normal Random Process and Semi-Infinite Medium

3.4.2   Log-Normal Random Processes

Once again, for a detailed derivation of the diffusion analysis given below, see Appendix B. The asymptotic analysis is slightly more complicated for a log-normal random process because it is not immediately obvious how the cross section should be scaled. Eq. 3.19 can also be written

$$
\begin{aligned}
\sigma_{KL}(x,\omega) &= e^{\langle w(x)\rangle}e^{\sqrt{v_w}\sum_{k=1}^{K}\sqrt{\gamma_k}\varphi_k(x)\xi_k(\omega)} \\
&= e^{\langle w(x)\rangle}e^{\sqrt{v_w}\rho(x,\omega)}
\end{aligned}
\tag{3.31}
$$

where $\gamma_k = \frac{\lambda_k}{v_w}$ and the KL expansion has been replaced by $\rho(x,\omega)$. Clearly, from Eq. 3.20,

$$
e^{\langle w(x)\rangle} = \frac{\langle\sigma\rangle}{\sqrt{\frac{v_\sigma}{\langle\sigma\rangle^2}+1}} = \frac{\langle\sigma\rangle}{\sqrt{y+1}}
\tag{3.32}
$$

where $y = \frac{v_\sigma}{\langle\sigma\rangle^2}$. Applying the scalings from Eq. 3.25 and setting

$$v_\sigma \sim \mathcal{O}\left(\frac{1}{\epsilon}\right)$$

yields

$$y = \frac{\tilde{v}_\sigma/\epsilon}{\langle\tilde{\sigma}\rangle^2/\epsilon^2} = \epsilon\frac{\tilde{v}_\sigma}{\langle\tilde{\sigma}\rangle^2} = \epsilon\tilde{y},$$

thus

$$e^{\langle w(x)\rangle} = \frac{\langle\tilde{\sigma}\rangle}{\epsilon\sqrt{\epsilon\tilde{y}+1}} \approx \frac{\langle\tilde{\sigma}\rangle}{\epsilon}\left(1 - \frac{\epsilon\tilde{y}}{2} + \frac{3(\epsilon\tilde{y})^2}{8} + \mathcal{O}(\epsilon^3)\right) \tag{3.33}$$

where the square root has been expanded in a Taylor series about $\epsilon\tilde{y} = 0$. The second term in Eq. 3.31, given Eq. 3.21, can be written

$$e^{\sqrt{v_w}\rho(x,\omega)} = e^{\sqrt{\ln(y+1)}\rho(x,\omega)}. \tag{3.34}$$

Clearly, another Taylor series is required in order to apply the scalings and proceed with the analysis. The series is taken about $y = 0$:

$$e^{\sqrt{\ln(y+1)}\rho} \approx 1 + \rho\sqrt{y} + \frac{\rho^2}{2}y + \left(\frac{\rho^3}{6} + \frac{\rho}{4}\right)y^{\frac{3}{2}} + \frac{\rho^4 - 6\rho^2}{24}y^2 + \mathcal{O}(y^{\frac{5}{2}}). \tag{3.35}$$

Thus,

$$e^{\sqrt{v_w}\rho(x,\omega)} \approx 1 + \rho\sqrt{\epsilon\tilde{y}} + \frac{\rho^2}{2}\epsilon\tilde{y} + \left(\frac{\rho^3}{6} + \frac{\rho}{4}\right)(\epsilon\tilde{y})^{\frac{3}{2}} + \frac{\rho^4 - 6\rho^2}{24}(\epsilon\tilde{y})^2 + \mathcal{O}(\epsilon^{\frac{5}{2}}). \tag{3.36}$$

Substituting these cross sections into the transport equation along with the rest of the diffusion scalings and proceeding with the analysis yields Eq. 3.28, the analytic diffusion equation obtained for the normal cross section.

Numerical results are shown for a KL order of 5, $\langle\sigma\rangle = 5$ cm^{-1}, $v_\sigma = 25$ cm^{-2}, $\lambda_c = 1$ cm, $c = 0.5$, $L = 5$ cm, $N = 8$ and $I = 250$. As can be seen, the individual flux realizations show more variation in Fig. 3.13(a) than they did in Fig. 3.11(a) since $v_\sigma = 25$ cm^{-2} as opposed to 2 cm^{-2}. However, as n gets larger, each individual realization still approaches the diffusion solution. The relative difference in each individual realization, shown in Fig. 3.13(b), scales as $\sqrt{\epsilon}$, just as it did in Fig. 3.11(b).
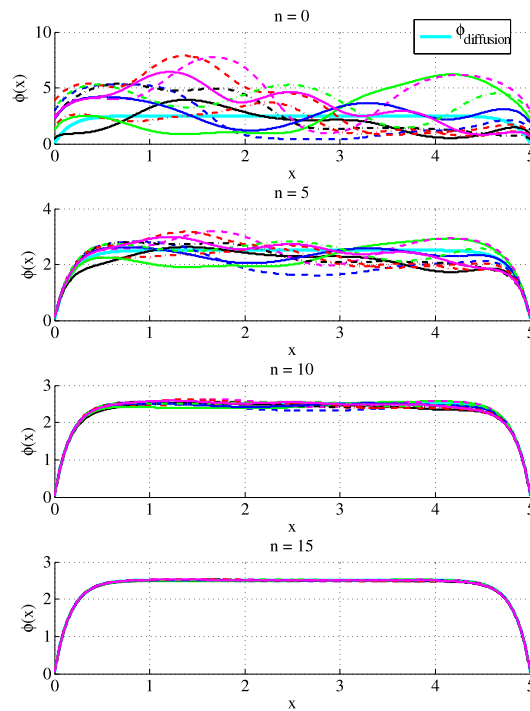
(a) Scalar Flux for 10 KL Realizations and Diffusion
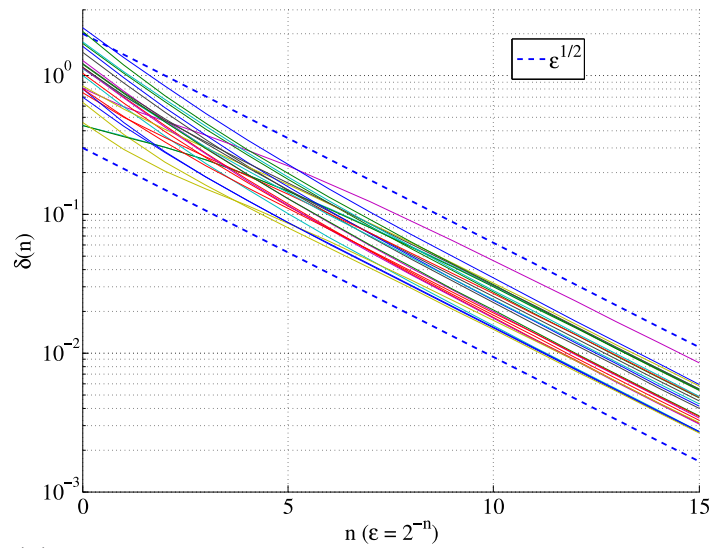
(b) Relative L_2 Norm of the Difference Between the Numerical and Diffusion Solutions for 25 KL Realizations

Figure 3.13: Diffusion Limit for a Log-Normal Random Process

Chapter 4

The Polynomial Chaos Expansion

The homogeneous form of polynomial chaos (PC) has long been used to represent Gaussian random processes in terms of Hermite polynomials, where the Hermite polynomials are given in terms of Gaussian random variables. Generalized PC (gPC) is a more recent development which extends the method to include other families of orthogonal polynomials and random variables. Both methods have been used in concert with the Stochastic Finite Element Method (SFEM), which combines PC expansions with projections onto the PC basis to yield systems of deterministic equations for the PC coefficients of the flux which are, in general, coupled. The Stochastic Collocation Method (SCM) has also been used to calculate the gPC coefficients directly. In section 4.1, homogeneous chaos and its extension to gPC are discussed. Section 4.2 details the application of SFEM and SCM to the transport equation, both when the cross section is a random variable and can be represented using a gPC expansion, and when it is a random process, requiring that a KL expansion be used. A detailed spectral analysis is conducted in section 4.3, including an analysis of the well-posedness of the SFEM equations, plots of the spectral radii of possible operators for analyzing the convergence of Richardson iteration and graphs of the eigenvalue spectra of the operators that yield insight into the convergence of Krylov iterative methods.

4.1 Polynomial Chaos

4.1.1 Homogeneous Chaos

Homogeneous chaos was first proposed by Wiener [29] and is closely related to the previous discussion on the KL expansion in Chapter 3 as it expands second-order random process in terms of Gaussian random variables. As before, the eigenvalues and eigenfunctions of the covariance function are necessary to construct the KL expansion, therefore the covariance function must be known. If we want to expand a quantity with unknown covariance function, a PC expansion in terms of the same Gaussian random variables, $\xi_k(\omega)$, can be used instead. A second-order random process, $\chi(\omega)$, can be represented by the following mean-square convergent expansion in terms of generalized Hermite polynomials of order n, H_n [33]:

$$
\begin{aligned}
\chi(\omega) = a_0 H_0 &+ \sum_{i_1=1}^{\infty} a_{i_1} H_1(\xi_{i_1}) \\
&+ \sum_{i_1=1}^{\infty} \sum_{i_2=1}^{i_1} a_{i_1 i_2} H_2(\xi_{i_1}, \xi_{i_2}) \\
&+ \sum_{i_1=1}^{\infty} \sum_{i_2=1}^{i_1} \sum_{i_3=1}^{i_2} a_{i_1 i_2 i_3} H_3(\xi_{i_1}, \xi_{i_2}, \xi_{i_3}) + \dots .
\end{aligned}
\tag{4.1}
$$

In order for this expansion to be useful, it is necessary to truncate by limiting both the number of random variables, K, as well as the maximum polynomial order, P,

to yield

$$\chi(\omega) = a_0 H_0 + \sum_{i_1=1}^{K} a_{i_1} H_1(\xi_{i_1})$$

$$+ \sum_{i_1=1}^{K} \sum_{i_2=1}^{i_1} a_{i_1 i_2} H_2(\xi_{i_1}, \xi_{i_2}) + \ldots$$

$$+ \sum_{i_1=1}^{K} \cdots \sum_{i_P=1}^{i_{P-1}} a_{i_1 \ldots i_P} H_P(\xi_{i_1}, \ldots, \xi_{i_P}) \tag{4.2}$$

$$= a_0 H_0 + a_1 H_1(\xi_1) + \ldots + a_K H_1(\xi_K)$$

$$+ a_{11} H_2(\xi_1, \xi_1) + a_{21} H_2(\xi_2, \xi_1) + \ldots + a_{KK} H_2(\xi_K, \xi_K)$$

$$+ \ldots + a_{1\ldots1} H_P(\xi_1, \ldots, \xi_1) + \ldots + a_{K\ldots K} H_P(\xi_K, \ldots, \xi_K)$$

$$= a_0 + a_1 \xi_1 + \ldots + a_K \xi_K$$

$$+ a_{11}(\xi_1^2 - 1) + a_{21} \xi_1 \xi_2 + \ldots + a_{KK}(\xi_K^2 - 1) + \ldots \tag{4.3}$$

where the total number of terms in the expansion is

$$(P_t + 1) = \frac{(K + P)!}{K! P!}. \tag{4.4}$$

P_t is defined in this way so that when there is a single random variable, $P_t = P$ is the maximum polynomial order. For notational convenience, Eq. 4.3 can be written as

$$\chi(\omega) = \sum_{i=0}^{P_t} \hat{a}_i \Psi_i(\{\xi_r\}) \tag{4.5}$$

where $\hat{a}_i$ and $\Psi_i(\{\xi_r\})$ correspond to the $a_{i_1 \ldots i_p}$ and $H_p(\xi_{i_1}, \ldots, \xi_{i_p})$, respectively. Increasing the number of random variables, K, accounts for higher frequency random fluctuations of the stochastic process itself, while increasing the maximum polynomial order, P, captures strong nonlinear dependence of the solution process on the stochastic process [40].

4.1.2 Generalized Polynomial Chaos

Homogeneous chaos is limited to a Hermite-type PC expansion in terms of Gaussian random variables. The method is efficient for Gaussian inputs and certain types of non-Gaussian (e.g., log-normal) input parameters [33, 40]; however, in general, when inputs are non-Gaussian, using another type of random variable may be more efficient. Generalized polynomial chaos (gPC), developed by Xiu and Karniadakis [31, 32], expands the method to so-called "Wiener-Askey chaoses" of orthogonal polynomials belonging to the Askey scheme [84], which are listed along with their corresponding random variable type and support in Table 4.1. As can be seen, the gPC of the Hermite type is homogeneous chaos.

Wiener-Askey Chaos $\{\Phi(\zeta)\}$	Random Variables ζ	Weight Function $w(\zeta)$	Support
Hermite	Gaussian	$\frac{1}{\sqrt{2\pi}}e^{-\frac{\zeta^2}{2}}$	$(-\infty, \infty)$
Laguerre	gamma	$\frac{\zeta^{\alpha-1}e^{-\zeta}}{\Gamma(\alpha)}$	$[0, \infty)$
Jacobi	beta	$\frac{\Gamma(\alpha+\beta+2)(1-\zeta)^\alpha(1+\zeta)^\beta}{2^{\alpha+\beta}(b-a)\Gamma(\alpha+1)\Gamma(\beta+1)}$	$[a, b]$
Legendre	uniform	$\frac{1}{(b-a)}$	$[a, b]$

Table 4.1: Continuous Wiener-Askey Polynomial Chaoses and their Underlying Random Variables and Corresponding Weight Functions

Once again, a second-order random process is expanded as [31, 32]

$$
\begin{aligned}
\chi(\omega) = c_0 I_0 &+ \sum_{i_1=1}^{K} c_{i_1} I_1(\zeta_{i_1}) \\
&+ \sum_{i_1=1}^{K}\sum_{i_2=1}^{i_1} c_{i_1 i_2} I_2(\zeta_{i_1}, \zeta_{i_2}) + \ldots \\
&+ \sum_{i_1=1}^{K}\cdots\sum_{i_P=1}^{i_{P-1}} c_{i_1 \ldots i_P} I_P(\zeta_{i_1}, \ldots, \zeta_{i_P})
\end{aligned}
\tag{4.6}
$$

which can be rewritten as

$$\chi(\omega) = \sum_{i=0}^{P_t} \hat{c}_i \Phi_i(\{\zeta_r\}). \tag{4.7}$$

The I_p are Askey polynomials of order p, the ζ_{i_p} are their corresponding random variables and the $\hat{c}_i$ and $\Phi_i(\{\zeta_r\})$ correspond to the $c_{i_1...i_p}$ and $I_p(\zeta_{i_1}, \ldots, \zeta_{i_p})$, respectively. Invoking the orthogonality of the basis functions, the coefficients in Eq. 4.7 are given by

$$\hat{c}_j = \frac{\langle \chi, \Phi_j(\zeta) \rangle}{\langle \Phi_j^2(\zeta) \rangle} \tag{4.8}$$

where

$$\langle f(\zeta), g(\zeta) \rangle = \int f(\zeta)g(\zeta)w(\zeta)d\zeta. \tag{4.9}$$

4.1.3 Representation of Arbitrary Random Inputs

The evaluation of the numerator in Eq. 4.7 must be dealt with carefully when χ, $\chi \in (\chi_0, \chi_1)$, and ζ, $\zeta \in (\zeta_0, \zeta_1)$, belong to different probability spaces. This difficulty can be overcome by mapping both variables onto a third variable, $u(\omega) \in (0, 1)$. Let the probability density functions (pdfs) of χ and ζ be $f(\chi)$ and $g(\zeta)$ with accompanying cumulative distribution functions (cdfs)

$$F(\chi) = \int_{\chi_0}^{\chi} f(\chi)d\chi'$$

and

$$G(\zeta) = \int_{\zeta_0}^{\zeta} g(\zeta')d\zeta'.$$

$F(\chi)$ and $G(\zeta)$, being cdfs, are defined on the interval $(0, 1)$, thus it is possible to define $u = F(\chi) = G(\zeta)$ to be a uniform random variable on interval such that $\chi = F^{-1}(u) = h(u)$ and $\zeta = G^{-1}(u) = \ell(u)$. Now

$$\hat{c}_j = \frac{\langle \chi, \Phi_j(\zeta) \rangle}{\langle \Phi_j^2(\zeta) \rangle} = \frac{1}{\langle \Phi_j^2(\zeta) \rangle} \int_0^1 h(u)\Phi_j(\ell(u))du. \tag{4.10}$$

4.2 Numerical Implementation: Computation of the Polynomial Chaos Coefficients

4.2.1 The Stochastic Finite Element Method

If the total cross section, $\sigma(\omega)$, does not vary spatially, a single random variable is sufficient to characterize it. The application of SFEM begins with the expansion of $\psi(x, \mu; \omega)$ and $\sigma(\omega)$ in gPC expansions:

$$\psi(x, \mu; \omega) = \sum_{i=0}^{P} \psi_i(x, \mu) \Phi_i(\zeta(\omega)) \tag{4.11}$$

$$\sigma(\omega) = \sum_{j=0}^{P_\sigma} \sigma_j \Phi_i(\zeta(\omega)). \tag{4.12}$$

The coefficients of the cross section are known since its distribution is known, however, the coefficients $\psi_i(x, \mu)$ must be determined in the solution process—they are the problem unknowns. Alternately, if the cross section can be written as a function of the random variable, $\sigma(\omega) = f(\zeta(\omega))$, this expression can be substituted into the transport equation in place of its gPC expansion.

The stochastic transport equation is formed by substituting $\psi(x, \mu; \omega)$ and $\sigma(\omega)$ from Eqs. 4.11 and 4.12 into the deterministic transport equation (Eq. 2.1) to yield

$$\mu \sum_{i=0}^{P} \frac{\partial \psi_i(x, \mu)}{\partial x} \Phi_i(\zeta(\omega)) + \sum_{i=0}^{P} \sum_{j=0}^{P_\sigma} \psi_i(x, \mu) \sigma_j \Phi_i(\zeta(\omega)) \Phi_j(\zeta(\omega)) =$$

$$\frac{c}{2} \sum_{i=0}^{P} \sum_{j=0}^{P_\sigma} \phi_i(x) \sigma_j \Phi_i(\zeta(\omega)) \Phi_j(\zeta(\omega)) + Q(x, \mu). \tag{4.13}$$

If $f(\zeta(\omega))$ is used in place of a gPC, the transport equation becomes

$$\mu \sum_{i=0}^{P} \frac{\partial \psi_i(x, \mu)}{\partial x} \Phi_i(\zeta(\omega)) + \sum_{i=0}^{P} \psi_i(x, \mu) f(\zeta(\omega)) \Phi_i(\zeta(\omega)) =$$

$$\frac{c}{2} \sum_{i=0}^{P} \phi_i(x) f(\zeta(\omega)) \Phi_i(\zeta(\omega)) + Q(x, \mu). \quad (4.14)$$

Since the Φ_i are orthogonal, taking Galerkin projections onto the polynomial basis yields a *deterministic* equation for each ψ_ℓ, $\ell = 0, 1, \ldots, P$:

$$\mu \frac{\partial \psi_\ell}{\partial x} \langle \Phi_\ell^2 \rangle + \sum_{i=0}^{P} \sum_{j=0}^{P_\sigma} \psi_i \sigma_j \langle \Phi_i \Phi_j \Phi_\ell \rangle = \frac{c}{2} \sum_{i=0}^{P} \sum_{j=0}^{P_\sigma} \phi_i \sigma_j \langle \Phi_i \Phi_j \Phi_\ell \rangle + Q_\ell \quad (4.15)$$

or

$$\mu \frac{\partial \psi_\ell}{\partial x} \langle \Phi_\ell^2 \rangle + \sum_{i=0}^{P} \psi_i \langle f \Phi_i \Phi_\ell \rangle = \frac{c}{2} \sum_{i=0}^{P} \phi_i \langle f \Phi_i \Phi_\ell \rangle + Q_\ell \quad (4.16)$$

where $Q_\ell = \langle \Phi_\ell Q \rangle$. Dividing through by $\langle \Phi_\ell^2 \rangle$ yields

$$\mu \frac{\partial \psi_\ell}{\partial x} + \sum_{i=0}^{P} b_{\ell i} \psi_i = \frac{c}{2} \sum_{i=0}^{P} b_{\ell i} \phi_i + q_\ell, \quad \ell = 0, 1, \ldots, P \quad (4.17)$$

where $b_{\ell i} = \sum_{j=0}^{P_\sigma} \sigma_j \frac{\langle \Phi_i \Phi_j \Phi_\ell \rangle}{\langle \Phi_\ell^2 \rangle}$ or $b_{\ell i} = \frac{\langle f \Phi_i \Phi_\ell \rangle}{\langle \Phi_\ell^2 \rangle}$ and $q_\ell = \frac{Q_\ell}{\langle \Phi_\ell^2 \rangle}$.

If, instead, the cross section varies spatially and is therefore a random process, it can be represented using a truncated KL expansion as in Chapter 3

$$\sigma(x, \omega) = \langle \sigma \rangle + \sum_{k=1}^{K} \sqrt{\lambda_k} \varphi_k(x) \xi_k(\omega). \quad (4.18)$$

There are now K random variables to contend with, therefore the PC expansion of the flux takes the form

$$\psi(x, \mu; \omega) = \sum_{i=0}^{P_t} \psi_i(x, \mu) \Phi_i(\{\zeta_r\}) \quad (4.19)$$

where there are K random variables, P is the maximum polynomial order and there are $(P_t + 1) = \frac{(K+P)!}{K!P!}$ terms in the PC expansion of ψ. The transport equation then

takes the form

$$\mu \sum_{i=0}^{P_t} \frac{\partial \psi_i(x,\mu)}{\partial x} \Phi_i(\{\zeta_k\})$$

$$+ \left[\langle \sigma \rangle + \sum_{k=1}^{K} \sqrt{\lambda_k} \varphi_k(x) \xi_k(\omega) \right] \sum_{i=0}^{P_t} \psi_i(x,\mu) \Phi_i(\{\zeta_r\}) =$$

$$\frac{c}{2} \left[\langle \sigma \rangle + \sum_{k=1}^{K} \sqrt{\lambda_k} \varphi_k(x) \xi_k(\omega) \right] \sum_{i=0}^{P_t} \phi_i(x) \Phi_i(\{\zeta_r\}) + Q(x,\mu). \quad (4.20)$$

Projecting onto the polynomial basis once again and dividing through by $\langle \Phi_\ell^2 \rangle$ yields a set of $(P_t + 1)$ fully coupled deterministic equations for $\psi_\ell(x,\mu)$:

$$\mu \frac{\partial \psi_\ell}{\partial x} \Phi_i(\{\zeta_k\}) + \langle \sigma \rangle \psi_\ell + \sum_{k=1}^{K} \sum_{i=0}^{P_t} \sqrt{\lambda_k} \varphi_k(x) \frac{\langle \xi_k \Phi_i \Phi_\ell \rangle}{\langle \Phi_\ell^2 \rangle} \psi_i =$$

$$\frac{c}{2} \langle \sigma \rangle \phi_\ell + \frac{c}{2} \sum_{k=1}^{K} \sum_{i=0}^{P_t} \sqrt{\lambda_k} \varphi_k(x) \frac{\langle \xi_k \Phi_i \Phi_\ell \rangle}{\langle \Phi_\ell^2 \rangle} \phi_i + Q_\ell, \quad \ell = 0, 1, \dots, P_t. \quad (4.21)$$

Eq. 4.21 can be written in the same way as Eq. 4.17 where

$$b_{\ell i}(x) = \langle \sigma \rangle \delta_{\ell i} + \sum_{k=1}^{K} \sqrt{\lambda_k} \varphi_k(x) \frac{\langle \xi_k \Phi_i \Phi_\ell \rangle}{\langle \Phi_\ell^2 \rangle}.$$

As can be seen, regardless of the type of expansion used to represented the cross section, the stochastic transport problem has been reduced to a system of $(P_t + 1)$ fully-coupled deterministic equations for $\psi_\ell(x,\mu)$, which must be solved iteratively.

The coupled equations in Eqs. 4.17 are reminiscent of multigroup transport problems with energy upscatter, for which there are several block iterative schemes available: Exact Block Gauss-Seidel (BGS), Inexact Block Gauss-Seidel (IBGS), Inexact Block Jacobi (BJ) and Inexact Block Jacobi (IBJ). In this case, each block corresponds to a particular PC coefficient of the flux, a structure which emerges when linear discontinuous finite element and discrete ordinates discretizations are applied to the spatial and angular variables, respectively. In total, then, there are $2IN(P_t+1)$

equations and unknowns, where I is the number of spatial cells and N is the number of discrete ordinates. The SFEM equations are rewritten in operator notation

$$\mathbf{L}\vec{\psi} = \mathbf{MSD}\vec{\psi} + \vec{Q} \qquad (4.22)$$

where

$$\vec{\psi} = [\vec{\psi}_0\,\vec{\psi}_1\,\cdots\,\vec{\psi}_{P_t}]^T \quad \text{and} \quad \vec{\phi} = [\vec{\phi}_0\,\vec{\phi}_1\,\cdots\,\vec{\phi}_{P_t}]^T.$$

$\mathbf{L}$ is the streaming and removal operator, which represents the left-hand side of Eq. 4.17; $\mathbf{M}$ maps the scalar flux coefficient vector, $\vec{\phi}$, onto the angular flux coefficient vector, $\vec{\psi}$; $\mathbf{S}$ is the scattering operator, which represents the summation on the right-hand side of Eq. 4.17; $\mathbf{D}$ maps $\vec{\psi}$ onto $\vec{\phi}$ (i.e., $\vec{\phi} = \mathbf{D}\tilde{\psi}$); and $\vec{Q}$ is a vector of the volume source moments. Since $\mathbf{L}$ and $\mathbf{S}$ perform summations over the PC moments of ψ and ϕ, respectively, each block in these matrices contain a smaller sub-matrix of dimension $2IN \times 2IN$ and $2I \times 2I$, respectively. $\mathbf{M}$ and $\mathbf{D}$ perform mappings on a single PC moment, therefore their block structure is diagonal and the blocks are of dimension $2IN \times 2I$ and $2I \times 2IN$, respectively.

By splitting $\mathbf{L}$ and $\mathbf{S}$ up into their block lower triangular ($\mathbf{L_L}$ and $\mathbf{S_L}$), block diagonal ($\mathbf{L_D}$ and $\mathbf{S_D}$) and block upper triangular ($\mathbf{L_U}$ and $\mathbf{S_U}$) parts, it is possible to write the block iterative schemes in the general form

$$\vec{\psi}^{(z+1)} = \mathbf{T}\vec{\psi}^{(z)} + \vec{q} \qquad (4.23)$$

where

$$\vec{q} = \mathbf{U}\vec{Q}$$

for iteration-unique $\mathbf{U}$ and $\mathbf{T}$ and z is the iteration index. For each scheme, $\mathbf{U}$ and $\mathbf{T}$ are listed in Table 4.2. The inexact schemes are so-named because the PC coefficients of the scalar flux on the right-hand side of Eq. 4.17 are not updated until the end of each outer iteration. In the exact schemes, the scalar flux is kept current

Method	T	U
BGS	$\mathbf{U}\left[-\mathbf{L_U} + \mathbf{MS_U D}\right]$	$\left[\mathbf{I} - (\mathbf{L_L} + \mathbf{L_D})^{-1}\mathbf{M}(\mathbf{S_L} + \mathbf{S_D})\mathbf{D}\right]^{-1}(\mathbf{L_L} + \mathbf{L_D})^{-1}$
IBGS	$\mathbf{U}\left[-\mathbf{L_U} + \mathbf{MSD}\right]$	$(\mathbf{L_L} + \mathbf{L_D})^{-1}$
BJ	$\mathbf{U}\left[-(\mathbf{L_L} + \mathbf{L_U}) + \mathbf{M}(\mathbf{S_L} + \mathbf{S_U})\mathbf{D}\right]$	$(\mathbf{I} - \mathbf{L_D}^{-1}\mathbf{MS_D D})^{-1}\mathbf{L_D}^{-1}$
IBJ	$\mathbf{U}\left[-(\mathbf{L_L} + \mathbf{L_U}) + \mathbf{MSD}\right]$	$\mathbf{L_D}^{-1}$

Table 4.2: $\mathbf{T}$ and $\mathbf{U}$ Matrices for Various Iterative Methods

at each outer iteration by conducting a series of inner source iterations for each PC coefficient. This inner iteration takes the form

$$\mathbf{L}_\ell \vec{\psi}_\ell^{(y+1)} = \mathbf{M}_\ell(\mathbf{S}_{\mathbf{s},\ell} + \mathbf{S}_{\mathbf{f},\ell})\mathbf{D}_\ell \vec{\psi}^{(y)} + \vec{Q}_\ell, \quad \ell = 0, 1, \ldots, P_t \tag{4.24}$$

is identical to Eq. 2.9 and is conducted independently for each PC coefficient. $\mathbf{M}_\ell$ and $\mathbf{D}_\ell$ are also identical to ℓ^{th} diagonal block of $\mathbf{M}$ and $\mathbf{D}$, respectively.

Given the potentially large number of coupled equations, computational effort should be reduced considerably by using a more powerful Krylov iterative method, which can be preconditioned using one of the iterative schemes mentioned above. This approach has been shown to be efficient for solving the two coupled Levermore-Pomraning equations, particularly in the atomic mix-diffusion limit [85]. For solution using a Krylov iterative method, each of the iterations listed above can then be rewritten in the form $\mathbf{A}\vec{x} = \vec{b}$ as

$$(\mathbf{I} - \mathbf{T})\vec{\psi} = \vec{q}. \tag{4.25}$$

4.2.2 The Stochastic Collocation Method

An alternative approach to calculating the PC coefficients is to use quadrature to evaluate the inner product in Eq. 4.8 directly

$$\hat{c}_j = \langle \chi, \Phi_j(\{\zeta_r\}) \rangle = \int_{\zeta_1} d\zeta_1 \cdots \int_{\zeta_K} d\zeta_K \cdot \chi(\zeta_1, \ldots, \zeta_K) \Phi_j(\zeta_1, \ldots, \zeta_K) w(\zeta_1, \ldots, \zeta_K)$$

$$\approx \sum_{m_1=1}^{M_1} w_{m_1} \cdots \sum_{m_K=1}^{M_K} w_{m_K} \chi(\zeta_{1,m_1}, \ldots, \zeta_{K,m_K}) \Phi_j(\zeta_{1,m_1}, \ldots, \zeta_{K,m_K}),$$

(4.26)

a procedure that has been termed the Stochastic Collocation Method (SCM). When $w(\{\zeta_r\})$ is the weight function for a set of classical orthogonal polynomials, as is the case with the gPC, a suitable Gaussian quadrature can be used.

4.3 Spectral Analysis of the SFEM Equations

4.3.1 Well-Posedness of the SFEM Equations

Since the flux, and possibly the cross section, have been replaced by an approximate expansion, the well-posedness of the systems of equations given in Eq. 4.17 must be examined. A similar analysis was given in [32] with more detailed proofs.

We begin by rewriting Eq. 4.17, where the source term has been omitted without loss of generality, in matrix form

$$\mu \frac{\partial \vec{\psi}}{\partial x} + B_{P+1} \vec{\psi} = \frac{c}{2} B_{P+1} \vec{\phi}$$

(4.27)

where $\vec{\psi} = [\psi_0, \psi_1, \ldots, \psi_P]^T$, $\vec{\phi} = [\phi_0, \phi_1, \ldots, \phi_P]^T$ and $B_{P+1} = [b_{\ell i}]$, $\ell, i = 0, 1, \ldots, P$, and assume that the PC expansion of the cross section is a linear function of the random variable—i.e., the cross section can be represented exactly by $\sigma =$

$\sigma_0 \Phi_0(\zeta) + \sigma_1 \Phi_1(\zeta)$. Then it can be shown that B_{P+1} has $(P + 1)$ real and distinct eigenvalues and eigenvectors [32]. Therefore, B_{P+1} can be diagonalized to form the matrix $\Lambda_{P+1} = S^{-1} B_{P+1} S$ whose diagonal entries are the eigenvalues of B_{P+1}, λ_i. The columns of the matrix S are then the eigenvectors of B_{P+1}. Eq. 4.27 can then be written as

$$\mu \frac{\partial \vec{U}}{\partial x} + \Lambda_{P+1} \vec{U} = \frac{c}{2} \Lambda_{P+1} \vec{V} \tag{4.28}$$

where $\vec{U} = S^{-1} \vec{\psi}$ and $\vec{V} = S^{-1} \vec{\phi}$. Since Λ_{P+1} is diagonal, Eq. 4.28 no longer represents a coupled system of equations, but a set of $(P + 1)$ independent equations:

$$\mu \frac{\partial U_i}{\partial x} + \lambda_i U_i = \frac{c}{2} \lambda_i V_i, \quad i = 0, \ldots, P. \tag{4.29}$$

Given that cross sections are only physically meaningful if they are non-negative, we conclude that the problem is well-posed if the eigenvalues of B_{P+1} are all non-negative—i.e., $\lambda_i \geq 0 \, \forall \, i$.

Distribution	Variance	Parameters	Support
Normal	1.0		$(-\infty, \infty)$
Log-Normal	1.0		$[0, \infty)$
Log-Normal	25.0		$[0, \infty)$
Gamma	1.0	$\alpha = 25, \beta = 0.2$	$[0, \infty)$
Gamma	5.0	$\alpha = 5, \beta = 1$	$[0, \infty)$
Beta	1.0	$\alpha = 11, \beta = 11$	$[0, 10]$
Beta	5.0	$\alpha = 5, \beta = 2$	$[0, 15]$
Uniform	1.0		$[5 - \sqrt{3}, 5 + \sqrt{3}]$
Uniform	5.0		$[5 - \sqrt{15}, 5 + \sqrt{15}]$

Table 4.3: Test Case Parameters

A series test cases, which are used throughout this thesis, were selected to represent a variety of different distributions all with mean $\langle \sigma \rangle = 5.0$ cm^{-1}. These distributions are shown in Fig. 4.1 and their particulars are delineated in Table 4.3. For the gamma, beta and uniform distributions, the various parameters and support were selected in such a way as to achieve the desired shape, mean and variance.

:
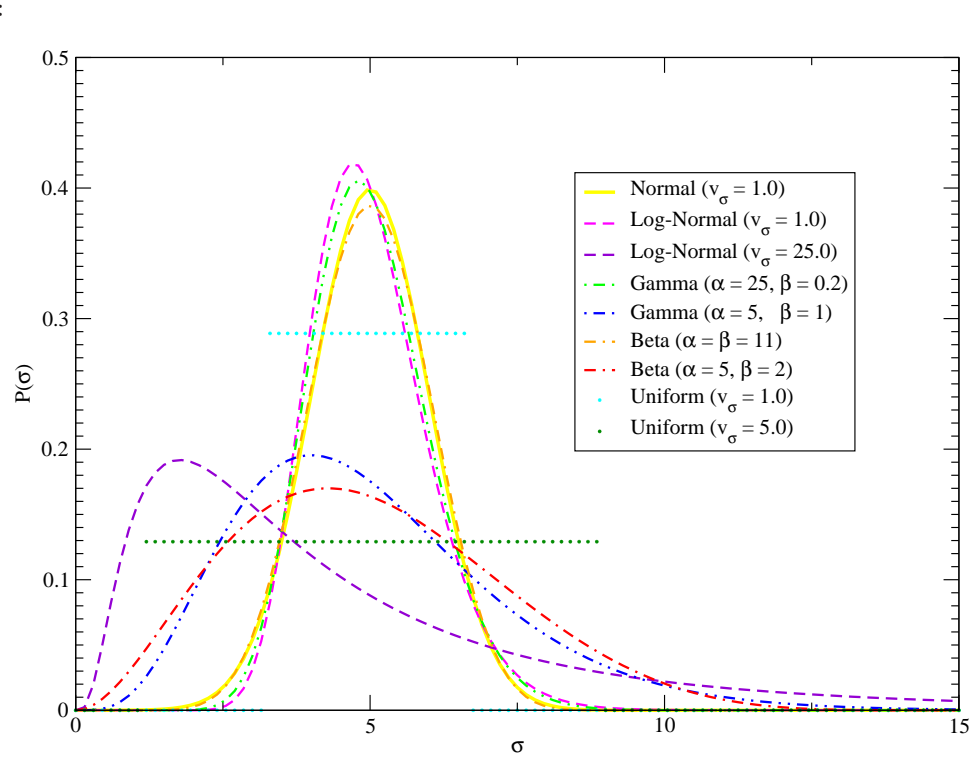
Figure 4.1: Plot of Test Case Total Cross Section Distributions for SFEM

The minimum values of λ are plotted in Fig. 4.2. As can be seen, the larger the PC order, the smaller the minimum eigenvalue. Also, for a particular distribution, larger variances lead to smaller minimum eigenvalues. This is particularly noticeable for the normal distribution where for $v_\sigma = 25$, the eigenvalue falls sharply to zero for P = 1 and is negative past that point. For $v_\sigma = 1$, the minimum eigenvalue is only positive up to P = 9, and for $v_\sigma = 0.25$, the eigenvalue does not fall below zero until P = 31. Thus, for the normal distribution, it is reasonable to conclude that there is always some PC order beyond which the SFEM solution will become ill-posed. This is not a failure of the method itself, but rather the result of representing strictly non-negative cross sections with a distribution that allows for negative numbers. For the other three distributions, the plots level out at some positive value and, since

:
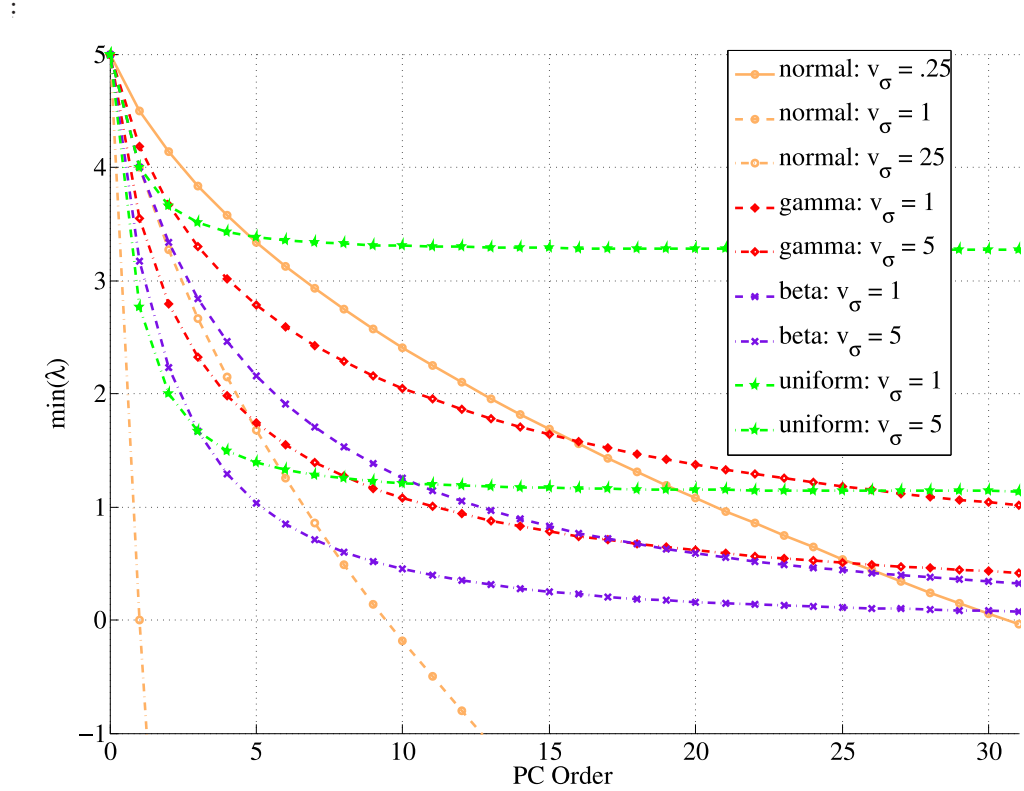
Figure 4.2: Plot of the Minimum Eigenvalues of Each Distribution

their support is strictly positive in the cases selected, it can be assumed that they do not ever fall below zero and therefore always form a well-posed systems of equations.

It was also observed that for an optimal gPC expansion and when $M = (P + 1)$, where M is the number of SCM quadrature points, the number of negative eigenvalues of B_{P+1} corresponds to the number of negative abscissas produced by the corresponding Gauss quadrature set used for SCM. Furthermore, $\lambda_i = \sigma_i$, where λ_i is the ith eigenvalue of B_{P+1} and σ_i is the ith SCM quadrature abscissa. This can be seen in Table 4.4, which lists σ_i and λ_i for various SCM quadrature and PC orders for two different quadrature sets their optimal gPC chaoses: The normal distribution with $\langle \sigma \rangle = 5.0$ cm and $v_\sigma = 1.0$ cm^{-2} represented using Hermite chaos and the beta distribution with $\alpha = \beta = 11$ defined on the interval $[-5, 15]$ represented

Distribution	M	$\sigma_i, i = 1 \dots M$
	P	$\lambda_i, i = 1 \dots P+1$
Normal	2	$\{6, 4\}$
	1	$\{6, 4\}$
	4	$\{7.33441421833900, 5.74196378430270, 4.25803621569730, 2.66558578166100\}$
	3	$\{7.33441421833898, 5.74196378430273, 4.25803621569727, 2.66558578166102\}$
	8	$\{9.14454718612590, 7.80248586128750, 6.63651904243510, 5.53907981135140,$ $4.46092018864860, 3.36348095756490, 2.19751413871250, 0.85545281387411\}$
	7	$\{9.14454718612588, 7.80248586128754, 6.63651904243510, 5.53907981135137,$ $4.46092018864862, 3.36348095756489, 2.19751413871246, 0.85545281387411\}$
	16	$\{11.63087819839300, 10.47222570594900, 9.49295530252000, 8.60087362417150,$ $7.76024504763070, 6.95198034571630, 6.16382910055500, 5.38676060450060,$ $4.61323939549940, 3.83617089944500, 3.04801965428370, 2.23975495236930,$ $1.39912637582850, 0.507044697479990, -0.472225705949340, -1.63087819839310\}$
	15	$\{11.63087819839313, 10.47222570594933, 9.49295530252000, 8.60087362417155,$ $7.76024504763071, 6.95198034571632, 6.16382910055496, 5.38676060450055,$ $4.61323939549943, 3.83617089944504, 3.04801965428367, 2.23975495236930,$ $1.39912637582845, 0.507044697479990, -0.47222570594934, -1.63087819839312\}$
Beta $\alpha = \beta = 11$ [-5,15]	2	$\{7, 3\}$
	1	$\{7, 3\}$
	4	$\{9.31664814502680, 6.43394698801960, 3.56605301198040, 0.68335185497321\}$
	3	$\{9.31664814502678, 6.43394698801964, 3.56605301198036, 0.68335185497321\}$
	8	$\{11.59435131344900, 9.77702630514080, 7.90204392629330, 5.97384144517530,$ $4.02615855482470, 2.09795607370670, 0.22297369485925, -1.59435131344940\}$
	7	$\{11.59435131344938, 9.77702630514074, 7.90204392629336, 5.97384144517534,$ $4.02615855482466, 2.09795607370666, 0.22297369485925, -1.59435131344939\}$
	16	$\{13.34601040970200, 12.42262779386900, 11.43457261997400, 10.37475412641600,$ $9.25081306863260, 8.07471734486130, 6.86037616324450, 5.62273311241410,$ $4.37726688758590, 3.13962383675550, 1.92528265513870, 0.74918693136744,$ $-0.37475412641636, -1.43457261997410, -2.42262779386870, -3.34601040970160\}$
	15	$\{13.34601040970155, 12.42262779386867, 11.43457261997414, 10.37475412641636,$ $9.25081306863256, 8.07471734486133, 6.86037616324449, 5.62273311241412,$ $4.37726688758588, 3.13962383675552, 1.92528265513867, 0.74918693136744,$ $-0.37475412641636, -1.43457261997414, -2.42262779386866, -3.34601040970156\}$

Table 4.4: Quadrature Abscissas for SCM and Eigenvalues of B_{P+1} for SFEM

using Jacobi chaos. As can be seen, both distributions have non-zero probabilities of negative cross sections, thus for large enough quadrature/PC order, at least one of the quadrature abscissas and eigenvalues of B_{P+1} become negative.

Since $\lambda_i = \sigma_i$, it follows that U_i and V_i in Eq. 4.29 are in fact the angular and scalar fluxes computed when σ_i is used as the cross section in the deterministic transport equation. Furthermore, since $\vec{\psi} = S\vec{U}$ and the elements of ψ are the PC coefficients of the angular flux,

$$\psi_p = \frac{\langle \psi \Phi_p \rangle}{\langle \Phi_p^2 \rangle},$$

multiplying the p$^{\text{th}}$ row of S, $S(p,:)$, by $\vec{U}$ must perform the quadrature summation

$$\psi_p = S(p,:)\vec{U} = \frac{1}{\langle \Phi_p^2 \rangle} \sum_{i=1}^{M} w_i \Phi_p(\zeta_i) U_i.$$

While this is hardly a rigorous proof, it would seem to indicate that SFEM and SCM are in fact *equivalent* when $M = (P+1)$. This result would also seem to confirm that the non-zero probability of negative cross sections is responsible for the ill-posedness of SFEM for the Gaussian distribution (and other distributions without positive support). While it is possible to truncate the distribution when SCM is used by ignoring terms, there is no clear way to do this in the SFEM equations, therefore they become unstable.

4.3.2 Spectral Radii of the Operators

The convergence of the iterative schemes presented above are analyzed using Fourier analysis. This is accomplished by taking the spectral Fourier transform of Eq. 4.17 with the discrete ordinates approximation in angle

$$\mu_n ik\bar{\psi}_{n,\ell} + \sum_{p=0}^{P} b_{\ell p}\bar{\psi}_{n,p} = \frac{c}{2}\sum_{p=0}^{P} b_{\ell p}\bar{\phi}_p + \bar{q}_\ell, \quad \ell = 0, 1, \ldots, P, \tag{4.30}$$

where the Fourier transforms of a function, f, and its derivative, $\frac{\partial f_{n,\ell}(x)}{\partial x}$, are defined to be

$$\bar{f}_{n,\ell}(k) = \int_{-\infty}^{\infty} e^{-ikx} f_{n,\ell}(x) dx$$

and

$$\frac{\overline{\partial f}_{n,\ell}}{\partial x}(k) = \int_{-\infty}^{\infty} e^{-ikx} f_{n,\ell}(x) dx = ik\bar{f}_{n,\ell}(k),$$

respectively. The spectral radius of a particular iterative scheme is then given by applying iteration indices and recasting Eq. 4.30 in the form

$$\vec{\bar{\Psi}}^{(m+1)} = \mathbf{G}(k)\vec{\bar{\Psi}}^{(m)} + \vec{q} \tag{4.31}$$

where (m) is the iteration index, $\vec{\Psi}$ is a vector of values $\bar{\psi}_{n,\ell}$, and $\mathbf{G}(k)$ is an iteration-specific coefficient matrix. The spectral radius, ρ, of $\mathbf{G}(k)$ offers valuable insight into the convergence of the iterative scheme; convergence is guaranteed if

$$\rho = \max_{-\infty < k < \infty} \|\mathbf{G}(k)\| < 1.$$

The spectral radii were computed for several different distributions represented by the optimal polynomial chaoses, with results shown below for various PC orders and scattering ratios, c.

In the previous analysis in Section 4.3.1, it was predicted that for the normal distribution with $\langle \sigma \rangle = 5.0$ cm^{-1} and $v_\sigma = 1.0$ cm^{-2}, the solution is only physical up to a PC order of 9. This is once again clearly demonstrated by the spectral radii of the Inexact Block Gauss-Seidel and Inexact Block Jacobi methods shown in Fig. 4.3, which are greater than unity for P > 9. Also shown are the spectral radii for $v_\sigma = 0.25$ and $v_\sigma = 25.0$ cm^{-2}. For the smaller variance case, it is expected that the spectral radius will exceed unity for P > 30, thus in this plot, where the P $\leq$ 15, all spectral radii are less than unity. For the larger variance, the spectral radius is greater than one for all PC orders greater than zero, which is the deterministic case, also as predicted. Fig. 4.4 shows spectral radii for the log-normal distribution for $v_\sigma = 1.0$ and $v_\sigma = 25.0$ cm^{-2}. The IBJ iteration is non-convergent when P > 1 for the larger variance, and the spectral radius rapidly approaches unity for the smaller variance when P > 6. The spectral radius of the IBGS iteration is convergent in all cases, however.

Figs. 4.5, 4.6 and 4.7(a) show spectral radii for the gamma, beta and uniform distributions for $v_\sigma = 1$ cm^{-2} and $v_\sigma = 5$ cm^{-2}, $c = 0.5$, and the optimal Laguerre, Jacobi and Legendre Chaos expansions, respectively. As predicted, for these three distributions there are no issues with convergence when the optimal gPC expansion is used. In general, it can be stated that smaller scattering ratios and cross section variances result in more rapid convergence of the SFEM solution. Also, IBGS should

always converge more rapidly than IBJ for serial computation. Fig. 4.7(b) shows the spectral radius of the SFEM equations when non-optimal Hermite chaos is used to model a uniform cross section. As can be seen, the spectral radii do not converge monotonically with PC order as they do when Legendre chaos is used, and the spectral radius exceeds unity for P > 8 for $v_\sigma = 1$ and for P = 6 and P > 8 for $v_\sigma = 5$. This is due to the same phenomenon encountered when Hermite chaos was used to represent the Gaussian distribution—it allows for negative cross sections that are unphysical and therefore destabilize the numerical system.

:
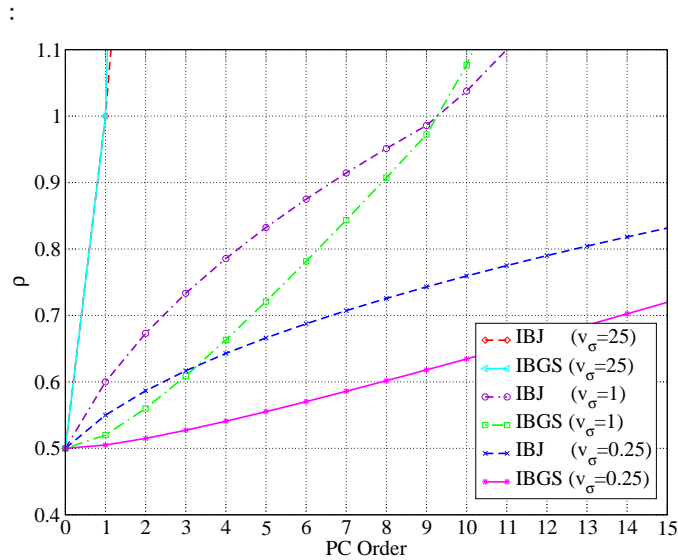
Figure 4.3: Spectral Radii vs. PC order: Hermite Chaos expansion of the Normal Distribution ($\langle\sigma\rangle = 5.0$ cm^{-1})

:
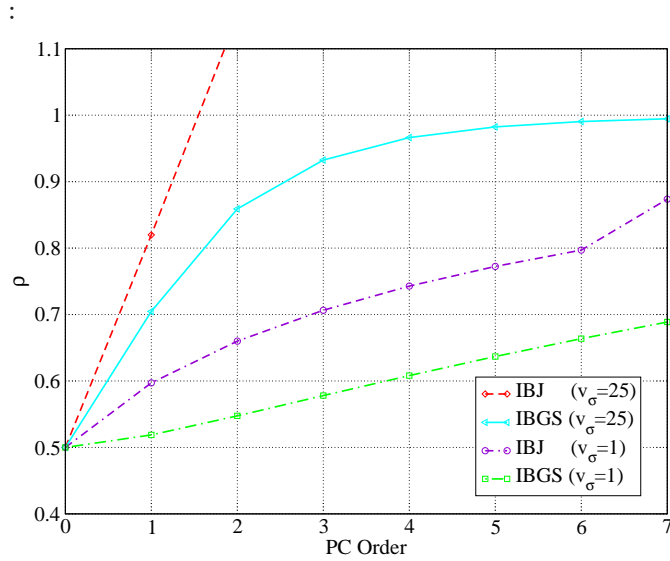
Figure 4.4: Spectral Radii vs. PC order: Hermite Chaos expansion of the Log-Normal Distribution ($\langle\sigma\rangle = 5.0$ cm^{-1}, $c = 0.5$)

:
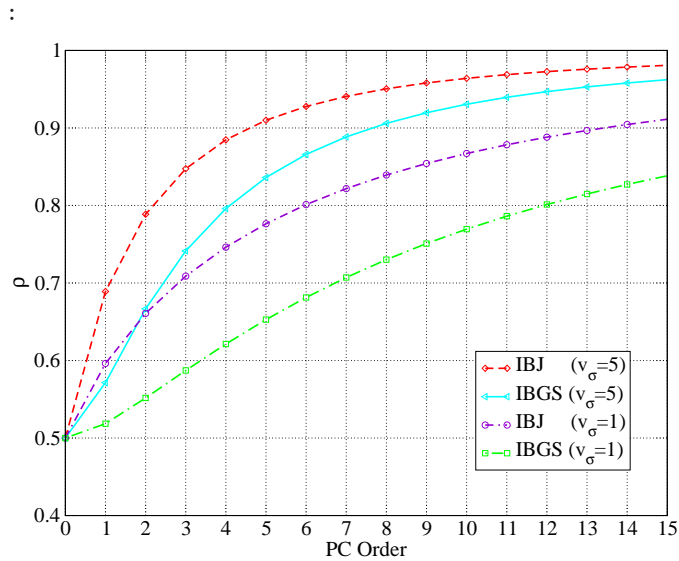
Figure 4.5: Spectral Radii vs. PC order: Laguerre Chaos expansion of the Gamma Distribution ($\langle\sigma\rangle = 5.0$ cm^{-1}, $c = 0.5$)

:
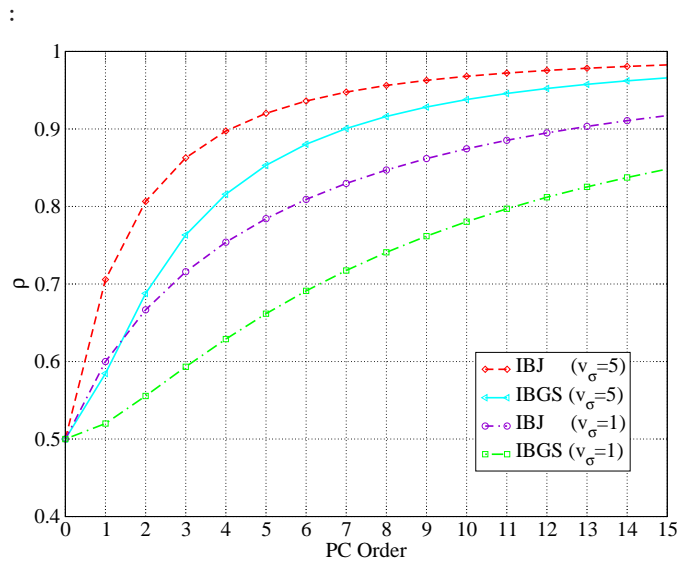
Figure 4.6: Spectral Radii vs. PC order: Jacobi Chaos expansion of the Beta Distribution ($\langle\sigma\rangle = 5.0$ cm^{-1}, $c = 0.5$)

:

(a) Legendre Chaos Expansion

:
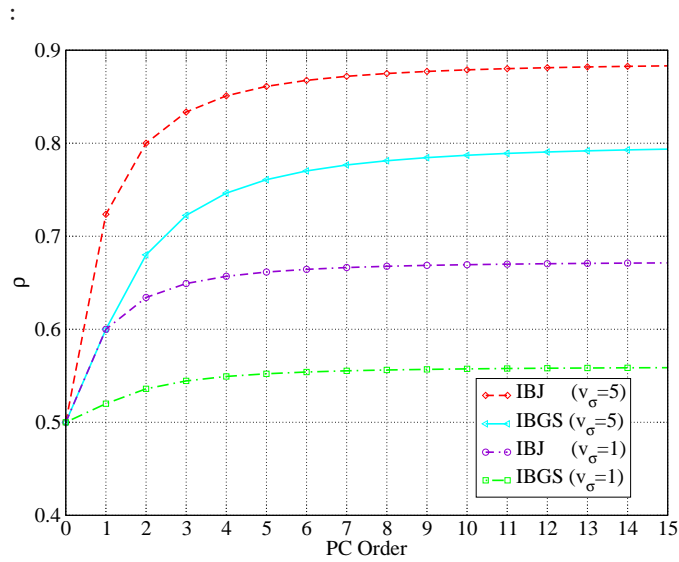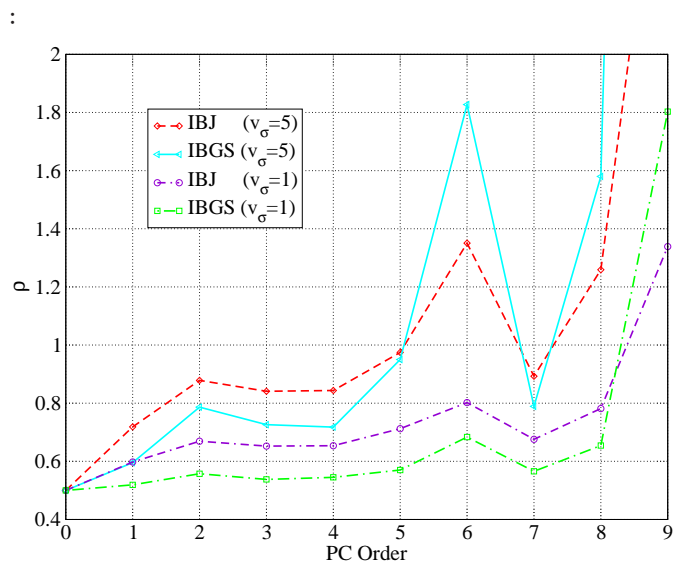
(b) Hermite Chaos Expansion

Figure 4.7: Spectral Radii vs. PC order: Uniform Distribution ($\langle\sigma\rangle = 5.0$ cm^{-1}, $c = 0.5$)

65

4.3.3 Eigenvalue Spectra of the Operators

The spectral radius of the operator $\mathbf{A}$ in the matrix equation $\mathbf{A}\vec{x} = \vec{b}$ can say much about the behavior of Krylov iterative method employed to solve it. The matrix equation takes the form

$$(\mathbf{I} - \mathbf{T})\vec{\psi} = \vec{q}, \tag{4.32}$$

for which the $\mathbf{T}$ matrices are given in Table 4.2. Therefore in this section, the eigenvalue spectra of the operators $(\mathbf{I} - \mathbf{T})$ are explored for the IBGS and IBJ iterations. Fig. 4.8 shows the eigenvalue spectra of the IBGS and IBJ for the Hermite chaos expansion of the normal cross section, with the imaginary part of the eigenvalue plotted vs. the real part, for $\langle \sigma \rangle = 5.0$ cm^{-1} and $v_\sigma = 1.0$ cm^{-2} for $c = 0.5$ and $c = 0.99$. As can be seen, the spectra are more tightly clustered around one for smaller PC orders and become more spread out as the order increases. The clusters also spread out as the material becomes more diffusive. This indicates that a Krylov iterative method will converge more rapidly for smaller PC orders and less diffusive materials. When P = 15, for which physically meaningful solutions do not exist and for which the spectral radii for the simple operators are larger than unity, the eigenvalue cluster is not only large, but also surrounds the origin in all cases. This indicates that the operator may be singular, or extremely close to singular, in which case GMRES is not likely to converge. Because the problem has been shown to be ill-posed, this result is not surprising.

In Figs. 4.9, 4.10, 4.11 and 4.12(a), eigenvalue spectra are shown for $c = 0.5$ for optimal gPC expansions of the log-normal, gamma, beta and uniform cross sections. Two different variances are shown in each case, and in general it can be concluded that larger PC orders and variances lead to eigenvalue clusters with larger radii and terms that sit extremely close to the origin. Although the plots are not shown, for larger scattering ratios the spectra have larger radii and are more spread out as was

observed in Fig. 4.8. Also shown in Fig. 4.12(b) is the eigenvalue spectrum for the uniform cross section represented using Hermite chaos. For the IBGS iteration, the spectra are similar in every case except P = 7 and $v_\sigma = 5$ for which the Hermite chaos cluster is larger. For the IBJ iteration, the spectra are similar in all cases. The P = 15 spectrum is not shown for Hermite chaos because the cluster is very large and numerical system clearly unstable for the same reasons that the spectral radius exceeds unity.
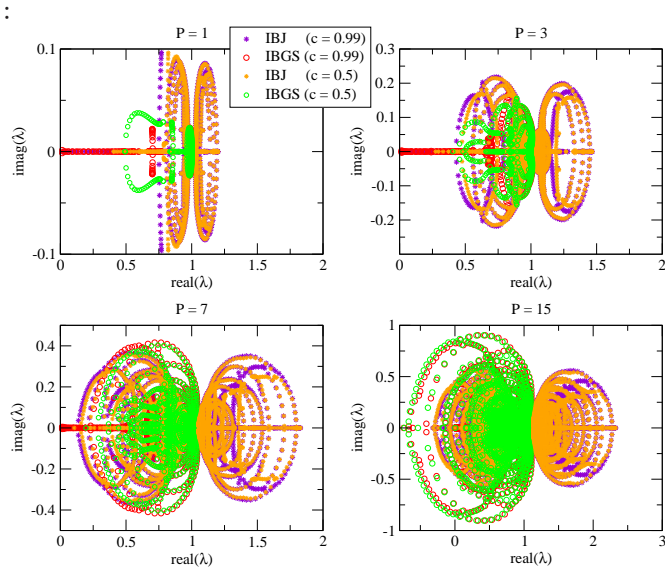
Figure 4.8: Eigenvalue spectrum for various PC orders: Hermite Chaos expansion of the Normal Distribution ($\langle\sigma\rangle = 5.0$ cm^{-1}, $v_\sigma = 1.0$ cm^{-2})
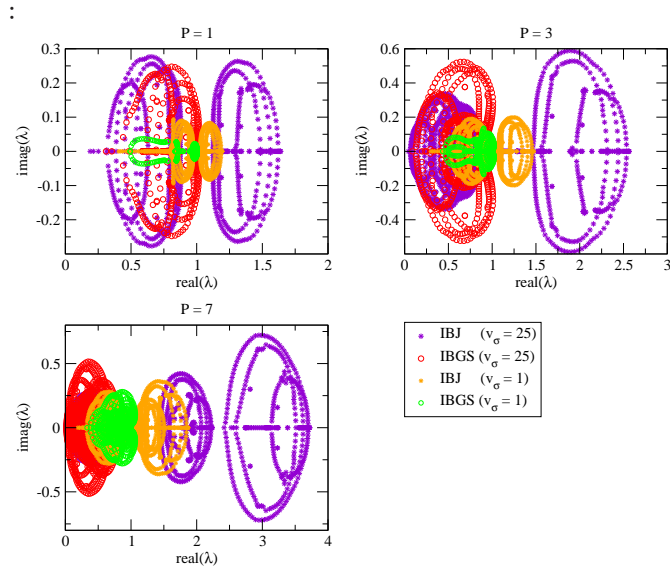
Figure 4.9: Eigenvalue spectrum for various PC orders: Hermite Chaos expansion of the Log-Normal Distribution ($\langle\sigma\rangle = 5.0$ cm^{-1}, $c = 0.5$)
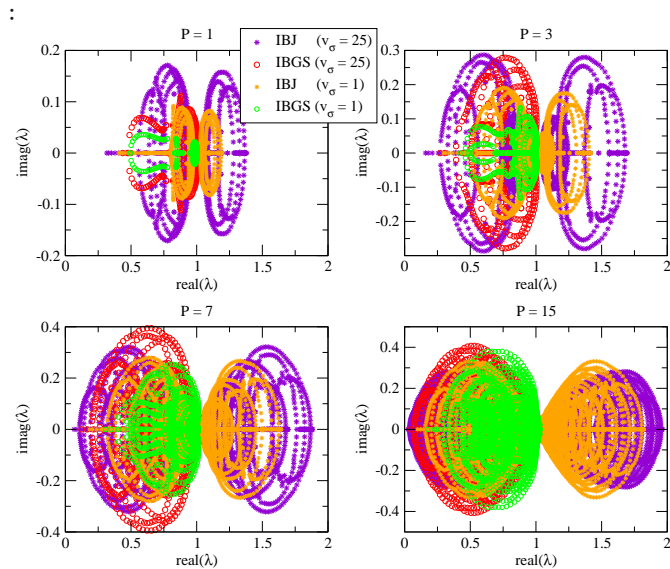
Figure 4.10: Eigenvalue spectrum for various PC orders: Laguerre Chaos expansion of the Gamma Distribution ($\langle\sigma\rangle = 5.0$ cm^{-1}, $c = 0.5$)
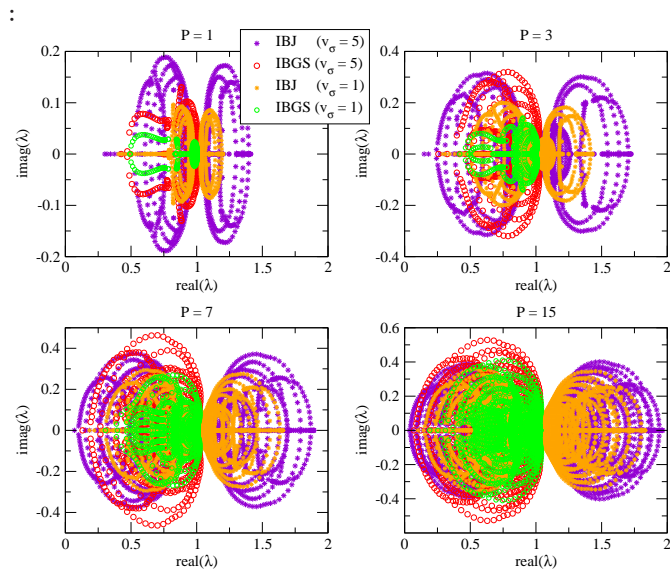
Figure 4.11: Eigenvalue spectrum for various PC orders: Jacobi Chaos expansion of the Beta Distribution ($\langle \sigma \rangle = 5.0$ cm^{-1}, $c = 0.5$)

(a) Legendre Chaos Expansion

(b) Hermite Chaos Expansion

Figure 4.12: Eigenvalue spectrum for various PC orders: Uniform Distribution ($\langle \sigma \rangle = 5.0$ cm^{-1}, $c = 0.5$)

Chapter 5

The Polynomial Chaos Expansion: Numerical Results

An extensive numerical study was conducted in order to test the convergence of the PC expansion and to compare the accuracy and computational efficiency of the SCM and SFEM solution methods. In Section 5.1, the convergence of the optimal gPC expansion is explored for each of the test cases delineated in Table 4.3. Results computed using both the SCM and the SFEM are shown and compared. Non-optimal Hermite chaos is also used to represent a uniform random variable in order to compare convergence with Legendre chaos. In Section 5.2, higher-order PC coefficients of the scalar flux are shown for several of the test cases. Section 5.3 shows similar results for the KL expansion, comparing the SCM with the SFEM. And finally, in Section 5.4, the computational efficiency of the SCM and SFEM are compared for these test cases.

5.1 Accuracy and Convergence of the PC Expansion for Various Random Variables

5.1.1 Optimal gPC Expansions

Figs. 5.1 to 5.10 show flux profiles and flux pdfs at various material depths for cross sections that are random variables of the normal, log-normal, gamma, beta and uniform varieties. In all cases, the mean cross section is $\langle \sigma \rangle = 5$ cm^{-1} and the cross sections are represented exactly using their corresponding random variables. In the flux profile graphs, M indicates the number of SCM quadrature point used, P indicates the order of PC expansion used in the SFEM and the number in parentheses indicates the number of Monte Carlo realizations required to achieve a relative sample standard deviation of 1% for the flux. In the flux pdf graphs, PC indicates the order of the PC expansion used to reconstruct the pdf. The pdf of the flux is defined to be

$$
\begin{aligned}
P(\phi) &= \int_{\zeta_{min}}^{\zeta_{max}} d\zeta \, \delta[\phi - \sum a_p \Phi_p(\zeta)] P(\zeta) \\
&= \frac{1}{2\pi} \int_{-\infty}^{\infty} dk \, e^{-ik\phi} \int_{\zeta_{min}}^{\zeta_{max}} d\zeta \, e^{ik \sum a_p \Phi_p(\zeta)} P(\zeta)
\end{aligned}
\tag{5.1}
$$

where $\zeta \in [\zeta_{min} \, \zeta_{max}]$ is the random variable with pdf $P(\zeta)$. However, the integral in Eq. 5.1 generally cannot be computed analytically, therefore the pdfs shown below were generated by sampling the random variable 10^6 times, computing the flux from its PC expansionusing this value, and tabulating the values to generate the histograms shown.

In Fig. 5.1, the flux as given by Gauss-Hermite quadrature and Hermite chaos is shown for the normal distribution for a variance of 1.0 cm^{-2} and scattering ratios of $c = 0.5$ and $c = 0.99$. There are several items of note:

1. As can been seen in Fig. 5.1(a) and as predicted by the analysis, it is not

possible to attain SFEM solutions for P = 15 and P = 31, although P = 7 is not sufficient to characterize the standard deviation. Once again, this is not a failure of Hermite chaos itself but rather a by-product of representing a strictly non-negative quantity as a normal random variable, thereby admitting negative values. Gauss-Hermite quadrature also struggles with negativities, producing 7 and 2 negative abscissas for M = 32 and M = 16, respectively, as indicated by the usable number of SCM quadrature points given in parentheses. These negative abscissas are discarded, so the distribution being sampled from is in fact not a true Gaussian, but a Gaussian truncated at zero so that it is only semi-infinite in scope. The quadrature weights are not renormalized, as perhaps they should be, but the sum of the weights in the quadrature set is 0.99999986890290 for M = 16 and 0.99999990884086 for M = 32 when 2 and 7 quadrature points are discarded, respectively. These sums are so close to unity, thus their exclusion does not profoundly impact the solution.

2. As c approaches unity—i.e., as the material becomes more diffusive—fewer PC terms are required to obtain an accurate solution. As can be seen in Fig. 5.2, the flux pdf is essentially normal near the incident edge in both cases, but becomes increasingly skewed as the beam penetrates the slab for $c = 0.5$, while it becomes only slightly skewed for $c = 0.99$. It would therefore be expected that a larger PC order would be required to converge $c = 0.5$ than $c = 0.99$ since the flux is clearly a higher-order function of the normal random variable used to represent it.

3. As the material becomes more diffusive, the deterministic solution computed for the mean cross section is a more accurate approximation of the true mean flux, although the deterministic solution always underestimates the mean value. This can once again be explained by turning to the pdf plot (Fig. 5.2), which shows that the flux profile is far narrower in the diffusive material, indicat-

ing that the solution is not as profoundly affected by the stochasticity of the material.

4. It requires higher SCM quadrature and PC orders to accurately represent the second moment of the flux, hence the standard deviation, than the mean. This indicates that the second moment of the flux is a higher-order function of the random variable than the first moment. It is expected that obtaining accurate higher-order moments of the flux would demand even higher SCM quadrature and PC orders.

5. The SCM with a SCM quadrature order of M is equivalent to the SFEM with a flux PC expansion of order $P = (M-1)$. The SCM computes the ith moment of the flux using a quadrature approximation of the integral $\langle \phi \Phi_i \rangle$ (see Eq. 4.26). Representing the flux using a PC order of P assumes that the flux can be well-represented using a polynomial of order P in terms of the random variable, thus the integrand can be assumed to be a polynomial of degree no greater than 2P. A Gauss quadrature order of M will exactly integrate a polynomial of order $(2M-1)$ weighted by the appropriate weight function. For $P = (M-1)$, the maximum polynomial order of the integrand is $2P = (2M-2)$, thus the integral computed by quadrature is exact for each term in the PC expansion. If higher-order terms are computed using a Gauss-Hermite quadrature of order M, they will be inaccurate since the polynomial order exceeds the accuracy of the SCM quadrature order. It is interesting to note that while the lower order PC coefficients could be computed using lower order SCM quadratures, this approach is ultimately more time consuming because the Gauss-Hermite quadrature is not nested. Each SCM quadrature order therefore contains an entirely unique set of abscissas and corresponding transport solutions.

As can been seen in Fig. 5.1(a) and as predicted by the analysis, it is not possible to attain SFEM solutions for $P = 15$ and $P = 31$, although $P = 7$ is not sufficient

to characterize the standard deviation. Once again, this is not a failure of Hermite chaos itself but rather a by-product of representing a strictly non-negative quantity as a normal random variable, thereby admitting negative values. Gauss-Hermite quadrature also struggles with negativities, producing 7 and 2 negative abscissas for M = 32 and M = 16, respectively, as indicated by the usable number of SCM quadrature points given in parentheses. These negative abscissas are discarded, so the distribution being sampled from is in fact not a true Gaussian, but a Gaussian truncated at zero so that it is only semi-infinite in scope. The quadrature weights are not renormalized, as perhaps they should be, but the sum of the weights in the quadrature set is 0.99999986890290 for M = 16 and 0.99999990884086 for M = 32 when 2 and 7 quadrature points are discarded, respectively. These sums are so close to unity, leading us to conclude that their exclusion did not profoundly impact the solution.

The effect of diffusivity on the accuracy of the deterministic solution and the required number of quadrature points or PC terms holds regardless of the cross-section distribution, therefore for the remaining distributions, flux profiles are given for two different variances and $c = 0.5$, for which the stochasticity of the material has a large effect on the solution and the deterministic solution quite inaccurate. Fig. 5.3 shows flux profiles for a cross section that is a log-normal random variable, also represented using Hermite chaos and the SCM solution computed using Gauss-Hermite quadrature. As would be expected, the stochastic solution varies from the deterministic solution more drastically for larger variances and, accordingly, larger SCM quadrature and PC orders are required to converge the flux for larger variances. In this case, for instance, the mean flux is converged for M = 4 and P = 3 when $v_\sigma = 1.0$, while when $v_\sigma = 25.0$, the mean flux is converged for M = 8 and P = 7 terms are required. Also, the relative standard deviation in the flux is, in general, larger for larger standard deviations in the cross section. Finally, in comparing Figs. 5.1(a) and 5.3(a) for which the standard deviations and scattering ratios are the

same, it can be seen that for a normally distributed cross section, the mean flux varies more drastically from the deterministic solution than for a log-normally distributed cross section. Accordingly, the relative standard deviation in the flux is also larger. This effect is attributable to the fact that the normal distribution is infinite in scope while the log-normal distribution is only semi-infinite. This particular distribution also stands out from the others in that the chaos and quadrature used were designed for the normal distribution. Since the log-normal distribution can be represented exactly as a function of the normal distribution, no approximations are required, however it is no longer true that retaining the same number of terms in the SCM quadrature and PC approximations yields equivalent solutions.

In Figs. 5.5, 5.7 and 5.9, flux profiles are shown for variances of 1.0 and 5.0 cm^{-2} for the gamma, beta and uniform distributions. Many of the observations made above apply in each instance. In general, a Gauss quadrature order of M is equivalent to a PC order of $(M-1)$ when both methods are based on the orthogonal polynomial set corresponding to the shape of the cross section distribution—e.g., Gauss-Legendre quadrature and Legendre Chaos. Also, for larger variances, the flux converges more slowly as a function of SCM quadrature/PC order and varies more drastically from the deterministic solution.

Finally, in Fig. 5.11, the pdfs of the fluxes for various cross section distributions are shown for two different depths and variances. As can be seen, the shape of the cross section distribution has a profound effect upon the distribution of the solution—i.e., the flux. This is even true when $v_\sigma = 1.0$ for which the normal, log-normal, gamma and beta cross section distributions appear to be quite similar (see Fig. 4.1). This demonstrates the importance of faithfully representing the cross section distribution pdf, not just its mean and variance.

Normal Distribution: Hermite Chaos

$\vdots$

(a) $c = 0.5$

$\vdots$

(b) $c = 0.99$
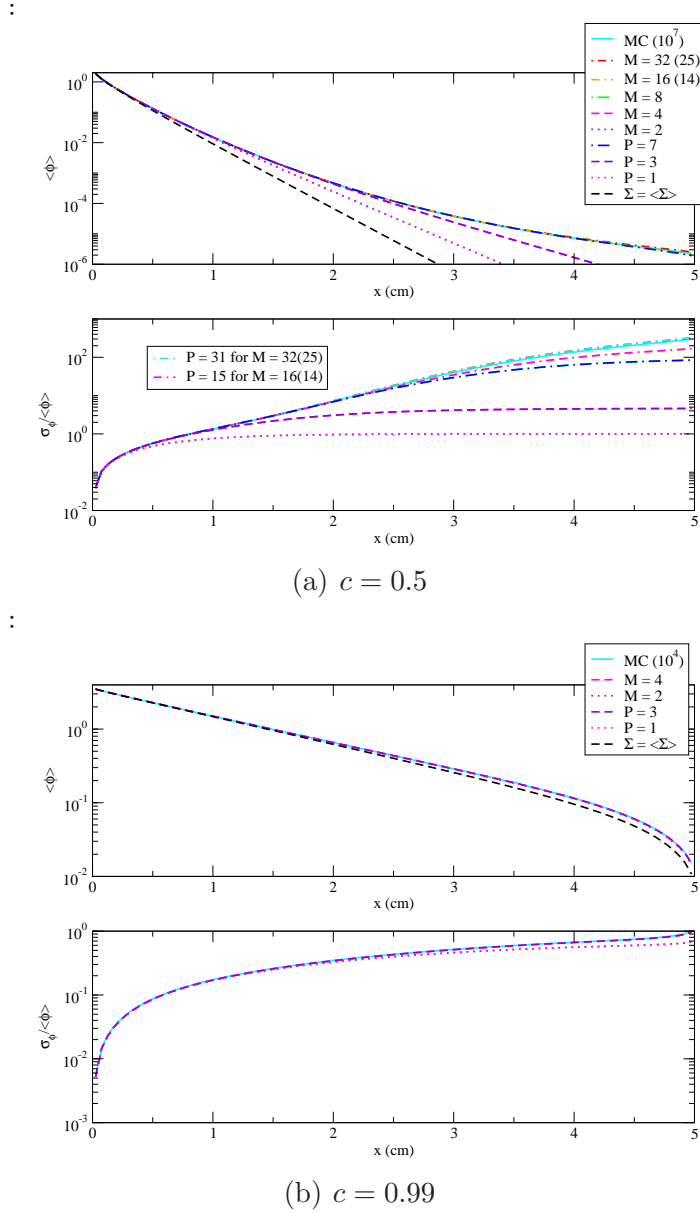
Figure 5.1: Scalar Flux: Hermite Chaos expansion of the Normal Distribution and Gauss-Hermite Quadrature ($\langle\sigma\rangle = 5.0$ cm^{-1}, $v_\sigma = 1.0$ cm^{-2})

⋮

(a) $c = 0.5$

⋮

(b) $c = 0.99$
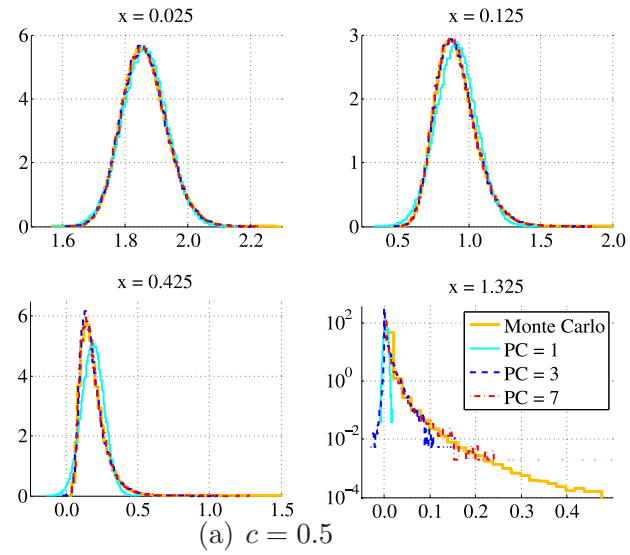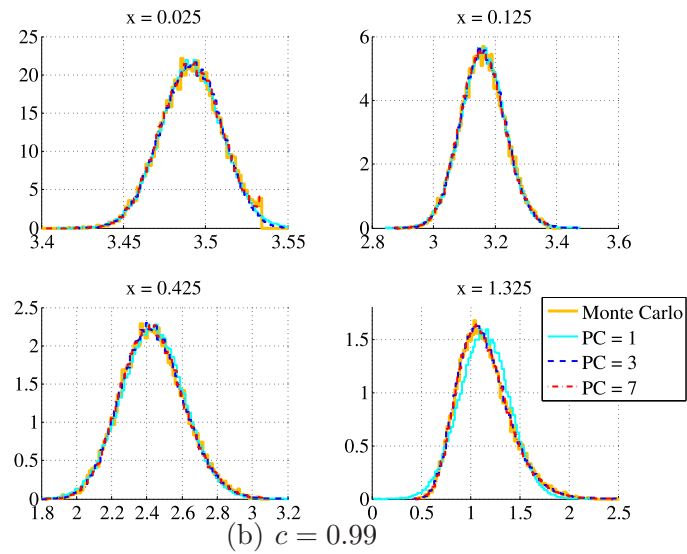
Figure 5.2: PDF of the Scalar Flux: Hermite Chaos expansion of the Normal Distribution ($\langle \sigma \rangle = 5.0$ cm^{-1}, $v_\sigma = 1.0$ cm^{-2})

Log-Normal Distribution: Hermite Chaos

:

(a) $v_\sigma = 1.0$ cm^{-2}

:
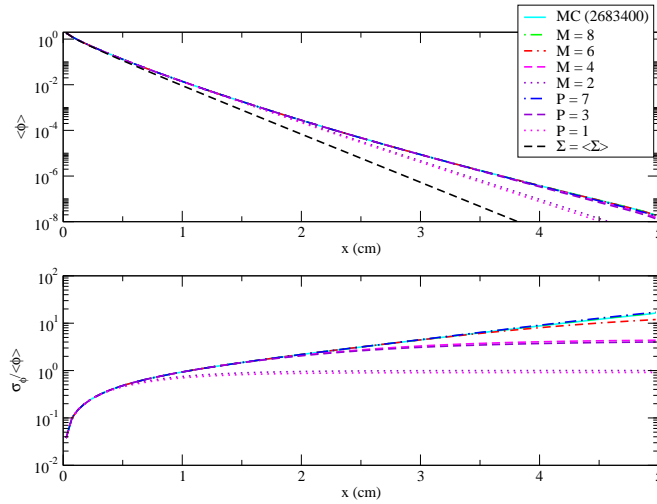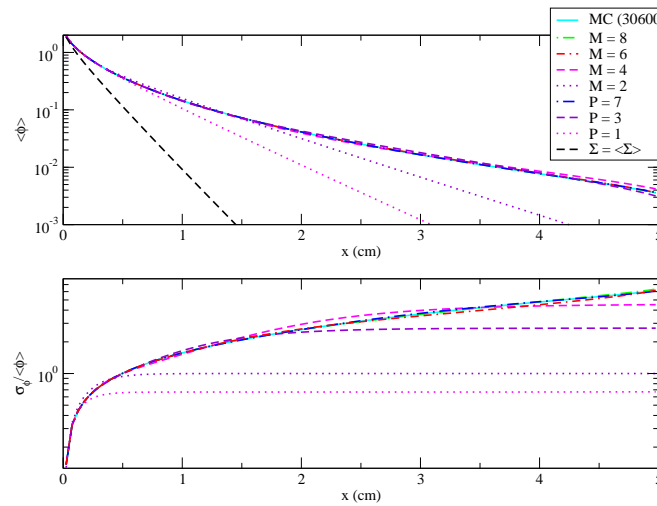
(b) $v_\sigma = 25.0$ cm^{-2}

Figure 5.3: Scalar Flux: Hermite Chaos expansion of the Log-Normal Distribution and Gauss-Hermite Quadrature ($\langle \sigma \rangle = 5.0$ cm^{-1}, $c = 0.5$)

:

(a) $v_\sigma = 1.0$ cm^{-2}

:

(b) $v_\sigma = 25.0$ cm^{-2}
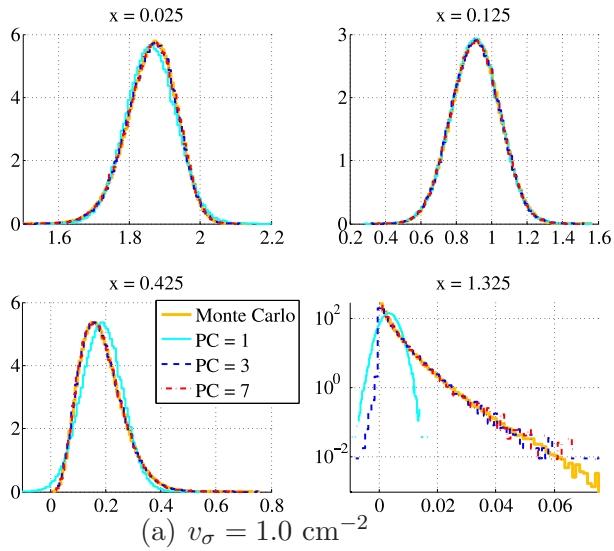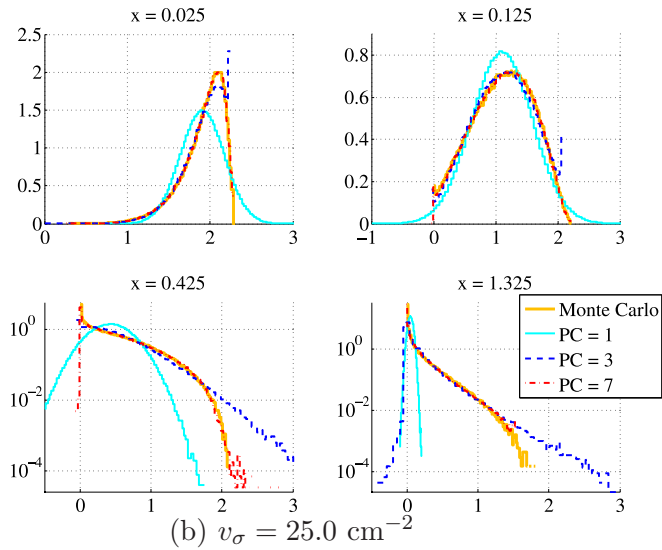
Figure 5.4: PDF of the Scalar Flux: Hermite Chaos expansion of the Log-Normal Distribution ($\langle\sigma\rangle = 5.0$ cm^{-1}, $c = 0.5$)

Gamma Distribution: Laguerre Chaos

(a) $v_\sigma = 1.0$ cm^{-2} ($\alpha = 25$, $\beta = 0.2$)

(b) $v_\sigma = 5.0$ cm^{-2} ($\alpha = 5$, $\beta = 1$)
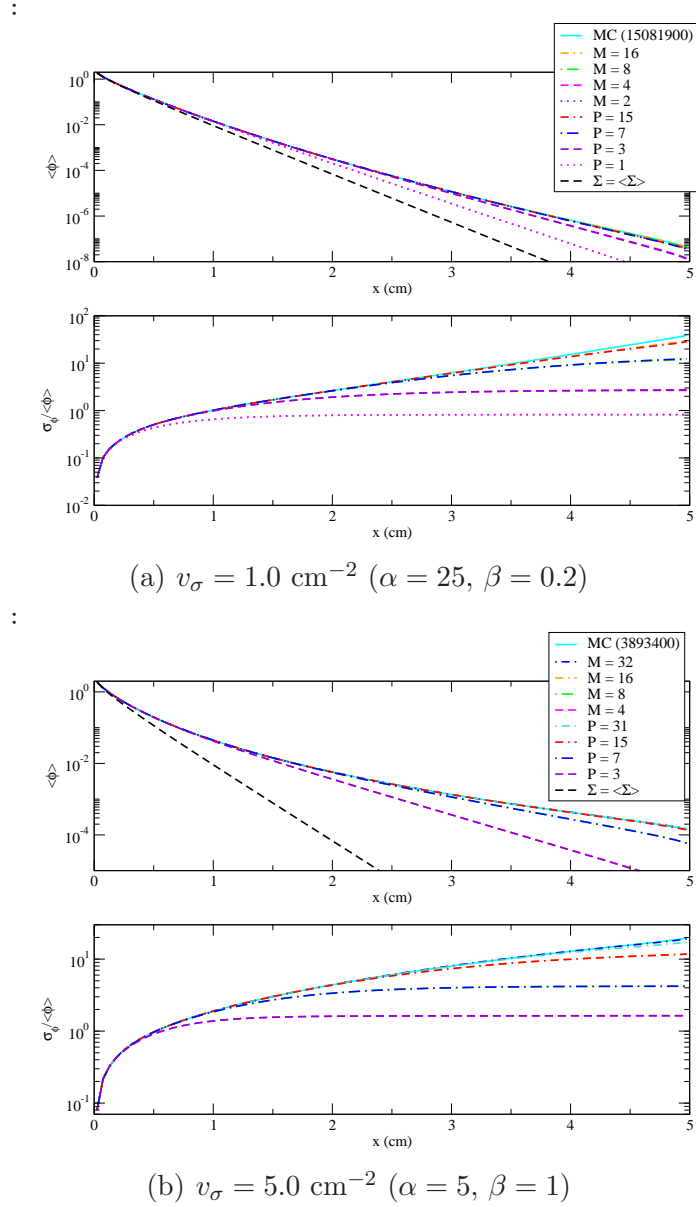
Figure 5.5: Scalar Flux: Laguerre Chaos expansion of the Gamma Distribution and Gauss-Laguerre Quadrature ($\langle\sigma\rangle = 5.0$ cm^{-1}, $c = 0.5$)

:

(a) $v_\sigma = 1.0$ cm^{-2} ($\alpha = 25$, $\beta = 0.2$)

:

(b) $v_\sigma = 5.0$ cm^{-2} ($\alpha = 5$, $\beta = 1$)
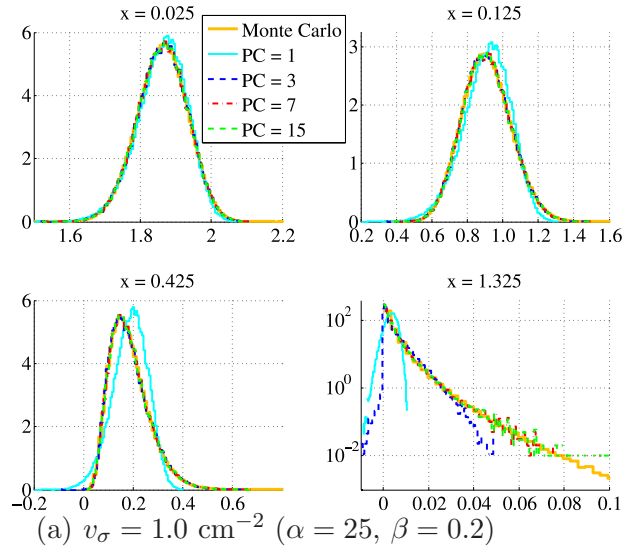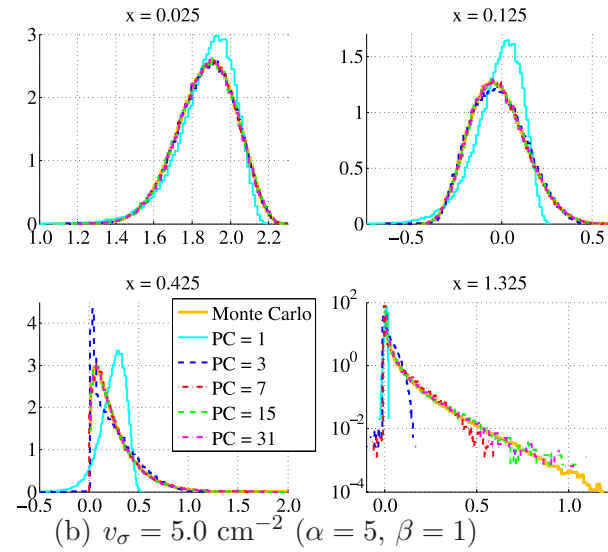
Figure 5.6: PDF of the Scalar Flux: Laguerre Chaos expansion of the Gamma Distribution ($\langle\sigma\rangle = 5.0$ cm^{-1}, $c = 0.5$)

Beta Distribution: Jacobi Chaos

:

(a) $v_\sigma = 1.0$ cm^{-2} ($\alpha = \beta = 11$, $\sigma \in (0, 10)$)

:

(b) $v_\sigma = 5.0$ cm^{-2} ($\alpha = 5$, $\beta = 2$, $\sigma \in (0, 15)$)
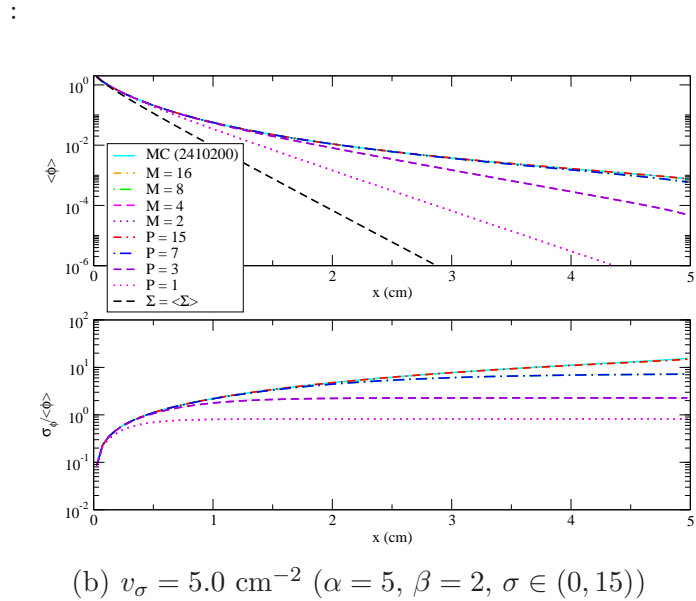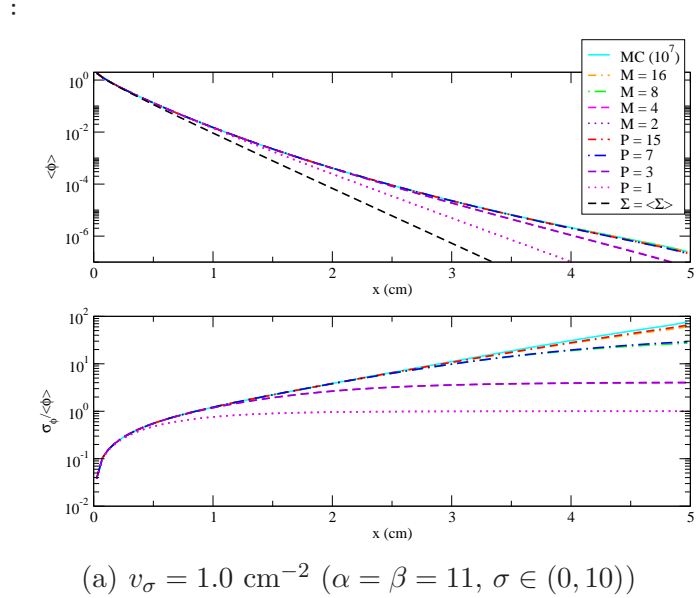
Figure 5.7: Scalar Flux: Jacobi Chaos expansion of the Beta Distribution and Gauss-Jacobi Quadrature ($\langle \sigma \rangle = 5.0$ cm^{-1}, $c = 0.5$)

:

(a) $v_\sigma = 1.0$ cm^{-2} $(\alpha = \beta = 11, \sigma \in (0, 10))$

:

(b) $v_\sigma = 5.0$ cm^{-2} $(\alpha = 5, \beta = 2, \sigma \in (0, 15))$
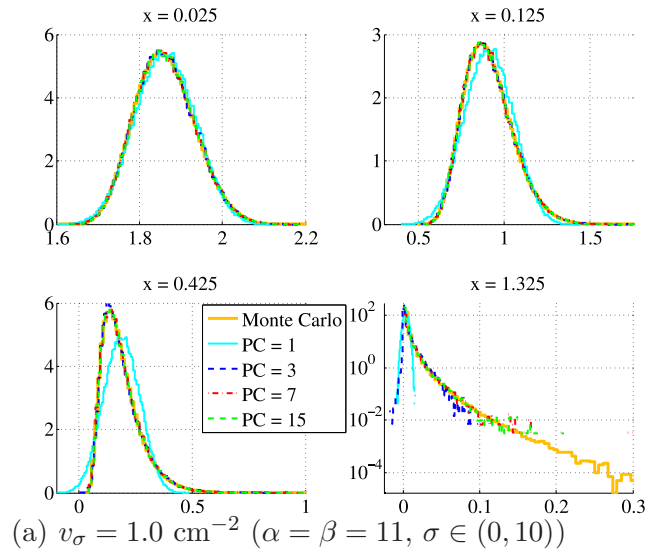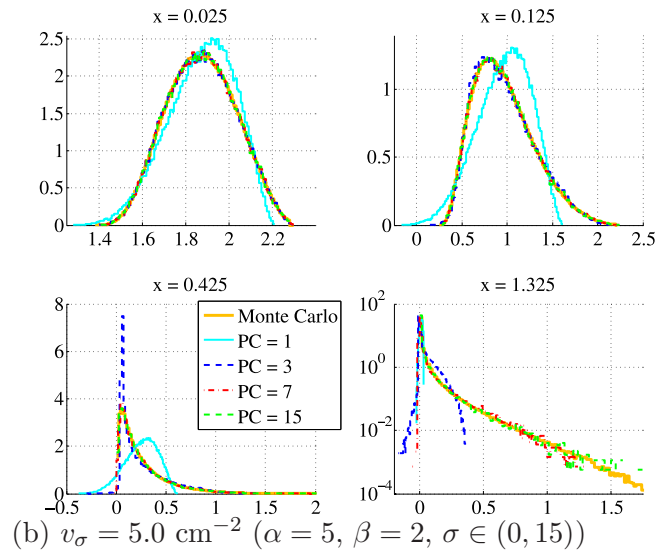
Figure 5.8: PDF of the Scalar Flux: Jacobi Chaos expansion of the Beta Distribution $(\langle\sigma\rangle = 5.0$ cm^{-1}, $c = 0.5)$

Uniform Distribution: Legendre Chaos

(a) $v_\sigma = 1.0$ cm^{-2} ($\sigma \in (3.2679, 6.7321)$)

(b) $v_\sigma = 5.0$ cm^{-2} ($\sigma \in (1.1270, 8.8730)$)
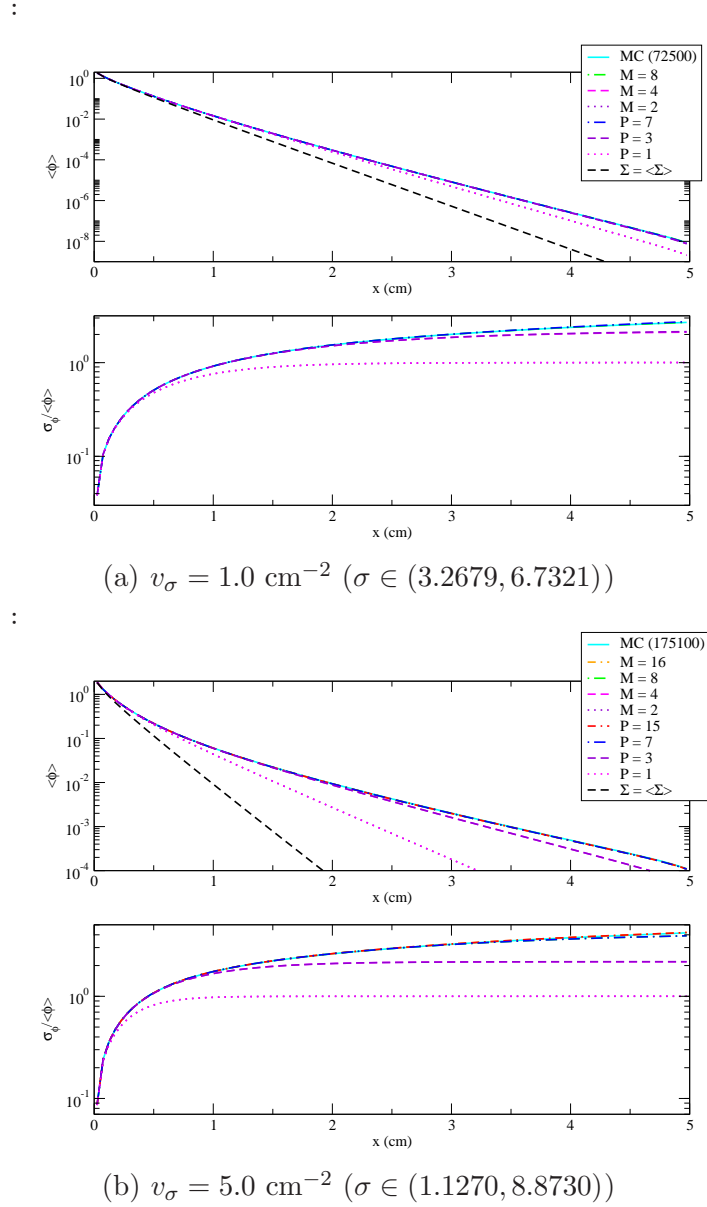
Figure 5.9: Scalar Flux: Legendre Chaos expansion of the Uniform Distribution and Gauss-Legendre Quadrature ($\langle\sigma\rangle = 5.0$ cm^{-1}, $c = 0.5$)

:

(a) $v_\sigma = 1.0$ cm^{-2} $(\sigma \in (3.2679, 6.7321))$

:
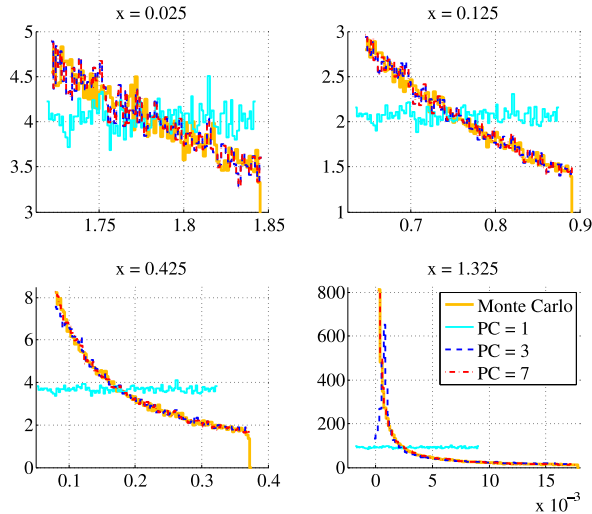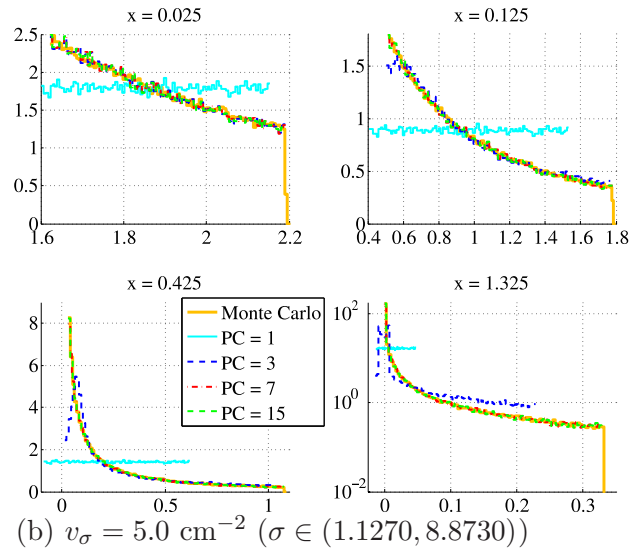
(b) $v_\sigma = 5.0$ cm^{-2} $(\sigma \in (1.1270, 8.8730))$

Figure 5.10: PDF of the Scalar Flux: Legendre Chaos expansion of the Uniform Distribution $(\langle\sigma\rangle = 5.0$ cm^{-1}, $c = 0.5)$

:

:

(a) $x = 0.025$ cm, $v_\sigma = 1.0$ cm^{-2}

(b) $x = 0.025$ cm, $v_\sigma = 5.0$ cm^{-2}

:

:

(c) $x = 0.425$ cm, $v_\sigma = 1.0$ cm^{-2}

(d) $x = 0.425$ cm, $v_\sigma = 5.0$ cm^{-2}
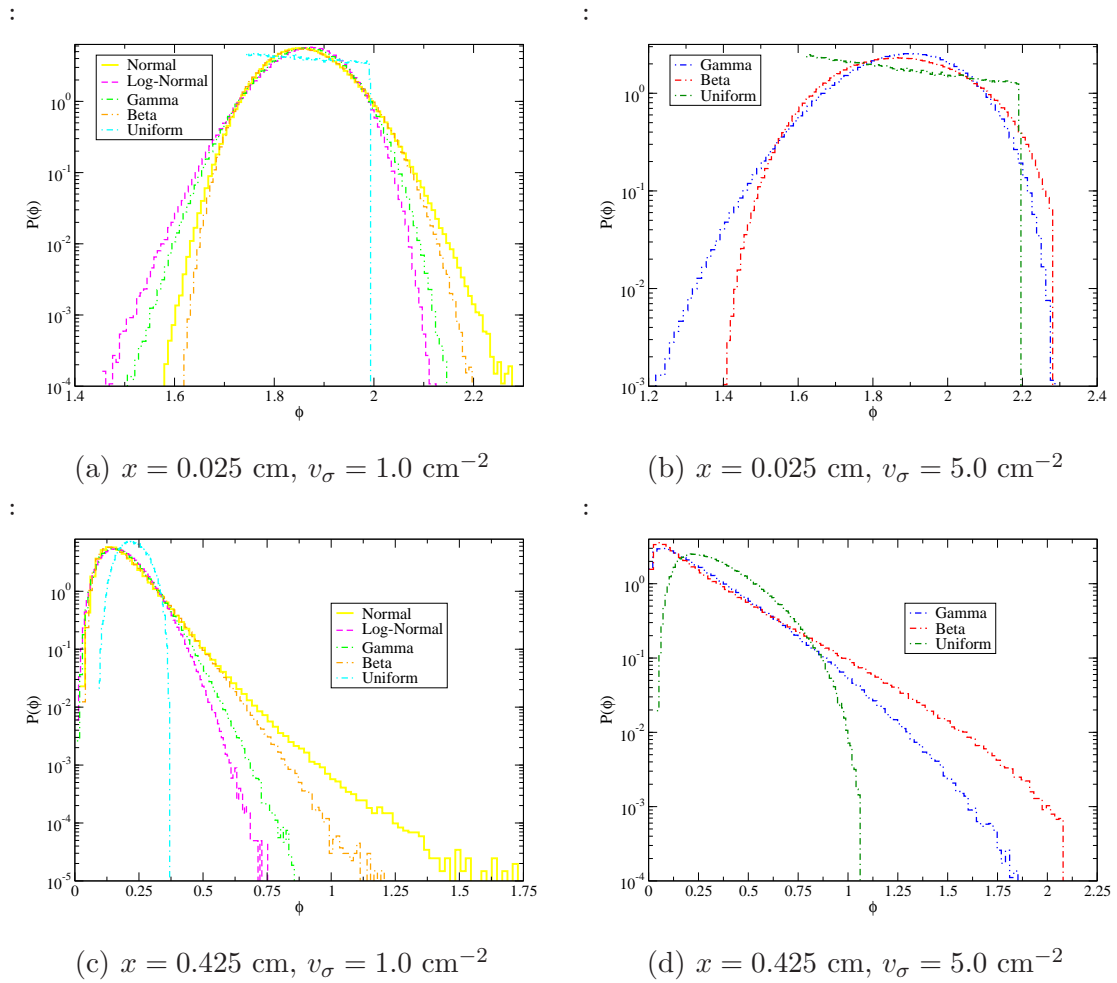
Figure 5.11: PDF of the Scalar Flux for Various Distributions ($\langle \sigma \rangle = 5.0$ cm^{-1}, $c = 0.5$)

5.1.2 Non-Optimal gPC Expansions

The uniform cross section was also represented using Hermite chaos using the methodology presented in Section 4.1.3. Fig. 5.12 shows the pdf of the cross section for $v_\sigma = 1.0$ cm^{-2} and $v_\sigma = 5.0$ cm^{-2} as a function of terms preserved in the PC expansion. As can be seen, the pdf generated using the PC expansion becomes more accurate as the PC order, P$_\sigma$, increases. However, a converged pdf of the cross section is not required in order for the SFEM to produce a converged solution, as can be seen in Fig. 5.13. For both variances, P $=$ P$_\sigma$ $= 7$ is sufficient to converge the flux and standard deviation. This is particularly interesting when $v_\sigma = 5.0$ since, when optimal Legendre chaos expansion is used to represent the cross section and the flux, P $= 15$ is required to converge the standard deviation. Although the cross section is not being represented exactly, a PC expansion in terms of the normal random variable is clearly better able to approximate the flux than a PC expansion in terms of a uniform random variable. In examining Figs. 5.11(b) and 5.11(d), it can be seen that the pdf of the flux is essentially uniform close to the incident boundary, but becomes a smoother function of ϕ as the beam penetrates the slab. It is not surprising, then, that a Hermite chaos expansion is better able to approximate the flux than a Legendre chaos expansion. It cannot be assumed, as often stated in the literature, that representing the cross section using an optimal gPC expansion is necessarily the most efficient option available.

⋮ ⋮

(a) $v_\sigma = 1.0$ cm$^2(\sigma \in (3.2679, 6.7321))$ (b) $v_\sigma = 5.0$ cm$^2(\sigma \in (1.1270, 8.8730))$
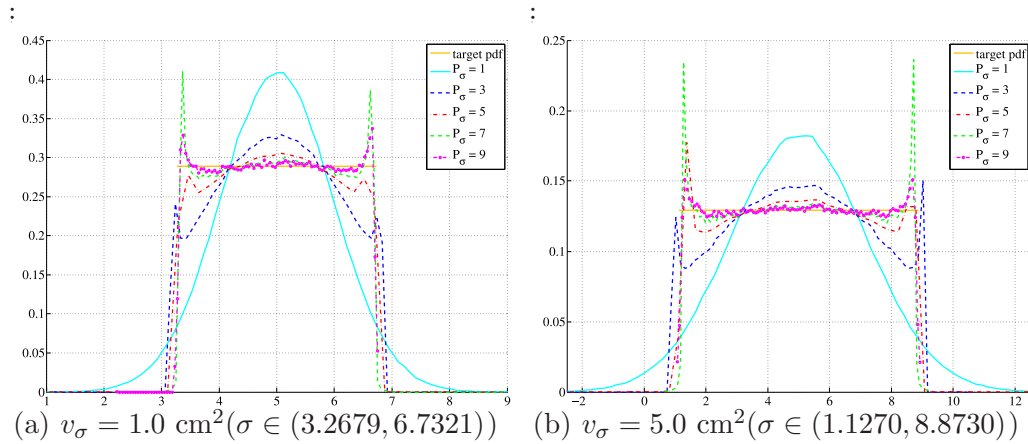
Figure 5.12: PDF of the Cross Section: Hermite Chaos Expansion of a Uniformly Distributed Cross Section ($\langle\sigma\rangle = 5.0$ cm^{-1})

⋮ ⋮

(a) $v_\sigma = 1.0$ cm$^2(\sigma \in (3.2679, 6.7321))$ (b) $v_\sigma = 5.0$ cm$^2(\sigma \in (1.1270, 8.8730))$
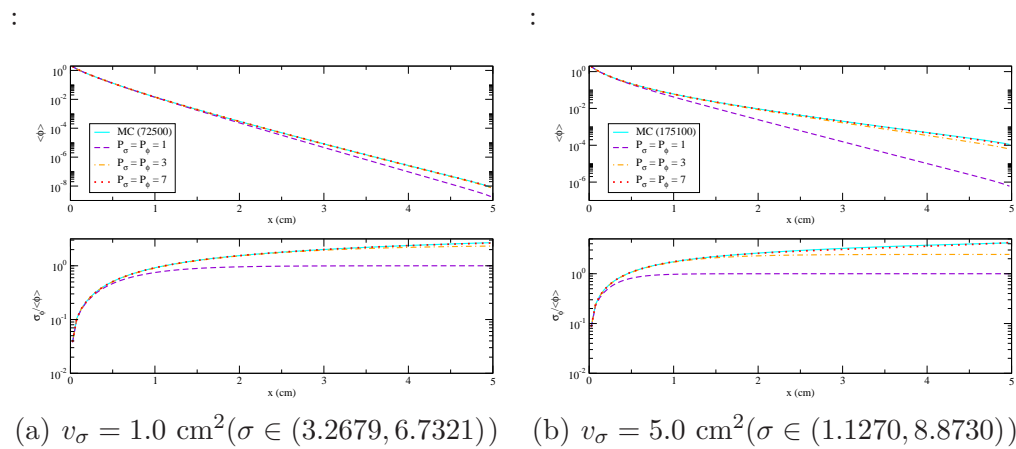
Figure 5.13: Scalar Flux: Hermite Chaos Expansion of a Uniformly Distributed Cross Section ($\langle\sigma\rangle = 5.0$ cm^{-1}, $c = 0.5$)

5.2   PC Coefficients of the Scalar Flux

Figs. 5.14, 5.15 and 5.16 show higher-order PC coefficients of the flux for several of the test cases. The mean (ϕ_0) is not shown because it is, in general, considerably larger than the other moments, is always positive and is shown in the previous section. Fig. 5.14 shows the PC moments of the flux for the normal distribution for two different scattering ratios. As can be seen, the higher-order moments are not always positive. Although negative fluxes are unphysical, this does not present a problem as long as the expansion itself remains positive. As can be seen, the coefficients get successively smaller, indicating that the series is converging. It is also interesting to note that while the coefficients are larger in magnitude for $c = 0.99$, they also fall to zero more quickly.

Fig. 5.15 shows the PC coefficents of the flux for the gamma distribution for two different variances. For the larger variance, the moments are larger indicating that the series is not converging as rapidly. As can be seen, the structure of the coefficients is quite different from those in the previous graph. In this case, all of the moments except for ϕ_1 start out negative at the incident boundary and, at some point, become positive. The magnitude of the minimum value (i.e., the most negative value) is on the same order as that of the maximum.

And finally, Fig. 5.16 shows the PC coefficents of the flux for the beta distribution for two different variances. Once again, the structure of the moments is quite different than those from the other two distributions. However, the moments are still larger when the variance is larger.

(a) $c = 0.5$ (M = 32)

(b) $c = 0.99$ (M = 4)
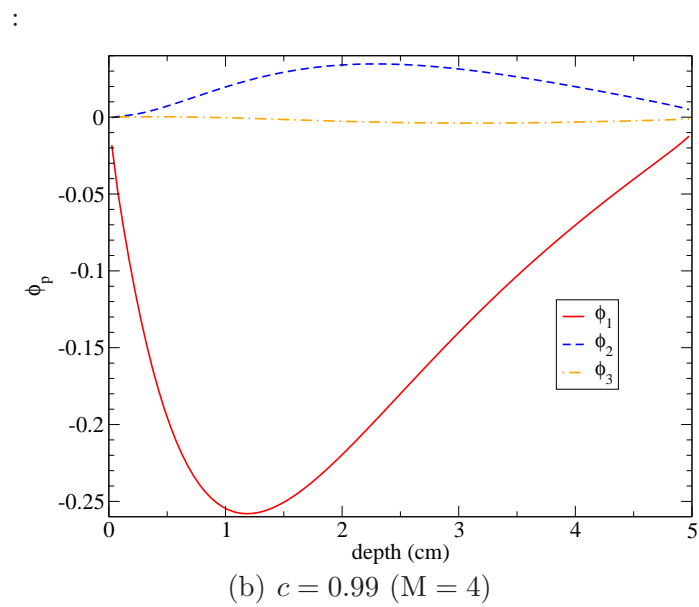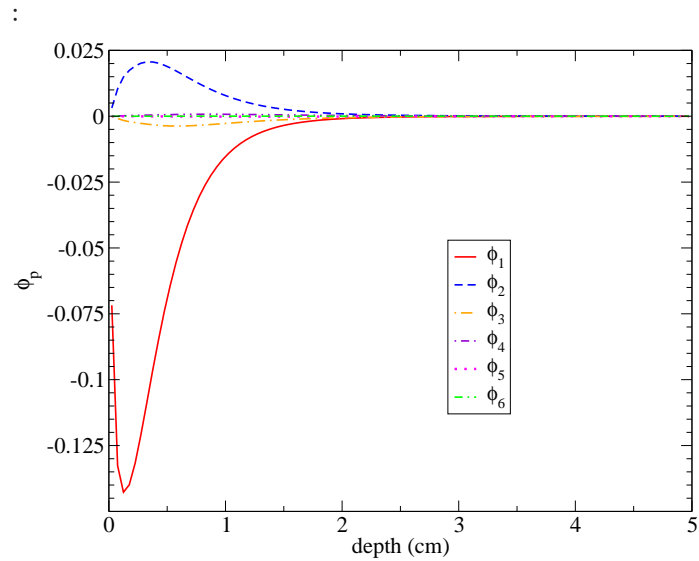
Figure 5.14: PC Coefficients of the Scalar Flux: Hermite Chaos expansion of the Normal Distribution ($\langle \sigma \rangle = 5.0$ cm^{-1}, $v_\sigma = 1.0$ cm^{-2})

:

(a) $v_\sigma = 1.0$ cm^{-2} ($\alpha = 25$, $\beta = 0.2$, M $= 16$)

:

(b) $v_\sigma = 5.0$ cm^{-2} ($\alpha = 5$, $\beta = 1$, M $= 32$)
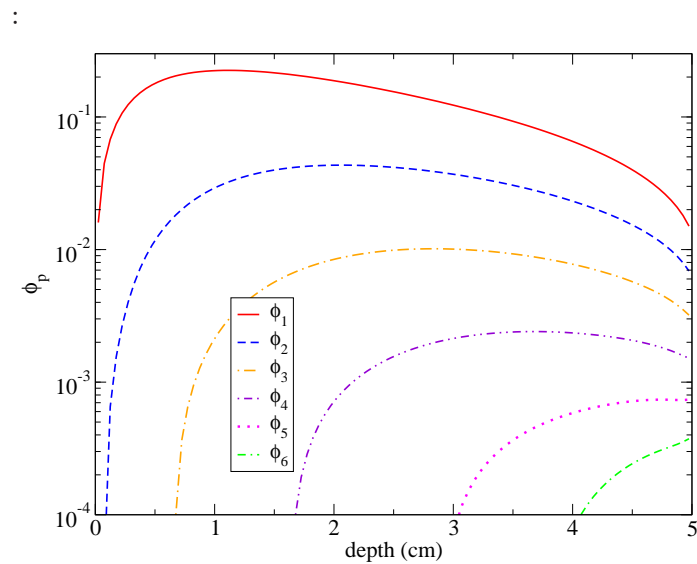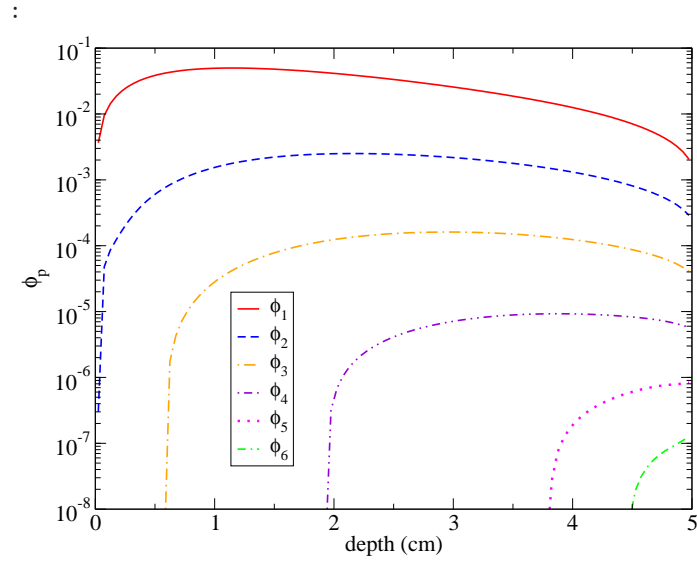
Figure 5.15: PC Coefficients of the Scalar Flux: Laguerre Chaos expansion of the Gamma Distribution ($\langle\sigma\rangle = 5.0$ cm^{-1}, $c = 0.5$)

:

(a) $v_\sigma = 1.0 \text{ cm}^{-2}$ ($\alpha = \beta = 11$, M = 16)

:

(b) $v_\sigma = 5.0 \text{ cm}^{-2}$ ($\alpha = 5$, $\beta = 2$, M = 16)
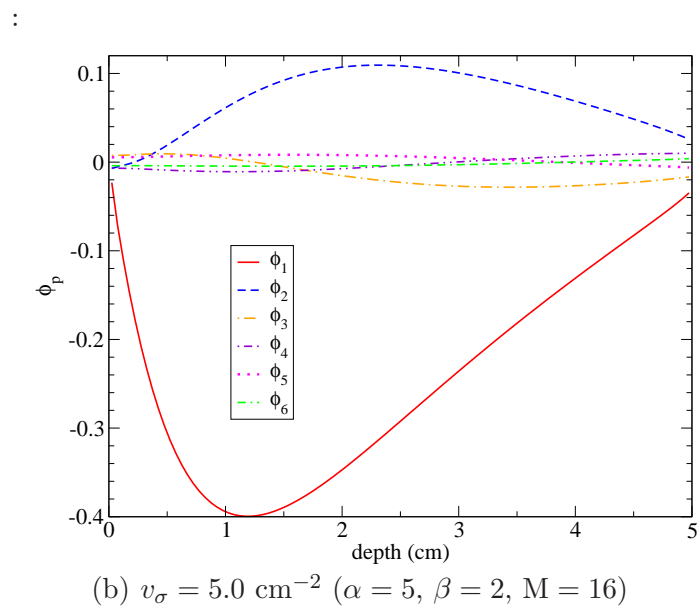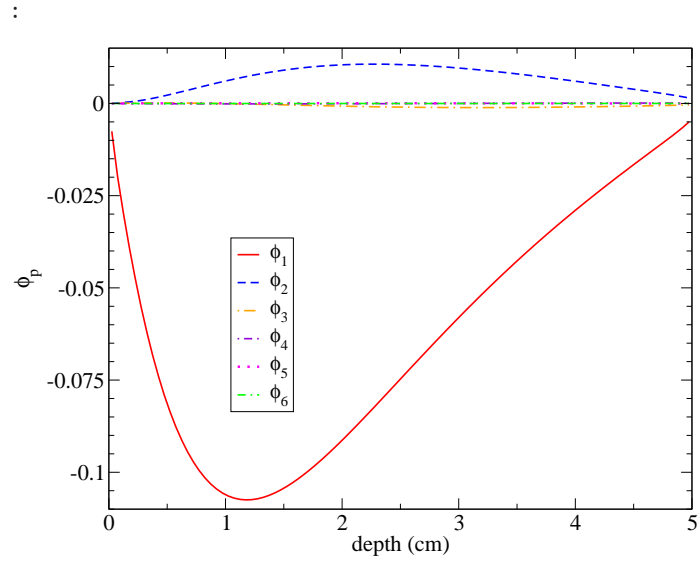
Figure 5.16: PC Coefficients of the Scalar Flux: Jacobi Chaos expansion of the Beta Distribution ($\langle\sigma\rangle = 5.0 \text{ cm}^{-1}$, $c = 0.5$)

5.3   Accuracy and Convergence of the PC Expansion for Gaussian Random Processes

Figs. 5.17 and 5.18 show fluxes and standard deviations for $c = 0.5$ and $c = 0.9$, respectively, computed using the SCM with quadrature order M and the SFEM for a maximum polynomial order of P and a KL order of 5. This translates to a PC order of $(P_t + 1) = \frac{(P+K)!}{P!K!}$ and a quadrature tensor product with M^K abscissas. In all cases, $\langle\sigma\rangle = 5.0$ cm^{-1}, $v_\sigma = 1.0$ cm^{-2}, $L = 5$ cm, $\lambda_c = 1$ cm, $N = 8$ and $I = 100$. As can be seen, once again the SCM with M $= (P + 1)$ is roughly equivalent to SFEM for a maximum polynomial order of P. There is some discrepancy between the two solutions, but it decreases as both solutions converge. Maximum polynomial orders of 5 and 3 are sufficient to converge the flux for $c = 0.5$ and $c = 0.9$, respectively, while maximum polynomial orders of 7 and 5 are necessary to converge the standard deviations.

.

(a) Scalar Flux

.
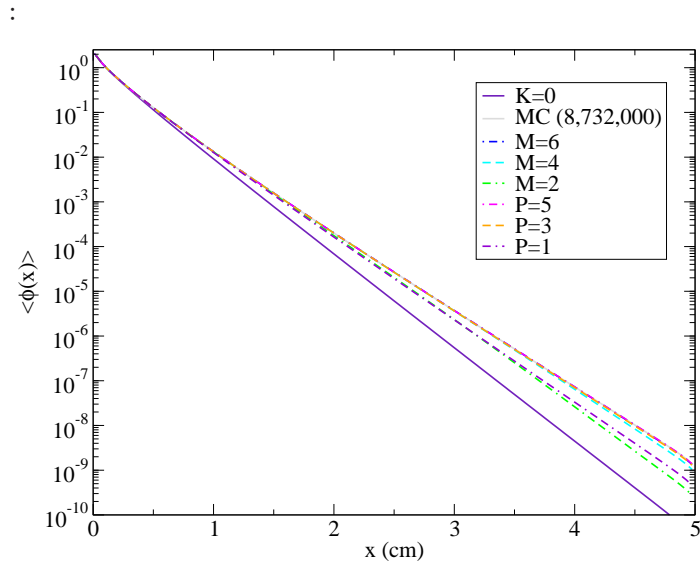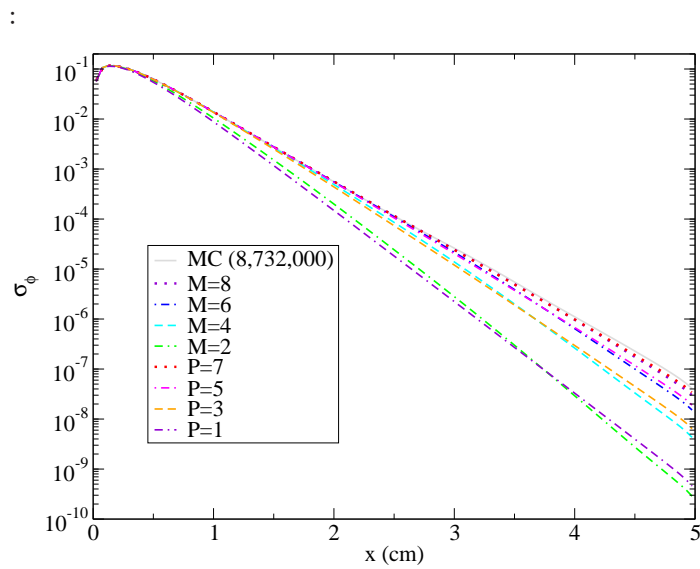
(b) Standard Deviation of the Scalar Flux

Figure 5.17: Normal Cross Section: Scalar Flux and its Standard Deviation for SFEM and SCM ($c = 0.5$)

:

(a) Scalar Flux

:
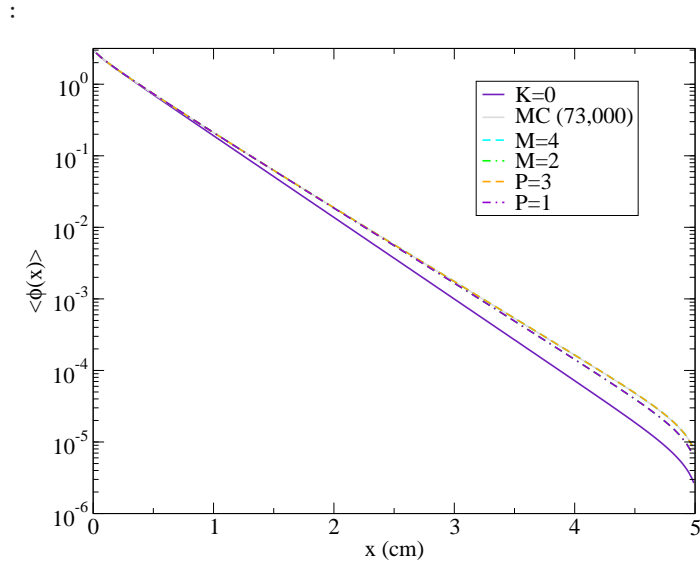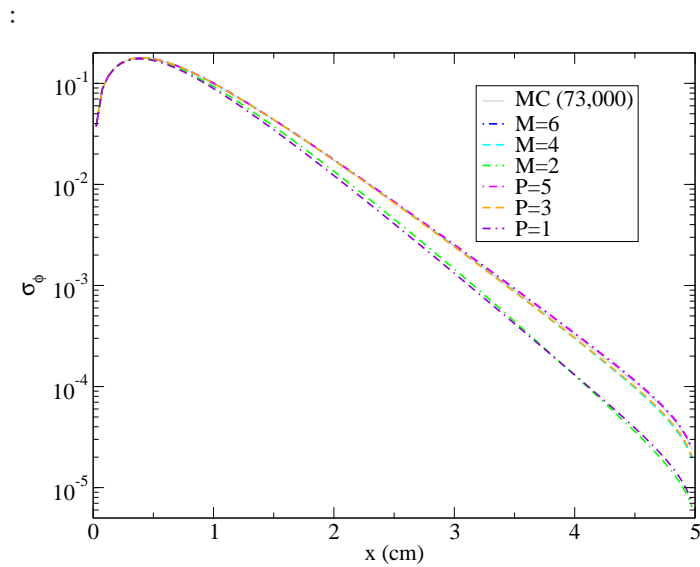
(b) Standard Deviation of the Scalar Flux

Figure 5.18: Normal Cross Section: Scalar Flux and its Standard Deviation for SFEM and SCM ($c = 0.9$)

5.4 Computational Efficiency of SFEM vs. SCM

5.4.1 Optimal gPC Expansions

Tables 5.1 through 5.4 show iteration counts and run times given as an average over 25 runs for $c = 0.5$ and $c = 0.99$ for each distribution. In each cell, the number on top is the result for SFEM and the number on the bottom is the result for SCM for a quadrature order of $M = (P + 1)$ and a PC order of P. For both methods, the iteration counts given are totals. Thus, for the SCM quadrature solution, the count is the total number of deterministic transport iterations for all quadrature abscissas. For the SFEM solution, the count is the total number of iterations for the coupled SFEM equations. Data is given for the IBGS scheme for Richardson, restarted GMRES with a restart of eight, and BiCGStab iterations. The GMRES restart parameter was chosen by testing different restarts on several of the test cases. A restart of eight was chosen because higher restart parameters did not drastically improve the speed of convergence, and it is desirable to keep the Krylov subspace as small as possible to conserve computer storage. There are several broad generalizations that can be made from the data:

- Larger iteration counts, hence larger run times, are required for larger scattering ratios, as expected in a transport setting when the material becomes more diffusive. For the SFEM, the iteration count also grows with the variance, and this effect increases with increasing PC order—i.e., for P = 1, there is only a difference of a few iterations between $v_\sigma = 1.0$ and $v_\sigma = 5.0$, but for P = 15, the iteration count is considerably larger for $v_\sigma = 5.0$ than $v_\sigma = 1.0$.

- As the SCM quadrature order doubles, the number of iterations, hence the run time, roughly doubles as well. This is due to the fact that for the deterministic solution, convergence is strongly influenced by the scattering ratio, which is

the same for the computation at each abscissa. This behavior can be observed in Figs. 4.8 through 4.12(a). As can be seen, the spectral radius for the IBGS iteration for a PC order of zero, which is in fact the spectral radius of the single deterministic equation, is roughly equal to the scattering ratio. Furthermore, the iteration count per quadrature point varies only slightly with quadrature order and variance—it is affected only by scattering ratio.

- Generally, as the number of terms in the PC expansion increases, the iteration count remains roughly constant when the variance is unity. However, the computational effort per iteration increases non-linearly with PC order, thus the run time more than doubles each time the PC order doubles. For larger variances and smaller scattering ratios, the iteration count increases more dramatically with PC order. This can be seen in the spectral analysis, where the spectral radius approaches unity more rapidly as a function of PC order when the variance is larger and exceeds unity for the normal distribution for P > 9.

- BiCGStab always requires the fewest iterations, followed by GMRES(8) and then Richardson iteration. Since each iterative method requires a different amount of computational effort, this does not mean that run times will follow the same trend, although generally they do.

- Although there are always fewer SFEM iterations than SCM iterations, each SFEM iteration involves inverting a much larger matrix, and is therefore more computationally intensive. Therefore, without exception, an M-term SCM quadrature solution always runs in a shorter time than an SFEM solution for P = (M − 1). Since these solutions are roughly equivalent, as shown in a previous section, SCM is shown to be the more efficient solution method *in these cases.*

In several cases, convergence was not achieved. For the normal distribution, when the PC order exceeds 9, the problem is no longer well-posed and the spectral radius of the matrix for Richardson iteration exceeds unity. The matrices for the Krylov iterations are also non-singular in that case. Consequently, for these PC orders, Richardson iteration is unstable, with the solution increasing without bound, restarted GMRES stagnates and BiCGStab breaks down numerically. Also, for the log-normal distribution, when P = 7, BiCGStab breaks down numerically for unknown reasons, but Richardson iteration and restarted GMRES converge without incident, albeit an extraordinarily large number of iterations. The spectral analysis reveals that the spectral radius is essentially unity and the eigenvalue cluster is quite large in this case. It is also interesting to note that this is the same case for which the spectral radius of IBJ is greater than unity for a PC order greater than one (see Fig. 4.4).

It can be concluded that the SCM is significantly more efficient than the SFEM when the inputs and unknowns are functions of a univariate random variable. This is particularly true as the variance grows because, for a given SCM quadrature order, the same number of transport iterations are required regardless of the variance—source iteration is sensitive only to the scattering ratio. The convergence of the SFEM, on the other hand, slows considerably with increasing variance because additional iterations are required. It is also possible to accelerate the individual SCM computations in problematic diffusive regimes using diffusion or S_2 synthetic accelerations [86, 87], which would make SCM even more efficient. BiCGStab is faster than restarted GMRES in general, and significantly faster than GMRES in diffusive regimes, although it does break down in instances where GMRES converges. In terms of choosing an iterative method, it would therefore seem to be prudent to always begin with BiCGStab and turn to restarted GMRES should it fail.

distribution	P M	IBGS	GMRES(8)	BiCGStab
normal $v_\sigma = 1$	1	28	13	7
	2	52	22	14
	3	32	16	9
	4	104	44	27
	7	60	31	18
	8	207	86	51
log-normal $v_\sigma = 1$	1	28	13	7
	2	52	22	14
	3	29	15	8
	4	104	44	27
	7	29	16	9
	8	208	88	51
log-normal $v_\sigma = 25$	1	50	24	14
	2	52	22	13
	3	184	112	62
	4	101	39	23
	7	4470	704	NC
	8	190	69	41
gamma $v_\sigma = 1$	1	28	13	7
	2	52	22	14
	3	30	15	8
	4	104	44	27
	7	34	17	9
	8	208	88	52
	15	35	16	9
	16	416	173	101
gamma $v_\sigma = 5$	1	32	15	8
	2	52	22	12
	3	54	25	13
	4	104	43	25
	7	112	52	32
	8	208	83	49
	15	242	112	62
	16	415	158	92
	31	466	199	NC
	32	827	298	174
beta $v_\sigma = 1$	1	28	13	7
	2	52	22	14
	3	31	15	8
	4	104	44	27
	7	36	18	10
	8	208	88	54
	15	38	21	11
	16	415	173	103
beta $v_\sigma = 5$	1	33	16	9
	2	52	22	13
	3	59	28	17
	4	104	44	26
	7	116	64	33
	8	206	86	49
	15	204	123	74
	16	407	165	97
uniform $v_\sigma = 1$	1	28	13	7
	2	52	22	14
	3	29	14	7
	4	104	44	27
	7	29	14	7
	8	208	88	54
uniform $v_\sigma = 5$	1	35	17	9
	2	52	22	13
	3	52	25	14
	4	104	44	26
	7	62	30	18
	8	208	87	52
	15	63	31	19
	16	416	174	105

Table 5.1: IBGS Iteration Counts: $c = 0.5$ and Single Random Variable Cross Section with Optimal gPC ($\epsilon = 10^{-9}$)

distribution	P M	IBGS	GMRES(8)	BiCGStab
normal $v_\sigma = 1$	1	0.0104	0.012	0.0104
	2	0.0072	0.0092	0.0084
	3	0.0284	0.034	0.0316
	4	0.0148	0.0188	0.0168
	7	0.1556	0.154	0.1492
	8	0.03	0.038	0.0324
log-normal $v_\sigma = 1$	1	0.01	0.012	0.0104
	2	0.0072	0.0092	0.0088
	3	0.0272	0.0332	0.0292
	4	0.0152	0.0188	0.0168
	7	0.0856	0.0864	0.0812
	8	0.0308	0.0384	0.0332
log-normal $v_\sigma = 25$	1	0.018	0.0208	0.0188
	2	0.0072	0.0092	0.0076
	3	0.17	0.2268	0.198
	4	0.014	0.0172	0.0148
	7	12.6904	3.5976	NC
	8	0.0276	0.0312	0.0284
gamma $\alpha = 25$	1	0.0104	0.012	0.0108
	2	0.0072	0.0092	0.0084
	3	0.028	0.032	0.028
	4	0.0148	0.0184	0.0168
	7	0.0908	0.088	0.076
	8	0.03	0.038	0.0336
	15	0.2476	0.2072	0.1912
	16	0.064	0.0788	0.068
gamma $\alpha = 5$	1	0.0116	0.014	0.0116
	2	0.0072	0.0088	0.0076
	3	0.0472	0.052	0.0444
	4	0.0144	0.018	0.0156
	7	0.288	0.2492	0.2432
	8	0.0304	0.036	0.0316
	15	1.6896	1.352	1.1996
	16	0.0624	0.0732	0.064
	31	9.214	6.372	NC
	32	0.138	0.151	0.135
beta $v_\sigma = 1$	1	0.01	0.012	0.0096
	2	0.0068	0.0088	0.0084
	3	0.0276	0.0312	0.0284
	4	0.0144	0.0184	0.0168
	7	0.0944	0.0916	0.0832
	8	0.03	0.0376	0.034
	15	0.2648	0.2668	0.2308
	16	0.0624	0.0784	0.07
beta $v_\sigma = 5$	1	0.012	0.0144	0.0128
	2	0.0072	0.0092	0.008
	3	0.0524	0.0584	0.0556
	4	0.0144	0.0184	0.016
	7	0.3004	0.3088	0.2492
	8	0.0296	0.0372	0.0316
	15	1.3844	1.4768	1.4152
	16	0.062	0.0748	0.0672
uniform $v_\sigma = 1$	1	0.01	0.012	0.01
	2	0.0072	0.0092	0.0084
	3	0.0268	0.0296	0.0244
	4	0.0144	0.0188	0.0168
	7	0.076	0.0724	0.0604
	8	0.0312	0.0376	0.0344
uniform $v_\sigma = 5$	1	0.0128	0.016	0.0124
	2	0.0068	0.0092	0.008
	3	0.0464	0.0524	0.046
	4	0.0144	0.018	0.0168
	7	0.16	0.15	0.1412
	8	0.03	0.0372	0.0328
	15	0.434	0.3844	0.378
	16	0.0632	0.0776	0.072

Table 5.2: IBGS Run Time in Seconds: Average over 25 Runs for $c = 0.5$ and Single Random Variable Cross Section with Optimal gPC ($\epsilon = 10^{-9}$)

distribution	P M	IBGS	GMRES(8)	BiCGStab
normal $v_\sigma = 1$	1	1177	111	44
	2	2277	202	56
	3	1162	134	64
	4	4365	388	110
	7	1162	242	119
	8	8058	703	213
log-normal $v_\sigma = 1$	1	1185	111	45
	2	2279	202	56
	3	1166	131	64
	4	4482	384	113
	7	1166	174	80
	8	8711	757	229
log-normal $v_\sigma = 25$	1	1272	158	64
	2	1766	162	52
	3	1990	796	221
	4	3364	280	101
	7	4217	3264	NC
	8	6498	474	202
gamma $\alpha = 25$	1	1087	107	44
	2	2324	205	57
	3	1075	121	63
	4	4656	395	119
	7	1074	154	77
	8	9346	801	254
	15	1074	199	100
	16	18841	1588	551
gamma $\alpha = 5$	1	1267	117	51
	2	2321	198	60
	3	1385	201	89
	4	4674	397	141
	7	1537	338	158
	8	9531	752	293
	15	1529	560	217
	16	19630	1450	618
	31	1516	626	NC
	32	40593	2700	1229
beta $v_\sigma = 1$	1	1120	108	44
	2	2277	202	56
	3	1109	126	59
	4	4404	384	110
	7	1109	163	86
	8	8416	749	215
	15	1109	222	107
	16	16050	1412	430
beta $v_\sigma = 5$	1	1214	126	51
	2	2212	181	58
	3	1315	214	99
	4	4263	381	120
	7	1425	424	182
	8	8380	726	246
	15	1458	678	257
	16	16623	1414	510
uniform $v_\sigma = 1$	1	1213	113	43
	2	2277	202	56
	3	1224	128	67
	4	4527	395	111
	7	1224	133	63
	8	9033	779	220
uniform $v_\sigma = 5$	1	1142	122	48
	2	2088	181	54
	3	1297	187	84
	4	4054	363	107
	7	1333	243	109
	8	8015	705	215
	15	1335	259	132
	16	15942	1413	426

Table 5.3: IBGS Iteration Counts: $c = 0.99$ and Single Random Variable Cross Section with Optimal gPC ($\epsilon = 10^{-9}$)

distribution	P M	IBGS	GMRES(8)	BiCGStab
normal $v_\sigma = 1$	1	0.4136	0.0936	0.054
	2	0.298	0.0732	0.0292
	3	0.9868	0.2656	0.1976
	4	0.573	0.141	0.0568
	7	2.9084	1.1396	0.8696
	8	1.05	0.255	0.111
log-normal $v_\sigma = 1$	1	0.414	0.0936	0.0564
	2	0.297	0.0736	0.029
	3	1.0532	0.2652	0.2012
	4	0.584	0.139	0.058
	7	3.2824	0.8904	0.6412
	8	1.14	0.278	0.12
log-normal $v_\sigma = 25$	1	0.4436	0.1332	0.0792
	2	0.23	0.0584	0.0268
	3	1.818	1.5956	0.6852
	4	0.438	0.102	0.0528
	7	11.858	16.5872	NC
	8	0.851	0.174	0.108
gamma $\alpha = 25$	1	0.3784	0.09	0.0548
	2	0.303	0.0748	0.0296
	3	0.9272	0.2416	0.1952
	4	0.607	0.143	0.0616
	7	2.706	0.7284	0.5692
	8	1.23	0.291	0.133
	15	7.244	2.3424	1.8572
	16	2.47	0.58	0.288
gamma $\alpha = 5$	1	0.4424	0.0976	0.0628
	2	0.302	0.0712	0.0308
	3	1.1768	0.4004	0.272
	4	0.609	0.143	0.0716
	7	3.8676	1.588	1.1628
	8	1.24	0.273	0.15
	15	10.3232	6.606	4.0132
	16	2.57	0.533	0.321
	31	29.9836	19.7056	NC
	32	5.33	0.999	0.652
beta $v_\sigma = 1$	1	0.392	0.0916	0.0544
	2	0.297	0.0724	0.0292
	3	0.9824	0.25	0.1832
	4	0.575	0.14	0.0576
	7	2.7956	0.7744	0.6376
	8	1.1	0.272	0.113
	15	7.4492	2.604	1.9768
	16	2.11	0.515	0.23
beta $v_\sigma = 5$	1	0.4244	0.1052	0.064
	2	0.29	0.0656	0.03
	3	1.1456	0.4172	0.3008
	4	0.555	0.139	0.0616
	7	3.614	1.9984	1.338
	8	1.1	0.264	0.128
	15	9.8356	8.0016	4.7088
	16	2.18	0.518	0.269
uniform $v_\sigma = 1$	1	0.4232	0.0964	0.0536
	2	0.297	0.0724	0.0284
	3	1.064	0.2528	0.2048
	4	0.59	0.143	0.0576
	7	3.124	0.6304	0.47
	8	1.18	0.284	0.116
uniform $v_\sigma = 5$	1	0.3996	0.1032	0.0596
	2	0.273	0.066	0.0276
	3	1.1324	0.3688	0.2552
	4	0.532	0.131	0.0556
	7	3.3752	1.144	0.7996
	8	1.05	0.256	0.113
	15	8.9488	3.0452	2.4496
	16	2.09	0.515	0.227

Table 5.4: IBGS Run Time in Seconds: Average over 25 Runs for $c = 0.99$ and Single Random Variable Cross Section with Optimal gPC ($\epsilon = 10^{-9}$)

5.4.2 Non-Optimal gPC Expansions

Table 5.5 shows iteration counts for the non-optimal gPC expansion of the uniform cross section. In comparing the convergence of Hermite chaos for the normal and uniform cross sections for $v_\sigma = 1.0$, the iteration counts for SFEM are similar for P = 1 and P = 3, but iteration counts for the normal cross section are considerably larger for the normal cross section than the uniform for P = 7. While both systems destabilize just after this point, for the normal cross section at P = 10 and for the uniform cross section at P = 9, the spectral radii are smaller for the uniform cross section than the normal and are roughly the same for P = 3 and P = 7 while those for the normal cross section increase rapidly between 3 and 7.

When convergence of the SFEM is compared against Legendre chaos, iteration counts are roughly the same for both variances. However, since the flux can be represented by a lower order Hermite chaos expansion (P = 7) than Legendre chaos expansion (P = 15) for $v_\sigma = 5.0$, Hermite chaos is actually more efficient.

c	distribution	P M	IBGS	GMRES(8)	BiCGStab
		1	28	13	7
		2	52	22	14
	uniform	3	28	14	8
	$v_\sigma = 1$	4	104	44	27
		7	27	15	8
0.5		8	208	88	53
		1	34	17	9
		2	52	22	13
	uniform	3	51	27	15
	$v_\sigma = 5$	4	103	42	25
		7	63	44	25
		8	206	85	48
		1	1176	111	44
		2	2279	202	56
	uniform	3	1169	120	63
	$v_\sigma = 1$	4	4457	379	110
		7	1165	130	74
0.99		8	8851	744	221
		1	1149	123	50
		2	2099	180	54
	uniform	3	1208	193	98
	$v_\sigma = 5$	4	3761	317	106
		7	1246	304	137
		8	7227	631	209

Table 5.5: IBGS Iteration Counts: Single Uniform Random Variable with Hermite gPC ($\epsilon = 10^{-9}$)

5.4.3 Gaussian Random Processes

Tables 5.6 and 5.7 show iteration counts and run times, respectively, for the SFEM and SCM when the cross section is a Gaussian random process represented by its KL expansion. Run times are given as averages over 40 runs for P = 1 and M = 2, 20 runs for P = 3 and M = 4, 15 runs for P = 5 and M = 6 and 10 runs for P = 7 and M = 8. Results are shown for two scattering ratios, three KL orders and several different PC and SCM quadrature orders. The number of equations for each PC and SCM quadrature order are listed, with the numbers in parentheses referring to the number of equations that had to be discarded due to negativities. Once again, for $v_\sigma = 1.0$, the SFEM iteration count remains roughly the same as the PC order increases, while the SCM iteration count per equation remains essentially constant. Furthermore, the SFEM iteration count remains roughly constant for increasing KL, as does the SCM iteration count per equation. For both methods, convergence slows in diffusive regimes.

When there is only a single random variable, the number of coupled equations in the SFEM system is equal to the number of quadrature points required by the SCM to achieve roughly the same accuracy and the SCM is faster. However, when there are additional random variables, the number of equations required by the SCM increases much more rapidly with increasing PC/quadrature and KL orders than the number of coupled SFEM equations does. Consequently, even though the SCM is more efficient than the SFEM for KL = 1, it is more efficient roughly half the time for KL = 3 and it almost never more efficient for KL = 5. This being said, the SCM yields good results even when it is necessary to discard terms. Although no problems were encountered with SFEM in this case, for a high enough PC order, the system will eventually destabilize since negative cross sections are possible. Therefore, although SFEM may be more efficient as the dimension of the problem grows, the fact that it will eventually break down ultimately renders it ineffective in this case.

c	KL	P M	equations	IBGS	GMRES(8)	BiCGStab
0.5	1	1	2	26	12	7
		2	2	52	22	14
		3	4	27	12	7
		4	4	104	44	28
		5	6	27	12	7
		6	6	156	66	42
		7	8	27	12	7
		8	8	208	88	55
	3	1	4	27	12	7
		2	8	208	88	56
		3	20	28	14	7
		4	64	1664	704	437
		5	56	30	15	8
		6	216	5617	2376	1464
		7	120	31	16	10
		8	512	12950	5479	3349
	5	1	6	27	12	7
		2	32	832	352	223
		3	56	29	14	8
		4	1024	26624	11264	6958
		5	252	30	16	9
		6	7776 (214)	196584	83182	50838
		7	792	32	18	10
		8	32768 (3366)	764042	323411	196003
0.9	1	1	2	159	32	20
		2	2	312	62	36
		3	4	159	33	19
		4	4	624	123	76
		5	6	160	34	19
		6	6	934	185	108
	3	1	4	159	32	19
		2	8	1249	248	148
		3	20	160	36	23
		4	64	9968	1963	1191
		5	56	160	39	25
		6	216	33522	6587	3955
	5	1	6	159	33	18
		2	32	4994	991	597
		3	56	160	37	24
		4	1024	159373	31388	18942
		5	252	160	41	25
		6	7776 (214)	1173362	230635	138501

Table 5.6: IBGS Iteration Counts: Gaussian Random Process with Hermite gPC $(v_\sigma = 1.0 \text{ cm}^{-2}, \epsilon = 10^{-9})$

c	KL	P M	equations	IBGS	GMRES(8)	BiCGStab
		1	2	0.0095	0.0112	0.01
		2	2	0.00725	0.009	0.0085
		3	4	0.024	0.026	0.0245
	1	4	4	0.015	0.018	0.017
		5	6	0.0427	0.038	0.0413
		6	6	0.022	0.026	0.022
		7	8	0.071	0.062	0.059
		8	8	0.031	0.037	0.035
		1	4	0.024	0.026	0.024
		2	8	0.0293	0.0367	0.0338
		3	20	0.294	0.252	0.222
0.5	3	4	64	0.26	0.311	0.289
		5	56	1.69	1.27	1.18
		6	216	1.07	1.24	1.17
		7	120	6.54	4.44	5.06
		8	512 (14)	3.15	3.59	3.37
		1	6	0.045	0.043	0.041
		2	32	0.118	0.145	0.137
		3	56	1.6	1.17	1.16
	5	4	1024	5.02	5.87	5.5
		5	252	25.2	17.5	17.8
		6	7776 (214)	70.4	76.1	73.1
		7	792	238	168	166
		8	32768 (3366)	562	600	573
		1	2	0.0568	0.028	0.0255
		2	2	0.0408	0.0265	0.0222
	1	3	4	0.141	0.0665	0.06
		4	4	0.082	0.053	0.048
		5	6	0.25	0.117	0.098
		6	6	0.123	0.0793	0.0687
		1	4	0.136	0.0648	0.06
		2	8	0.162	0.104	0.0917
0.9	3	3	20	1.6	0.614	0.632
		4	64	1.32	0.854	0.764
		5	56	8.77	3.09	3.31
		6	216	4.62	3.07	2.75
		1	6	0.258	0.114	0.0963
		2	32	0.649	0.42	0.372
	5	3	56	8.65	2.95	3.19
		4	1024	22	14.5	13.1
		5	252	135	43.6	45.7
		6	7776 (214)	194	139	129

Table 5.7: IBGS Run Time: Gaussian Random Process with Hermite gPC $(v_\sigma = 1.0 \text{ cm}^{-2}, \epsilon = 10^{-9})$

Chapter 6

K-Eigenvalue Problems

In many radiation transport applications, multiplying materials are present, therefore it is useful to explore the application of polynomial chaos (PC) expansions in these regimes. In section 6.1, the cross sections are taken to be functions of a single random variable, and both the Stochastic Finite Element Method (SFEM) and the Stochastic Collocation Method (SCM) are used to solve for the PC coefficients. The application of SFEM is described in detail, since the non-linearity introduced by the k-eigenvalue necessitates a Newton iteration. The accuracy and computational efficiency of SCM and SFEM are compared for uniform random variables and Legendre chaos. The SCM is then used to generate PC coefficients and pdfs for the various distributions explored previously in this thesis. In section 6.2, in a slightly different application, the fuel enrichment is assumed to a Gaussian random process. The test problem is a single fuel cell, modeled as a uranium dioxide fuel pin surrounded by a water moderator with periodic boundary conditions. The base case is a critical reactor, and SCM is used to generate the PC coefficients and pdfs of the k-eigenvalue for various correlation lengths and standard deviations in the fuel enrichment.

6.1   The Cross Sections as Single Random Variables

To begin, the total cross section is taken to be a single random variable and the scattering and fission cross sections to be linear functions of the total cross section. The flux and k-eigenvalue are also functions of the random variable and the transport equation can then be written as

$$\mu \frac{\partial \psi(x, \mu; \omega)}{\partial x} + \sigma(\omega)\psi(x, \mu; \omega) = \frac{\sigma(\omega)}{2}\left(c + \frac{\nu f}{k(\omega)}\right)\phi(x; \omega) \tag{6.1}$$

where $\sigma_s(\omega) = c\sigma(\omega)$ and $\sigma_f(\omega) = f\sigma(\omega)$. Once again, the problem could be solved using Monte Carlo, where numerous realizations of the fission cross section are generated and each corresponding value of k is computed, generally using the power iteration (Eq. 2.12), and tabulated. Alternatively, polynomial chaos (PC) expansions could be used to represent the stochastic quantities and either the Stochastic Finite Element Method (SFEM) or the Stochastic Collocation Method (SCM) could be used to compute the PC expansion coefficients.

6.1.1   The SFEM Approach

Applying PC expansions to each function of the random variable in Eq. 6.1 yields:

$$\mu \sum_{i=0}^{P} \Phi_i \frac{\partial \psi_i(x, \mu)}{\partial x} + \sum_{i=0}^{P}\sum_{j=0}^{P_\sigma} \Phi_i \Phi_j \left(\psi_i(x, \mu) - \frac{c}{2}\phi_i(x)\right)\sigma_j =$$
$$\frac{\nu f}{2} \sum_{m=0}^{P}\sum_{i=0}^{P}\sum_{j=0}^{P_\sigma} \Phi_m \Phi_i \Phi_j \lambda_m \phi_i(x)\sigma_j \tag{6.2}$$

where k has been represented in terms of its inverse,

$$\frac{1}{k(\omega)} = \lambda(\omega) \approx \sum_{j=0}^{P} \Phi_j \lambda_j,$$

so that all of the basis functions are in the numerator. Projecting onto the basis yields the following system of SFEM equations

$$\mu \frac{\partial \psi_\ell(x,\mu)}{\partial x} + \sum_{i=0}^{P} \sum_{j=0}^{P_\sigma} \frac{\langle \Phi_\ell \Phi_i \Phi_j \rangle}{\langle \Phi_\ell^2 \rangle} \left(\psi_i(x,\mu) - \frac{c}{2}\phi_i(x) \right) \sigma_j =$$

$$\frac{\nu f}{2} \sum_{m=0}^{P} \sum_{i=0}^{P} \sum_{j=0}^{P_\sigma} \frac{\langle \Phi_\ell \Phi_m \Phi_i \Phi_j \rangle}{\langle \Phi_\ell^2 \rangle} \lambda_m \phi_i(x) \sigma_j \quad (6.3)$$

which can be rewritten as

$$\mu \frac{\partial \psi_\ell}{\partial x} + \sum_{i=0}^{P} b_{\ell i} \left(\psi_i - \frac{c}{2}\phi_i \right) = \frac{\nu}{2} \sum_{m=0}^{P} \lambda_m \sum_{i=0}^{P} f_{\ell m i} \phi_i, \qquad \ell = 0, \ldots, P \qquad (6.4)$$

where

$$b_{\ell i} = \sum_{j=0}^{P_\sigma} \sigma_j \frac{\langle \Phi_\ell \Phi_i \Phi_j \rangle}{\langle \Phi_\ell^2 \rangle}$$

and

$$f_{\ell m i} = \sum_{j=0}^{P_\sigma} \frac{\langle \Phi_\ell \Phi_m \Phi_i \Phi_j \rangle}{\langle \Phi_\ell^2 \rangle} \sigma_j.$$

Application of the angular and spatial discretization refashions Eq. 6.4 in the form of a matrix equation

$$\sum_{i=0}^{P} \left(\mathbf{L}_{\ell i} - \mathbf{MS}_{\ell i} \mathbf{D} \right) \vec{\psi}_i = \sum_{m=0}^{P} \lambda_m \sum_{i=0}^{P} \mathbf{MS}_{f,\ell m i} \mathbf{D} \vec{\psi}_i, \qquad \ell = 0, \ldots, P \qquad (6.5)$$

where $\mathbf{L}_{\ell i}$ is the streaming and removal operator, $\mathbf{M}$ is the moment-to-discrete operator, $\mathbf{S}_{\ell i}$ and $\mathbf{S}_{f,\ell m i}$ are the scattering and fission source matrices, respectively, and $\mathbf{D}$ is the discrete-to-moment operator. Thus, in total there are $2IN(P+1)$ equations, where I is the number of spatial cells and N is the number of quadrature angles, while the solution vector,

$$\vec{x} = [\vec{\psi}_0, \ldots, \vec{\psi}_P, \lambda_0, \ldots, \lambda_P]^T,$$

contains $(2IN+1)(P+1)$ unknowns. The additional $(P+1)$ equations can be derived from the normalization condition on the eigenfunction

$$\vec{\phi}^T \vec{\phi} = \left(\mathbf{D}\vec{\psi}\right)^T \left(\mathbf{D}\vec{\psi}\right) = 1 \tag{6.6}$$

where $\vec{\psi}$ is the exact eigenfunction and is a function of the random dimension. Since the norm of $\vec{\phi}$ is a deterministic quantity, Eq. 6.6 states that for *each realization* of the material, the L$_2$-norm of the eigenfunction vector is unity. The eigenfunction can then be replaced by its PC expansion to yield

$$\sum_{i=0}^{P} \sum_{j=0}^{P} \left(\mathbf{D}\vec{\psi}_i\right)^T \left(\mathbf{D}\vec{\psi}_j\right) \Phi_i \Phi_j = 1. \tag{6.7}$$

Projecting onto the basis gives the final $(P+1)$ equations:

$$\sum_{i=0}^{P} \sum_{j=0}^{P} \left(\mathbf{D}\vec{\psi}_i\right)^T \left(\mathbf{D}\vec{\psi}_j\right) \langle \Phi_i \Phi_j \Phi_\ell \rangle = \delta_{\ell 0}, \qquad \ell = 0, \ldots, P. \tag{6.8}$$

As can be seen in Eq. 6.5, the matrix equation is non-linear since both the eigenvalue and the eigenfunction are unknown, therefore it is necessary to use a non-linear iterative solver such as Newton-Raphson. The system of equations is first written in the form

$$F(\vec{x}) = [F_0(\vec{x}) \cdots F_P(\vec{x}) F_{P+1}(\vec{x})]^T = 0$$

where $\vec{x}$ is the solution vector, and the F_ℓ are given by

$$F_\ell(\vec{x}) = \sum_{i=0}^{P} \left(\mathbf{L}_{\ell i} - \mathbf{MS}_{\ell i}\mathbf{D}\right) \vec{\psi}_i - \sum_{m=0}^{P} \lambda_m \sum_{i=0}^{P} \mathbf{MS}_{f,\ell m i}\mathbf{D}\vec{\psi}_i \tag{6.9a}$$

$$F_{P+1,\ell}(\vec{x}) = \sum_{i=0}^{P} \sum_{j=0}^{P} \left(\mathbf{D}\vec{\psi}_i\right)^T \left(\mathbf{D}\vec{\psi}_j\right) \langle \Phi_i \Phi_j \Phi_\ell \rangle - \delta_{\ell 0} \tag{6.9b}$$

for $\ell = 0, \ldots, P$.

Expanding $F(\vec{x})$ in a Taylor series around $\vec{x}$ yields

$$F(\vec{x} + \vec{\delta x}) = F(\vec{x}) + J \cdot \vec{\delta x} + O(\vec{\delta x}^2)$$

where J is the Jacobian matrix with elements

$$J_{ij} = \frac{\partial F_i}{\partial x_j}.$$

Since the zeros of $F(\vec{x})$ are desired, the condition $F(\vec{x} + \vec{\delta x}) = 0$ is imposed and, neglecting higher-order terms, the equation for the update, $\vec{\delta x}$, becomes

$$J \cdot \vec{\delta x}^{(i)} = -F(\vec{x}^{(i)}) \tag{6.10}$$

where i is the iteration index. This equation is solved for $\vec{\delta x}^{(i)}$ using an iterative method such as a Krylov subspace method and the solution vector is then updated:

$$\vec{x}^{(i+1)} = \vec{x}^{(i)} + \vec{\delta x}^{(i)}. \tag{6.11}$$

The terms in the Jacobian are determined by taking the derivatives of F (Eq. 6.9) with respect to the eigenfunctions and eigenvalues (for a detailed derivation of Eq. 6.12c, see Appendix C):

$$\frac{\partial F_\ell}{\partial \vec{\psi}_p} = \mathbf{L}_{\ell p} - \mathbf{MS}_{\ell p}\mathbf{D} - \sum_{m=0}^{P} \lambda_m \mathbf{MS}_{f,\ell m p}\mathbf{D} \tag{6.12a}$$

$$\frac{\partial F_\ell}{\partial \lambda_p} = -\sum_{i=0}^{P} \mathbf{MS}_{f,\ell p i}\mathbf{D}\vec{\psi}_i \tag{6.12b}$$

$$\frac{\partial F_{P+1,\ell}}{\partial \psi_{p,k}} = 2w_m \sum_{i=0}^{P} \left(\sum_{n=1}^{N} w_n \psi_{i,k-m+n} \right) \langle \Phi_i \Phi_p \Phi_\ell \rangle \tag{6.12c}$$

$$\frac{\partial F_{P+1}}{\partial \lambda_p} = 0 \tag{6.12d}$$

where $0 \le \ell \le P$, $\psi_{p,k}$ is the kth element of ψ_p for $1 \le k \le 2IN$ and $m = \text{mod}(k, N)$, $1 \le m \le N$, is the index of the quadrature angle corresponding to $\psi_{p,k}$.

Newton-Raphson shows quadratic convergence near the solution point, but can diverge if the initial guess is not sufficiently accurate. Here, the solution is initialized using either Monte Carlo or the SCM, although there are other possible intializing algorithms. It is expected that the three methods will yield the same answer for the PC coefficients of the eigenmode when a sufficient number of terms is kept in each case. As was shown previously, the SCM using a Gaussian quadrature order of M is equivalent to SFEM for $P = (M - 1)$ in non-multiplying media. This is an important consideration since Newton-Raphson may diverge if the initial guess is not sufficiently accurate.

6.1.2   The SCM Approach

The PC coefficients of the flux and k-eigenvalue can also be computed using SCM, and is one option for initializing the Newton-Krylov SFEM iteration. The SCM involves a series of M, where M is the SCM quadrature order, deterministic power iterations given by Eq. 2.12. Iteration proceeds until

$$\frac{|k^{(\ell+1)} - k^{(\ell)}|}{k^{(\ell+1)}} \leq \varepsilon$$

where ε is the tolerance. Power iteration requires an inner source iteration, also deterministic, to compute the flux. This iteration is given by Eq. 2.9 and proceeds until

$$\frac{\|\vec{\phi}^{(\ell+1)} - \vec{\phi}^{(\ell)}\|_2}{\|\mathbf{D}\vec{Q}\|_2} \leq \varepsilon.$$

6.1.3   Numerical Results

Numerical results were obtained for a critical reactor with uncertain macroscopic cross sections, which were taken to be functions of a single random variable. This

was accomplished by defining a constant scattering ratio, c, and 'fission ratio', f, such that $\sigma_s(\omega) = c\sigma_t(\omega)$ and $\sigma_f(\omega) = f\sigma_t(\omega)$. The test problem was taken from an analytical benchmark test set originally intended for criticality code verification [88]. The system is a bare slab reactor composed of uranium dioxide with the following material parameters:

ν	1.70
σ_f	0.054628
σ_c	0.027314 cm^{-1}
σ_s	0.464338 cm^{-1}
σ_t	0.54628 cm^{-1}

Table 6.1: Test Problem Parameters

The analytic critical size of the reactor is given as 20.74213 cm in [88]. Using 100 spatial cells and 32 discrete ordinates, by trial and error the critical size was found to be 20.742942196391 cm. Using this critical size and the mean cross sections listed in Table 6.1, the total cross section is assumed to be randomly distributed according to one of the pdfs explored previously. The relative accuracy and computational efficiency of the SFEM and the SCM are compared for a uniformly distributed cross section pdf and Legendre chaos. The pdfs of the flux and k-eigenvalue as well as the probability that $k > 1$, $P(k > 1)$, are also computed using the PC coefficients of the eigenmode (computed using SCM with a quadrature order of M = (P + 1)). This is done by sampling the random variable, computing k from its PC expansion and tabulating the results to generate the pdf and $P(k > 1)$. The results are then compared with Monte Carlo for various distributions.

Accuracy and Computational Efficiency of the SFEM vs. the SCM

Newton's iteration requires a 'good' inital guess which can be estimated using SCM or Monte Carlo. SCM is used here to initialize Newton's method, in part because it

is more efficient and in part because there are interesting implications to choosing an initial guess that is not accurate enough, a relationship best explored in the context of quadrature. Table 6.2 shows iteration counts, run times and L_2-Norms of F for the SCM initialization and a single Newton-Krylov SFEM iteration. The SCM initialization produces a solution with $\parallel F_{\text{SCM}} \parallel_2$ on the order of 10^{-3} or 10^{-4} in all cases. A single Newton-Krylov SFEM iteration then produces an $\parallel F_{\text{SFEM}} \parallel_2$ on the order of 10^{-6} or 10^{-7}. Note, however, that these are L_2 norms—the individual elements of F_{SCM} and F_{SFEM} are generally smaller than the norm.

In the previous chapter, it was shown that SCM using a quadrature order of M is equivalent to SFEM using a PC order of $P = (M - 1)$. The same cannot be said for multiplying media due to the non-linear nature of the SFEM equations. As can be seen in Fig. 6.1, the size of $\parallel F_{\text{SCM}} \parallel_2$ is strongly dependent on the tolerance set for the power iteration used to compute the k-eigenvalue (see Eq. 2.12) and the inner source iteration used to compute the flux updates (see Eq. 2.9). For $\frac{\sqrt{v_\sigma}}{\langle \sigma \rangle} = \frac{1}{5}$, as the tolerance decreases, $\parallel F_{\text{SCM}} \parallel_2$ decreases as well and is on the order of 10^{-8} for a tolerance of 10^{-12} for $P = 7$ and 15. However, for $P = 1$ and 3, $\parallel F_{\text{SCM}} \parallel_2$ is approximately 10^{-4} and 10^{-5}, respectively. Even with a very small tolerance, $\parallel F_{\text{SCM}} \parallel_2$ is quite large for small P, indicating that SCM with a quadrature order of $M = (P + 1)$ is not in fact equivalent to SFEM with a PC order of P. (In comparison, consider that if σ_f and ν are set to zero and a volume source is placed in the system, SCM with a quadrature order of $M = (P + 1)$ yields $\parallel F_{\text{SCM}} \parallel_2$ on the order of 10^{-12} or 10^{-13} for $P = 1, 3, 7$ and 15.) However, the fact that $\parallel F_{\text{SCM}} \parallel_2$ gets very small for $P = 7$ as the tolerance gets small indicates that the solution is essentially converged and that the two methods do eventually converge to the same answer, as would be expected. Similar conclusions can be drawn for $\frac{\sqrt{v_\sigma}}{\langle \sigma \rangle} = \frac{1}{\sqrt{5}}$, although clearly the solution does not converge as quickly as it does for the smaller variance. In Table 6.3, run times are also shown for $\frac{\sqrt{v_\sigma}}{\langle \sigma \rangle} = \frac{1}{5}$ (run times are almost identical for $\frac{\sqrt{v_\sigma}}{\langle \sigma \rangle} = \frac{1}{\sqrt{5}}$ and are therefore not shown) for various tolerances and PC orders. Although it is

much more expensive to use a smaller tolerance in SCM, it is not nearly as expensive as doing even a single SFEM Newton-Krylov iteration. Although doing that SFEM iteration does produce more accurate results for P = 1 and 3, these solutions are not converged therefore there is little point in doing the extra work.

$\frac{\sqrt{v_\sigma}}{\langle\sigma\rangle}$	PC	M	SCM Initialize			SFEM		
			GMRES(8)	run time (s)	$\parallel F_{\text{SCM}} \parallel_2$	GMRES(25)	run time (s)	$\parallel F_{\text{SFEM}} \parallel_2$
$\frac{1}{5}$	1	2	102	0.217	3.2355e-04	20	0.723875	2.6288e-07
	3	4	211	0.45	3.0228e-04	39	5.9535	2.3297e-07
	7	8	420	0.904	3.2456e-04	90	60.283	2.5748e-07
	15	16	847	1.8	3.2652e-04	125	536.956	1.9739e-07
$\frac{1}{\sqrt{5}}$	1	2	108	0.228	2.2224e-03	21	0.7538	1.4410e-06
	3	4	214	0.457	1.3736e-03	98	9.4105	8.5795e-07
	7	8	433	0.924	4.3315e-04	187	130.33	4.8508e-07
	15	16	862	1.84	4.2298e-04	253	1148.068	5.2655e-07

Table 6.2: Iteration Counts, Run Times and Errors for the SCM and a Single SCM-initialized SFEM Iteration in a Multiplying Material: Uniform Random Variable and Legendre Chaos (SCM tolerance = 10^{-6})
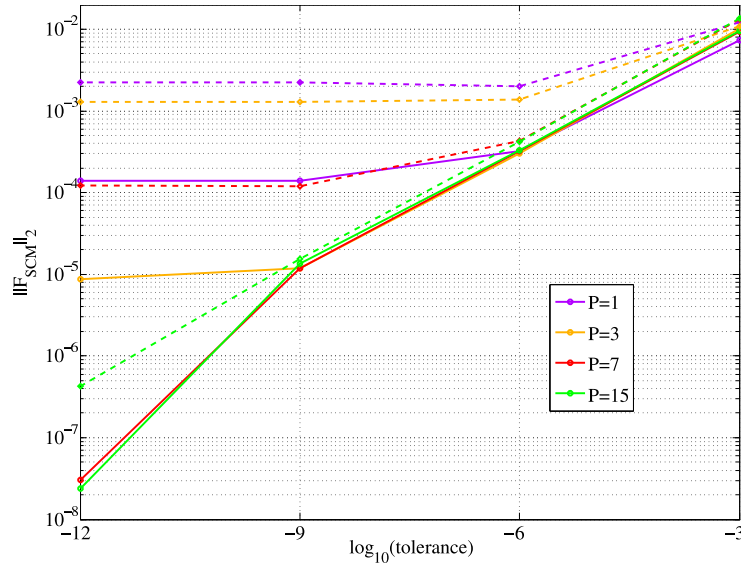
Figure 6.1: $\parallel F_{\text{SCM}} \parallel_2$ as a Function of Tolerance for Various PC Orders (Solid Lines: $\frac{\sqrt{v_\sigma}}{\langle\sigma\rangle} = \frac{1}{5}$, Dashed Lines: $\frac{\sqrt{v_\sigma}}{\langle\sigma\rangle} = \frac{1}{\sqrt{5}}$)

It is also interesting to explore the effect of using a quadrature order other than

tolerance	P = 1	P = 3	P = 7	P = 15
10^{-3}	0.08	0.16	0.39	0.64
10^{-6}	0.217	0.45	0.904	1.8
10^{-9}	0.36	0.76	1.44	2.9
10^{-12}	0.66	1.29	2.58	5.04

Table 6.3: Runtime for SCM for M = (P + 1) in seconds: Uniform Random Variable and Legendre Chaos ($\frac{\sqrt{v_\sigma}}{\langle\sigma\rangle} = \frac{1}{5}$)

M = (P + 1) to initialize Newton's method. Fig. 6.2 shows $\| F_{\text{SCM}} \|_2$ and Newton iteration counts necessary to obtain $\| F_{\text{SFEM}} \|_2 \leq 10^{-6}$ as a function of M for various PC orders and a tolerance of 10^{-6} for the power and source iterations in SCM. As can be seen, M = (P + 1) is generally optimal (a single Newton iteration is required), and choosing an M that is too small produces an initial guess that causes Newton to diverge (thus the missing data points). When M < (P + 1) and Newton's iteration will converge, $\| F_{\text{SCM}} \|_2$ is large, and numerous Newton iterations are required in the SFEM step. The number of iterations grows with PC order and is larger when the variance is larger. For $\frac{\sqrt{v_\sigma}}{\langle\sigma\rangle} = \frac{1}{5}$, when P = 1, $\| F_{\text{SCM}} \|_2$ jumps up sharply for M = 4, but then levels off. This indicates that M = 4 produces converged results for the two PC coefficients, therefore increasing the quadrature order does not affect the solution. For P = 3, there is a slight jump in the plot between M = 4 and M = 8 and then the line levels out, once again indicating that M = 8 produces converged results. For P = 7 and 15, M ≥ (P + 1) produce roughly the same results, indicating that for P = 7 the PC expansion is converged as is SCM with M = (P + 1). Similar conclusions can be drawn for $\frac{\sqrt{v_\sigma}}{\langle\sigma\rangle} = \frac{1}{\sqrt{5}}$, except in this case, the jumps between M = (P + 1) and 2(P + 1) are much more pronounced. Also, the solution clearly requires P = 15 and M = 16 to converge.

:

(a) $\| \ \mathrm{F_{SCM}} \ \|_2$

:

(b) Newton Iterations
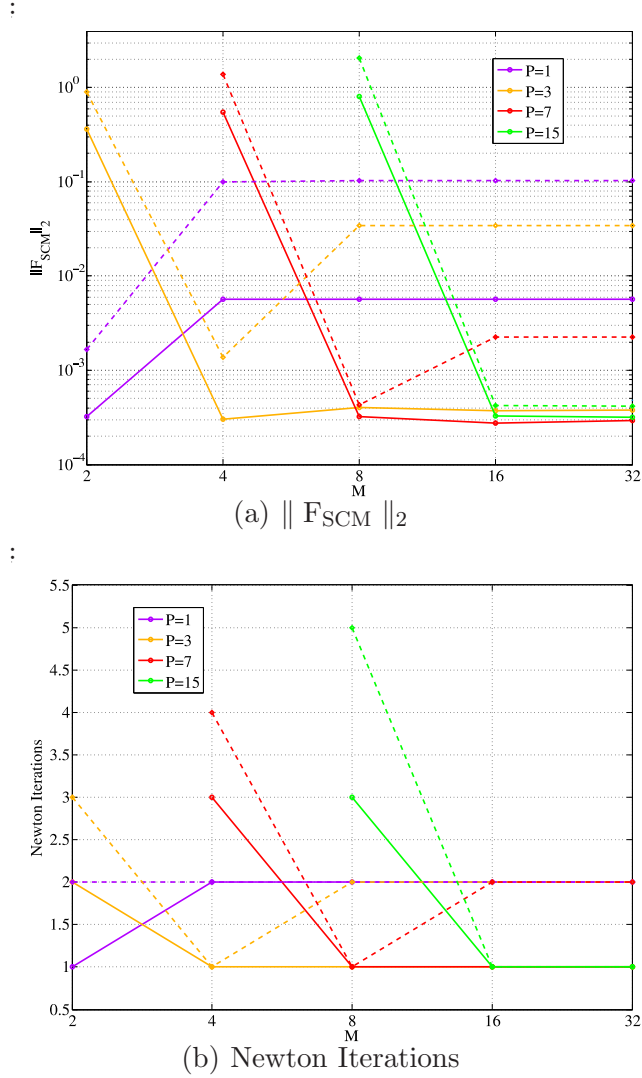
Figure 6.2: $\| \ \mathrm{F_{SCM}} \ \|_2$ and Newton Iteration Counts Necessary to Achieve $\| \ \mathrm{F_{SCM}} \ \|_2 \le 10^{-6}$ as a Function of Quadrature Order for Various PC Orders: Uniform Random Variable and Legendre Chaos (Solid Lines: $\frac{\sqrt{v_\sigma}}{\langle \sigma \rangle} = \frac{1}{5}$, Dashed Lines: $\frac{\sqrt{v_\sigma}}{\langle \sigma \rangle} = \frac{1}{\sqrt{5}}$)

Convergence of the PC Expansion

Using a PC order of P assumes—though the assumption may not be correct—that the eigenmode can be well-approximated using a P-dimensional polynomial. Therefore the integral with the highest-order polynomial is the one used for calculating the Pth moment of the k-eigenvalue, $\langle k\Phi_P \rangle$, or flux, $\langle \phi\Phi_P \rangle$, with the integrand assumed to be a polynomial of order 2P. A quadrature order of $M = (P + 1)$ can calculate the integral of a (2P+1)-dimensional polynomial exactly, and is therefore the smallest quadrature order that will yield 'exact' results if the eigenmode is, as assumed, well-approximated using a P-dimensional polynomial. Clearly, there is no point in computing coefficients of order M and greater because the quadrature will not yield an exact result. Tables 6.4 through 6.10 show the PC coefficients of the k-eigenvalue computed using several different quadrature orders and Monte Carlo for various distributions using their optimal gPCs. Figs. 6.3 through 6.9 show the pdfs of k for various PC orders, P, computed using a quadrature order of $M = (P + 1)$ for the same distributions and gPCs. Several general conclusions can be drawn:

1. Higher-order PC coefficients require higher-order quadrature orders to achieve convergence. This is expected given that the ith coefficient is defined to be the inner product of k with an ith-order polynomial. This also explains why the mean (k_0) converges more quickly than the standard deviation.

2. For larger standard deviations, higher quadrature and PC orders are required to achieve convergence of the mean, the standard deviation and the pdf of k.

3. Even when the mean and standard deviation of the cross section are similar, different distributions yield dissimilar pdfs, means and standard deviations of k. To reiterate, it is important to represent the pdf of the uncertain input faithfully in order to achieve accurate results.

4. Although PC orders of 15 and 31 generally yield converged results for the mean and reasonably accurate estimations of the standard deviation, the higher-order PC coefficients are clearly not converged. Because these coefficients are small (their magnitudes decrease as the order increases), this does not seem to impact the accuracy of the standard deviation or the pdfs.

Table 6.11 shows the probability that $k > 1$, $P(k > 1)$, as computed using various PC orders and Monte Carlo. As can be seen, the probability is generally close to 50%, but varies somewhat between distributions. For the uniform distribution, the probability appears to be unaffected by different variances (0.50037 in both cases), while the probabilities are quite different for the beta distribution (0.51520 for $\frac{\sqrt{v_\sigma}}{\langle \sigma \rangle} = \frac{1}{5}$ vs. 0.46884 for $\frac{\sqrt{v_\sigma}}{\langle \sigma \rangle} = \frac{1}{\sqrt{5}}$). It should also be noted that the PC result reproduces the Monte Carlo result quite accurately.

M	2	4	8	16	32
PC					
0	9.9048926e-01	9.8984298e-01	9.8984507e-01	9.8984493e-01	9.8984490e-01
1	4.3205783e-02	4.7289937e-02	4.7291405e-02	4.7291271e-02	4.7291315e-02
2	–	-1.1109893e-02	-1.1159513e-02	-1.1159306e-02	-1.1159495e-02
3	–	1.9970501e-03	2.1786374e-03	2.1782935e-03	2.1785835e-03
4	–	–	-3.5366639e-04	-3.5304162e-04	-3.5337401e-04
5	–	–	4.3702816e-05	4.2824039e-05	4.3121872e-05
6	–	–	-2.7295965e-06	-1.8000414e-06	-2.0055542e-06
7	–	–	-2.4120222e-07	-9.7200317e-07	-8.6072010e-07
8	–	–	–	4.0831278e-07	3.6071365e-07
9	–	–	–	-1.0698041e-07	-9.1590640e-08
10	–	–	–	2.1499390e-08	1.8285807e-08
11	–	–	–	-2.8261174e-09	-2.7424409e-09
12	–	–	–	-1.2939309e-10	1.1963629e-10
13	–	–	–	2.2757532e-10	1.1346185e-10
14	–	–	–	-7.8351707e-11	-5.1092879e-11
15	–	–	–	1.3994970e-11	1.1728086e-11
stdev	4.3205783e-02	5.0071218e-02	5.0172323e-02	5.0171972e-02	5.0172226e-02

Table 6.4: Normal Distribution: Hermite chaos coefficients and standard deviation of the k-eigenvalue calculated using M-dimensional Gauss-Hermite quadrature ($\frac{\sqrt{v_\sigma}}{\langle \sigma \rangle} = \frac{1}{5}$). The mean and standard deviation given by Monte Carlo are 9.8989716e-01 and 5.0070048e-02, respectively.

Figure 6.3: PDF of the k-eigenvalue: Hermite Chaos expansion of the Normal Distribution ($\frac{\sqrt{v_\sigma}}{\langle \sigma \rangle} = \frac{1}{5}$)

M	2	4	8	16	32
PC					
0	9.9117110e-01	9.9063547e-01	9.9063510e-01	9.9063510e-01	9.9063510e-01
1	-7.9124638e-03	-8.5647794e-03	-8.5666363e-03	-8.5666355e-03	-8.5666355e-03
2	–	-7.0355653e-04	-7.0732669e-04	-7.0732540e-04	-7.0732540e-04
3	–	-6.5316396e-05	-7.1276946e-05	-7.1275191e-05	-7.1275191e-05
4	–	–	-8.1681261e-06	-8.1660532e-06	-8.1660532e-06
5	–	–	-1.0088119e-06	-1.0067049e-06	-1.0067049e-06
6	–	–	-1.2742634e-07	-1.2572146e-07	-1.2572149e-07
7	–	–	-1.5010370e-08	-1.4293198e-08	-1.4293225e-08
8	–	–	–	-9.7816246e-10	-9.7819425e-10
9	–	–	–	1.9328363e-10	1.9324084e-10
10	–	–	–	1.3036439e-10	1.3031426e-10
11	–	–	–	4.9384935e-11	4.9334075e-11
12	–	–	–	1.5972332e-11	1.5927449e-11
13	–	–	–	4.7701879e-12	4.7392684e-12
14	–	–	–	1.3281553e-12	1.3212833e-12
15	–	–	–	3.1058141e-13	3.3930500e-13
stdev	3.9562319e-02	4.4802201e-02	4.4873599e-02	4.4873564e-02	4.4934167e-02

Table 6.5: Gamma Distribution: Laguerre chaos coefficients and standard deviation of the k-eigenvalue calculated using M-dimensional Gauss-Laguerre quadrature ($\frac{\sqrt{v_\sigma}}{\langle\sigma\rangle} = \frac{1}{5}$). The mean and standard deviation given by Monte Carlo are 9.9063305e-01 and 4.4871171e-02, respectively.

Figure 6.4: PDF of the k-eigenvalue: Laguerre Chaos expansion of the Gamma Distribution ($\frac{\sqrt{v_\sigma}}{\langle\sigma\rangle} = \frac{1}{5}$)

M	2	4	8	16	32
PC					
0	9.6224972e-01	9.5207180e-01	9.5190828e-01	9.5191928e-01	9.5191913e-01
1	-3.3482827e-02	-4.5909100e-02	-4.6428891e-02	-4.6413108e-02	-4.6413242e-02
2	–	-1.3613081e-02	-1.4566236e-02	-1.4546635e-02	-1.4546801e-02
3	–	-3.6908415e-03	-5.1284574e-03	-5.1071834e-03	-5.1073827e-03
4	–	–	-1.9356586e-03	-1.9158681e-03	-1.9160854e-03
5	–	–	-7.5764394e-04	-7.4353962e-04	-7.4376211e-04
6	–	–	-2.9321399e-04	-2.9001190e-04	-2.9022470e-04
7	–	–	-9.5833612e-05	-1.0964111e-04	-1.0982562e-04
8	–	–	–	-3.7602625e-05	-3.7736569e-05
9	–	–	–	-9.5739211e-06	-9.6318299e-06
10	–	–	–	4.7722969e-07	5.2317629e-07
11	–	–	–	3.3132436e-06	3.4917656e-06
12	–	–	–	3.4100748e-06	3.7485854e-06
13	–	–	–	2.6057514e-06	3.1275591e-06
14	–	–	–	1.6255223e-06	2.3466654e-06
15	–	–	–	7.3124926e-07	1.6570647e-06
stdev	7.4869877e-02	1.1745105e-01	1.2343850e-01	1.2331635e-01	1.2331795e-01

Table 6.6: Gamma Distribution: Laguerre chaos coefficients and standard deviation of the k-eigenvalue calculated using M-dimensional Gauss-Laguerre quadrature ($\frac{\sqrt{v_\sigma}}{\langle \sigma \rangle} = \frac{1}{\sqrt{5}}$). The mean and standard deviation given by Monte Carlo are 9.5179068e-01 and 1.2346672e-01, respectively.

Figure 6.5: PDF of the k-eigenvalue: Laguerre Chaos expansion of the Gamma Distribution ($\frac{\sqrt{v_\sigma}}{\langle \sigma \rangle} = \frac{1}{\sqrt{5}}$)

M	2	4	8	16	32
PC					
0	9.9048926e-01	9.8992239e-01	9.8992304e-01	9.8992289e-01	9.8992296e-01
1	1.8002409e-02	1.9486510e-02	1.9487668e-02	1.9487655e-02	1.9487677e-02
2	–	-3.3316200e-03	-3.3418840e-03	-3.3418571e-03	-3.3418661e-03
3	–	5.9792078e-04	6.3897759e-04	6.3898153e-04	6.3897539e-04
4	–	–	-1.2536296e-04	-1.2535749e-04	-1.2535722e-04
5	–	–	2.3083333e-05	2.3042586e-05	2.3043511e-05
6	–	–	-3.3502510e-06	-3.2534967e-06	-3.2527970e-06
7	–	–	1.8003082e-07	-1.2150618e-08	-1.1677261e-08
8	–	–	–	2.6936837e-07	2.6899917e-07
9	–	–	–	-1.4457367e-07	-1.4491513e-07
10	–	–	–	5.4956140e-08	5.5022594e-08
11	–	–	–	-1.6676232e-08	-1.6826328e-08
12	–	–	–	3.2651509e-09	3.3236039e-09
13	–	–	–	2.4665237e-10	8.3946253e-10
14	–	–	–	-5.6707110e-10	-6.7947352e-10
15	–	–	–	3.2351697e-10	-3.1111449e-10
stdev	4.3205783e-02	4.9111833e-02	4.9166884e-02	4.9166818e-02	4.9166875e-02

Table 6.7: Beta Distribution: Jacobi chaos coefficients and standard deviation of the k-eigenvalue calculated using M-dimensional Gauss-Jacobi quadrature ($\frac{\sqrt{v_\sigma}}{\langle\sigma\rangle} = \frac{1}{5}$). The mean and standard deviation given by Monte Carlo are 9.8987671e-01 and 4.9139733e-02, respectively.
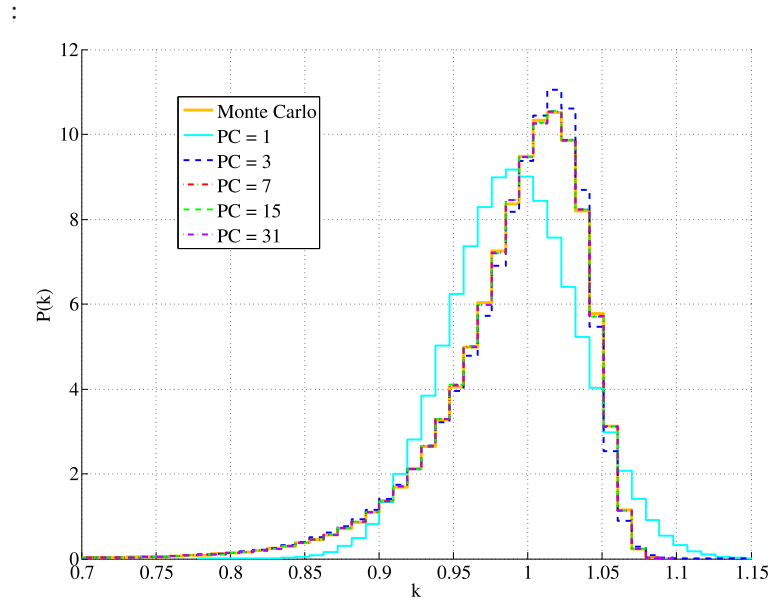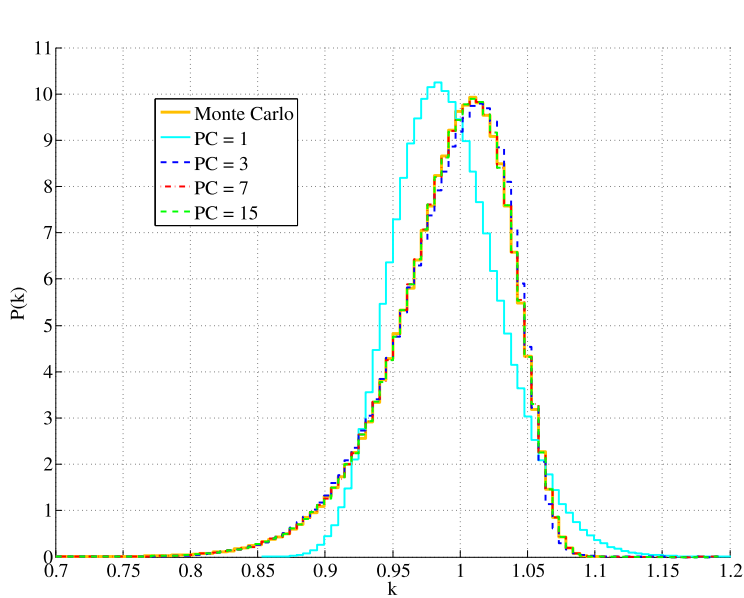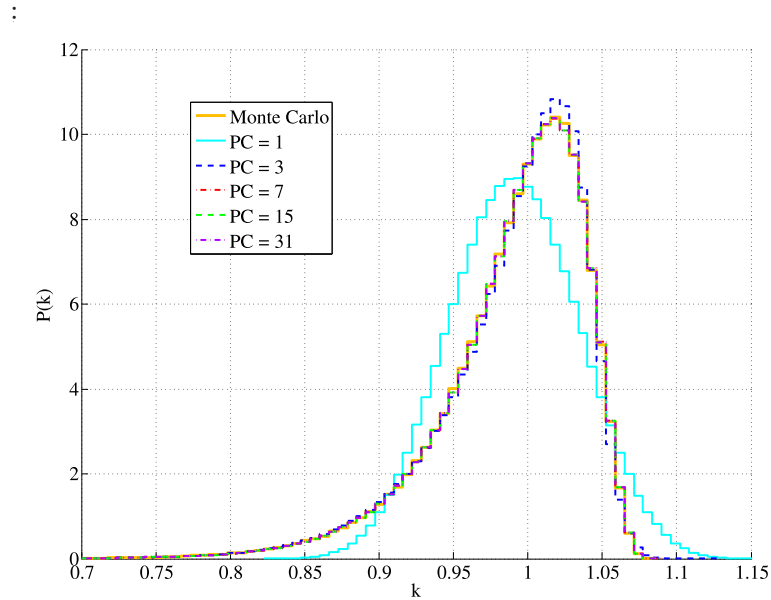

Figure 6.6: PDF of the k-eigenvalue: Jacobi Chaos expansion of the Beta Distribution ($\frac{\sqrt{v_\sigma}}{\langle\sigma\rangle} = \frac{1}{5}$)

M	2	4	8	16	32
PC					
0	9.5467453e-01	9.4398979e-01	9.4418209e-01	9.4417876e-01	9.4417866e-01
1	6.9317150e-02	9.2760635e-02	9.2712940e-02	9.2718270e-02	9.2718366e-02
2	–	-4.4179281e-02	-4.4902664e-02	-4.4909303e-02	-4.4909410e-02
3	–	1.7405680e-02	2.0424498e-02	2.0428979e-02	2.0429180e-02
4	–	–	-8.3810278e-03	-8.3743112e-03	-8.3746218e-03
5	–	–	2.9121999e-03	2.8765395e-03	2.8769452e-03
6	–	–	-7.3995888e-04	-6.4882081e-04	-6.4935346e-04
7	–	–	8.3937338e-05	-8.5840000e-05	-8.5112948e-05
8	–	–	–	2.2292803e-04	2.2195481e-04
9	–	–	–	-1.7135114e-04	-1.7008850e-04
10	–	–	–	9.2744826e-05	9.1106593e-05
11	–	–	–	-3.5814469e-05	-3.3693807e-05
12	–	–	–	5.2543709e-06	2.4923979e-06
13	–	–	–	6.6701960e-06	1.0400704e-05
14	–	–	–	-8.2214058e-06	-1.3372338e-05
15	–	–	–	5.0018343e-06	1.2086451e-05
stdev	9.2998715e-02	1.4439623e-01	1.4668761e-01	1.4669649e-01	1.4669683e-01

Table 6.8: Beta Distribution: Jacobi chaos coefficients and standard deviation of the k-eigenvalue calculated using M-dimensional Gauss-Jacobi quadrature ($\frac{\sqrt{v_\sigma}}{\langle\sigma\rangle} = \frac{1}{\sqrt{5}}$). The mean and standard deviation given by Monte Carlo are 9.4413453e-01 and 1.4656023e-01, respectively.
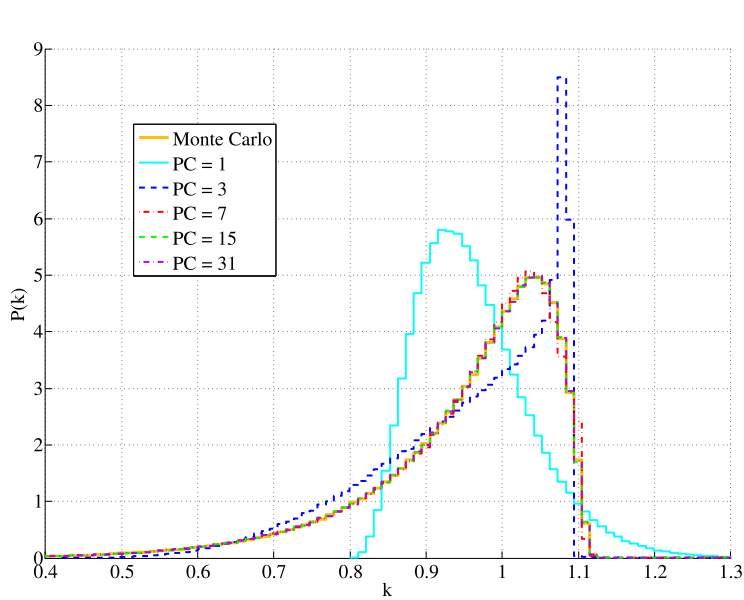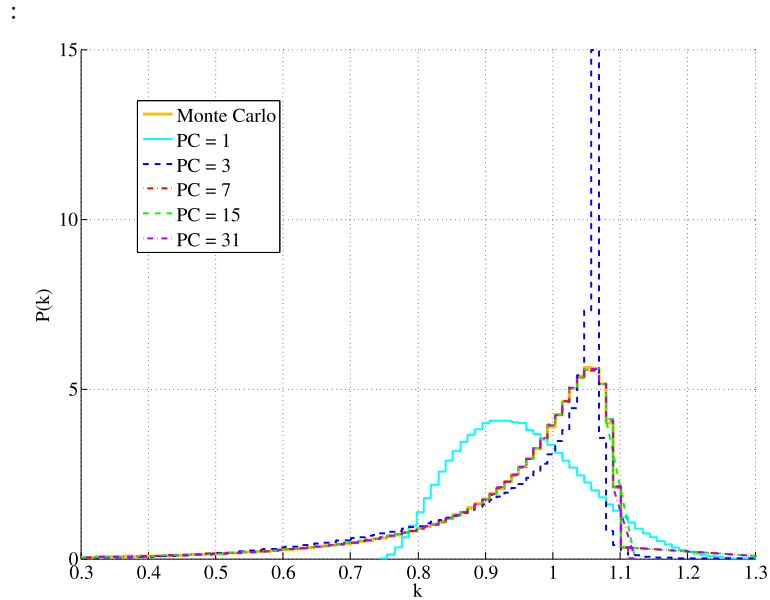

Figure 6.7: PDF of the k-eigenvalue: Jacobi Chaos expansion of the Beta Distribution ($\frac{\sqrt{v_\sigma}}{\langle\sigma\rangle} = \frac{1}{\sqrt{5}}$)

M	2	4	8	16	32
PC					
0	9.9048926e-01	9.9024514e-01	9.9024506e-01	9.9024519e-01	9.9024514e-01
1	7.4834610e-02	7.7446692e-02	7.7447096e-02	7.7447138e-02	7.7447142e-02
2	–	-1.9970666e-02	-1.9976612e-02	-1.9976831e-02	-1.9976745e-02
3	–	3.8271161e-03	3.8974476e-03	3.8973630e-03	3.8973713e-03
4	–	–	-6.3352402e-04	-6.3354386e-04	-6.3359736e-04
5	–	–	8.7652225e-05	8.7562341e-05	8.7546595e-05
6	–	–	-1.0000429e-05	-9.8359568e-06	-9.8723376e-06
7	–	–	8.2906323e-07	9.0514046e-07	9.2006423e-07
8	–	–	–	6.0098411e-08	1.5379122e-07
9	–	–	–	5.9547242e-08	-4.7999585e-08
10	–	–	–	1.5888445e-08	-5.3018272e-08
11	–	–	–	-2.4264053e-07	-1.4885961e-07
12	–	–	–	-1.3932848e-07	-3.6822944e-08
13	–	–	–	-2.2772697e-07	-1.0147724e-07
14	–	–	–	-1.1314019e-08	-1.4428400e-07
15	–	–	–	2.4933391e-07	4.4898787e-08
stdev	4.3205783e-02	4.5620039e-02	4.5622135e-02	4.5622177e-02	4.5622172e-02

Table 6.9: Uniform Distribution: Legendre chaos coefficients and standard deviation of the k-eigenvalue calculated using M-dimensional Gauss-Legendre quadrature ($\frac{\sqrt{v_\sigma}}{\langle\sigma\rangle} = \frac{1}{5}$). The mean and standard deviation given by Monte Carlo are 9.9024757e-01 and 4.5642910e-02, respectively.

Figure 6.8: PDF of the k-eigenvalue: Legendre Chaos expansion of the Uniform Distribution ($\frac{\sqrt{v_\sigma}}{\langle\sigma\rangle} = \frac{1}{5}$)

M	2	4	8	16	32
PC					
0	9.4609085e-01	9.3863470e-01	9.3868757e-01	9.3868753e-01	9.3868753e-01
1	1.9826274e-01	2.3779240e-01	2.3768979e-01	2.3768991e-01	2.3768991e-01
2	−	-1.3622486e-01	-1.3663493e-01	-1.3663512e-01	-1.3663513e-01
3	−	5.3841896e-02	5.7784918e-02	5.7784809e-02	5.7784861e-02
4	−	−	-1.9372933e-02	-1.9371860e-02	-1.9371855e-02
5	−	−	4.9475895e-03	4.9401349e-03	4.9400463e-03
6	−	−	-7.0918450e-04	-6.7864940e-04	-6.7875303e-04
7	−	−	-9.8700897e-05	-1.8911494e-04	-1.8918880e-04
8	−	−	−	2.0139181e-04	2.0154512e-04
9	−	−	−	-1.0199455e-04	-1.0188037e-04
10	−	−	−	3.8285453e-05	3.8252275e-05
11	−	−	−	-1.1053492e-05	-1.1033282e-05
12	−	−	−	1.9252220e-06	2.1341570e-06
13	−	−	−	5.6814130e-08	1.6997990e-07
14	−	−	−	-3.3195335e-07	-5.3813780e-07
15	−	−	−	3.6792861e-07	4.8149779e-08
stdev	1.1446705e-01	1.5157172e-01	1.5194389e-01	1.5194395e-01	1.5194395e-01

Table 6.10: Uniform Distribution: Legendre chaos coefficients and standard deviation of the k-eigenvalue calculated using M-dimensional Gauss-Legendre quadrature ($\frac{\sqrt{v_\sigma}}{\langle\sigma\rangle} = \frac{1}{\sqrt{5}}$). The mean and standard deviation given by Monte Carlo are 9.3865797e-01 and 1.5201495e-01, respectively.

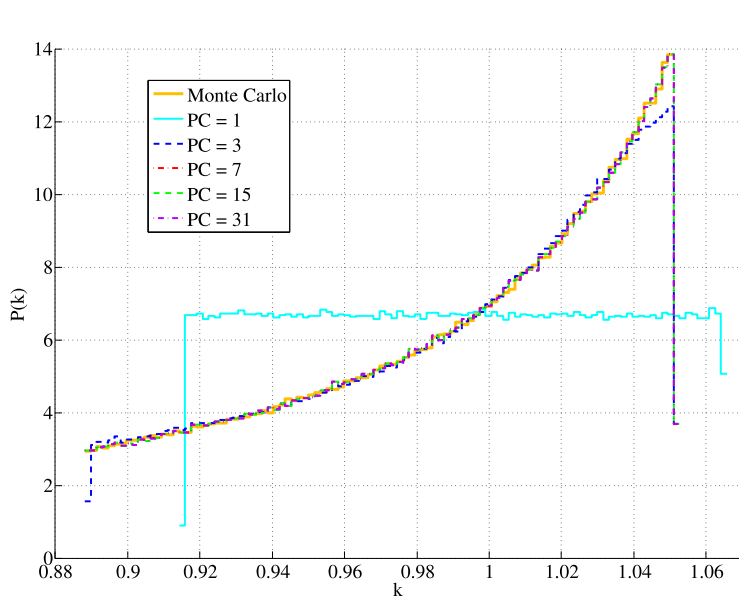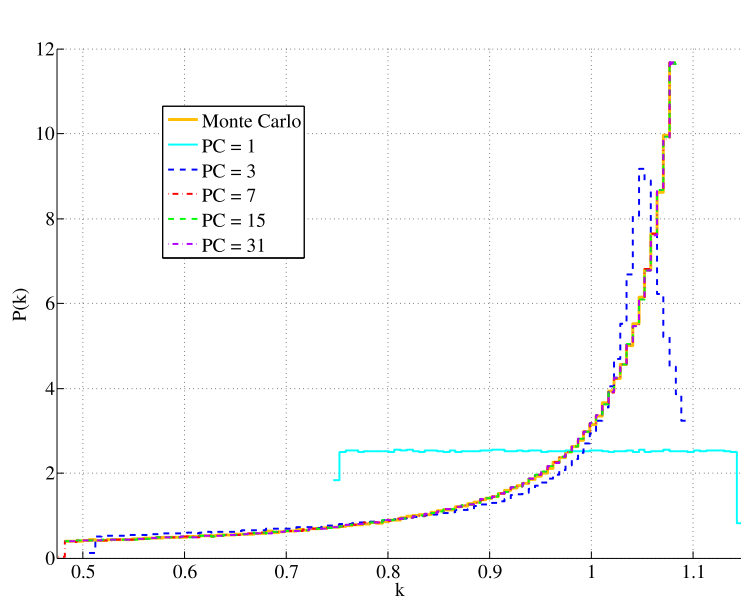Figure 6.9: PDF of the k-eigenvalue: Legendre Chaos expansion of the Uniform Distribution ($\frac{\sqrt{v_\sigma}}{\langle\sigma\rangle} = \frac{1}{\sqrt{5}}$)

Distribution	Normal	Gamma		Beta		Uniform	
	$\frac{\sqrt{v_\sigma}}{\langle\sigma\rangle}=\frac{1}{5}$	$\frac{\sqrt{v_\sigma}}{\langle\sigma\rangle}=\frac{1}{5}$	$\frac{\sqrt{v_\sigma}}{\langle\sigma\rangle}=\frac{1}{\sqrt{5}}$	$\frac{\sqrt{v_\sigma}}{\langle\sigma\rangle}=\frac{1}{5}$	$\frac{\sqrt{v_\sigma}}{\langle\sigma\rangle}=\frac{1}{\sqrt{5}}$	$\frac{\sqrt{v_\sigma}}{\langle\sigma\rangle}=\frac{1}{5}$	$\frac{\sqrt{v_\sigma}}{\langle\sigma\rangle}=\frac{1}{\sqrt{5}}$
PC Order							
1	0.413364	0.386870	0.268801	0.414601	0.303021	0.435864	0.363985
3	0.509628	0.477960	0.435462	0.506159	0.494431	0.501563	0.520201
7	0.500329	0.473100	0.441543	0.499182	0.467738	0.499945	0.499794
15	0.500498	0.473130	0.440362	0.499199	0.467479	0.499946	0.499908
31	0.500417	0.470020	0.440672	0.499199	0.467480	0.499946	0.499908
MC	0.500056	0.471200	0.440901	0.501520	0.468840	0.500370	0.500373

Table 6.11: Probability that $k > 1$ for various PC orders and Cross Section Distributions as computed by (P+1)-dimensional Gaussian Quadrature and Monte Carlo

6.2 The Fission Cross Section as a Random Process

6.2.1 Modeling a Critical Reactor with Uncertain Fuel Density

We now consider a reactor assembly in which the fuel enrichment contains some uncertainty, although the analysis could easily be extended to accomodate uncertainties in the number density or microscopic cross section. The test case is a reactor modeled in one-dimension as a single assembly, consisting of a uranium dioxide fuel pin surrounded by a light water moderator of equal thickness on each side, with periodic boundary conditions. The uranium is enriched to $1^w/_o$ ^{235}U on average, and the remainer of the uranium is ^{238}U. It is assumed that the enrichment varies randomly within the pin, thus the macroscopic cross section also varies as a function of space and the pin material itself appears to be stochastic. The weight percent of ^{235}U, w_{235}, is assumed to be a second-order Gaussian random process with covariance kernel C_w and expectation value $E\left[w_{235}(x)\right] = \langle w_{235}(x)\rangle$. For notational clarity, a zero-mean 'random part,' $\tilde{w}_{235}(x,\omega) = w_{235}(x,\omega) - \langle w_{235}(x)\rangle$, is defined. The number density

is then the expanded in the following KL expansion:

$$w_{235}(x,\omega) = \langle w_{235}(x) \rangle + \sum_{k=1}^{K} \sqrt{\lambda_k} \phi_k(x) \xi_k(\omega) \tag{6.13}$$

where the expansion is truncated at order k. The exponential kernel is again used to represent the covariance (equation 3.1).

In order to study the effect that stochasticity has on the criticality of the system, a critical system is created by manually adjusting the dimensions of the fuel pins through trial and error. Then, by setting the mean of the fission cross section to the critical value, it is possible to explore the effect that variability in the fuel enrichment has on k for various variances. Among the quantities of interest are the moments and pdfs of the k-eigenvalues, which are computed using SCM.

6.2.2 Numerical Results

The critical size of the system, with periodic boundary conditions, was found to be $L = 0.37400115$ cm UO_2 enriched to $1^w/_o$ ^{235}U with 3.0 cm of water on either side. The weight percent ^{235}U was expanded in a KL expansion with standard deviations, σ_w, of $0.05^w/_o$, $0.10^w/_o$ and $0.20^w/_o$ and correlation lengths of L cm, $0.5L$ cm, $0.1L$ cm and $0.05L$ cm. The macroscopic cross sections for the water reflector were taken to be $\sigma_f = 0.0$ cm^{-1}, $\sigma_\gamma = 0.022211$ cm^{-1} and $\sigma_t = 2.1667$ cm^{-1}. The data used for Uranium is shown in Table 6.12.

	^{238}U	^{235}U
M (g/mole)	238.0507847	235.0439242
ν	2.492088	2.436700
σ_f (barns)	1.680824E-5	585.2935
σ_γ (barns)	2.684817	98.75446
σ_t (barns)	11.98424	699.1633

Table 6.12: Test Problem Parameters: Uranium

The PC coefficients of the k-eigenvalue were computed using SCM with M $= (P+1)$ for each random variable. Pdfs were then generated by sampling the Gaussian random variables 10^6 times and using the sampled values to compute k from its PC expansion. Figure 6.10 shows the PDF of k-eigenvalues for $\lambda_c = L$, $\lambda_c = 0.5L$, $\lambda_c = 0.1L$ and $\lambda_c = 0.05L$ for various σ_w. In all cases, KL $= 5$ and P $= 3$, for which the pdfs were found to be converged. As can be seen, the distributions are slightly skewed, with peaks at $k > 1$, but falling off more quickly on the right than the left. This effect is most noticeable for $\sigma_w = 0.20^w/_o$. As would be expected, for larger standard deviations, the distribution is more spread out, so the probability of k departing from unity in either direction is larger. As the correlation length gets larger, the distribution also becomes more spread out.

From the same set of data, it is possible to generate the probability that the reactor will be supercritical, with results shown in Table 6.13 for various standard deviations and correlation lengths for various KL and PC orders. The model predicts that the reactor will be supercritical approximately 50% of the time in all cases. This number is essentially unaffected by the standard deviation of the enrichment or the correlation length, although, as mentioned before, the distributions vary drastically between these various cases. Since the enrichment and, by extension, the macroscopic cross section are Gaussian random processes, they are distributed according to the Gaussian distribution, which is symmetric, at each point in space. Given the symmetry of the representation, the fact that the pdfs of k are essentially symmetric about unity and that $P(k > 1) \approx 0.5$ is not entirely surprising.

The mean and standard deviation of the k-eigenvalues computed using the PC expansion of k are shown in Table 6.14. The mean and standard deviation of k are shown for $\lambda_c = L$, $\lambda_c = 0.5L$, $\lambda_c = 0.1L$ and $\lambda_c = 0.05L$, and the PC coefficients for a PC order of P are computed using a Gauss-Hermite quadrature of order M $= (P+1)$. As can be seen, the mean is essentially converged for P $= 1$ for $\lambda_c = 0.05L$ and

(a) $\lambda_c = L$

(b) $\lambda_c = 0.5L$

(c) $\lambda_c = 0.1L$

(d) $\lambda_c = 0.05L$
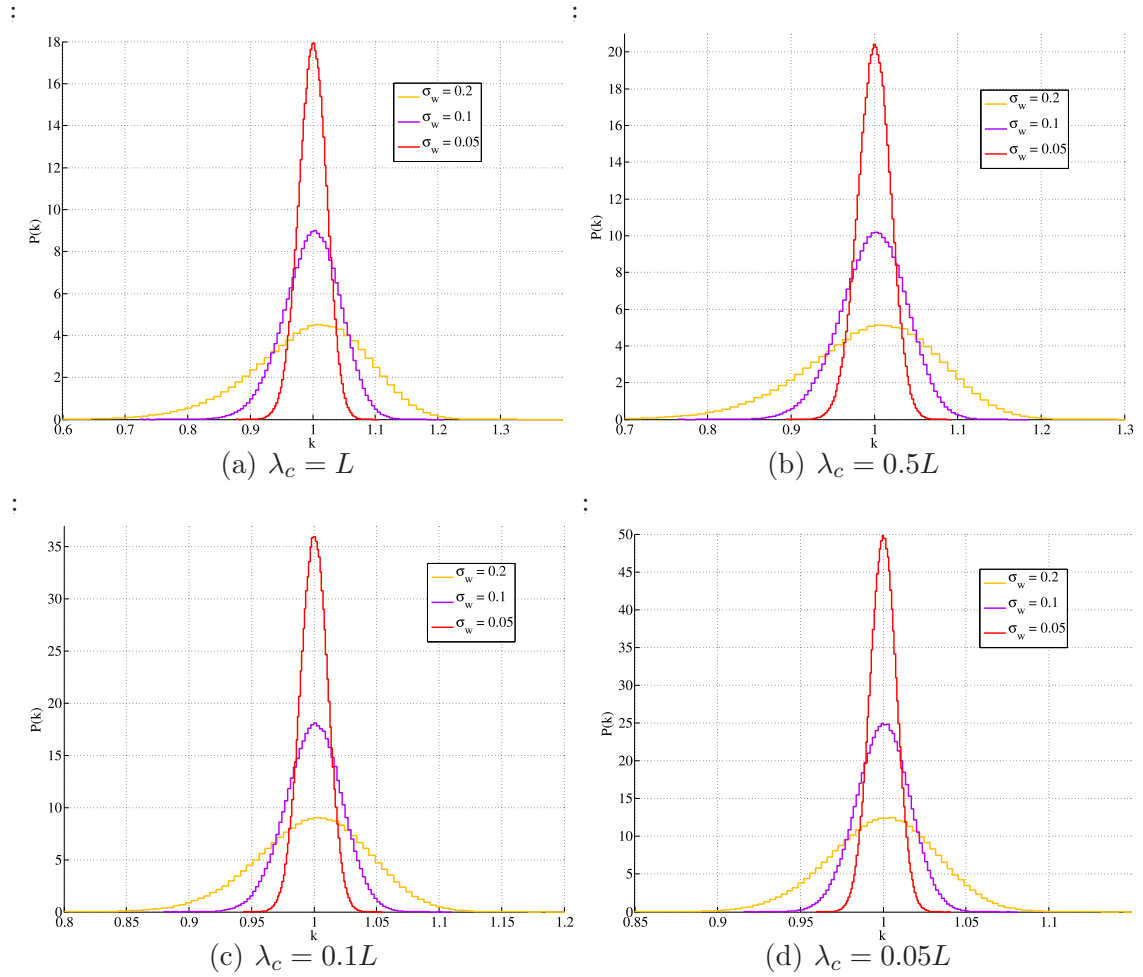
Figure 6.10: PDF of k-eigenvalues (KL = 5, P = 3)

KL	PC \ σ_w \ λ_c	1			3			5		
		0.20	0.10	0.05	0.20	0.10	0.05	0.20	0.10	0.05
1	L	0.467633	0.483968	0.492239	0.501149	0.500569	0.500497	0.500462	0.500488	0.500489
	$0.5L$	0.471583	0.485961	0.493238	0.500931	0.500537	0.500494	0.500475	0.500488	0.500489
	$0.1L$	0.484527	0.492517	0.496494	0.500556	0.500495	0.500489	0.500488	0.500489	0.500489
	$0.05L$	0.489208	0.494930	0.497670	0.500509	0.500489	0.500489	0.500489	0.500489	0.500489
3	L	0.467959	0.484138	0.492258	0.501638	0.500812	0.500619	0.500919	0.500719	0.500603
	$0.5L$	0.472129	0.486320	0.493289	0.501542	0.500782	0.500564	0.501049	0.500724	0.500560
	$0.1L$	0.485034	0.492556	0.496396	0.501363	0.500763	0.500497	0.501260	0.500755	0.500496
	$0.05L$	0.489235	0.494686	0.497386	0.500977	0.500545	0.500352	0.500951	0.500542	0.500351
5	L	0.467969	0.484127	0.492268	0.501681	0.500811	0.500629	0.499917	0.499714	0.499607
	$0.5L$	0.472140	0.486350	0.493359	0.501505	0.500759	0.500509	0.500195	0.499849	0.499654
	$0.1L$	0.485360	0.492840	0.496645	0.501687	0.501046	0.500744	0.500932	0.500370	0.500098
	$0.05L$	0.489675	0.495018	0.497714	0.501405	0.500916	0.500660	0.500760	0.500257	0.499982

Table 6.13: Probability that $k > 1$

$\lambda_c = 0.1L$, but P = 3 is required when $\lambda_c = 0.5L$ and $\lambda_c = L$. Given the fact that the pdfs of k are more spread out for larger λ_c, this result is to be expected. Also, the standard deviation does not converge as quickly as the mean, requiring P = 3 for smaller λ_cs. The standard deviation in k also increases with σ_w, as can been seen in the pdf graphs.

λ_c	σ_w	P = 1	P = 3	P = 5
	0.20	0.992705	0.992601	0.992601
		0.0899584	0.0918768	0.0918798
L	0.10	0.998184	0.9981781	0.998178
		0.0447627	0.0449926	0.0449927
	0.05	0.999547	0.999546	0.999546
		0.0223544	0.0223828	0.0223828
	0.20	0.994444	0.994383	0.994383
		0.0789263	0.0802071	0.0802085
$0.5L$	0.10	0.998615	0.998611	0.998611
		0.0393231	0.0394783	0.0394783
	0.05	0.999654	0.999654	0.999654
		0.0196440	0.0196633	0.0196633
	0.20	0.998326	0.998321	0.998321
		0.0442899	0.0444983	0.0444983
$0.1L$	0.10	0.999582	0.999581	0.999581
		0.0221200	0.0221458	0.0221458
	0.05	0.999895	0.999895	0.999895
		0.0110569	0.0110601	0.0110601
	0.20	0.999134	0.999133	0.999133
		0.0320465	0.0321210	0.0321210
$0.05L$	0.10	0.999784	0.999784	0.999784
		0.0160127	0.0160220	0.0160220
	0.05	0.999946	0.999946	0.999946
		0.00800502	0.00800618	0.00800618

Table 6.14: $< k >$ (top) and $\sigma_{<k>}$ (bottom): KL=5

Chapter 7

Conclusions and Future Work

The Stochastic Finite Element Method (SFEM) and Stochastic Collocation Method (SCM) have been used in a variety of fields to apply PC expansions to uncertainty quantification. The work conducted here is a preliminary examination of the effectiveness and efficiency of these methods when applied to uncertainty quantification in radiation transport. Two types of problems were explored: Those in which the uncertain inputs are functions of single random variables, uniform in space, and those in which the uncertain inputs are random processes, varying in space. In all cases, the SCM and SFEM were shown to yield accurate results in comparison with Monte Carlo or analytic solutions. In the single random variable case, the SCM was shown to be much more efficient than the SFEM, yielding comparable results for $M = (P + 1)$ at a fraction of the cost. The SCM becomes increasingly more efficient than SFEM as the number of PC terms in the expansion increases. In addition, the SCM requires a series of *independent* deterministic transport computations and can therefore be 'wrapped around' an existing transport code, requiring no modification to the tranport computation itself. SFEM, on the other hand, produces a coupled system of transport equations and its solution requires an entirely new algorithm. Furthermore, SFEM is plagued with convergence issues when an unphysical distri-

bution such as a Gaussian is used to represent a strictly positive parameter. While the extra work associated with the SFEM in comparison with the SCM is clearly not worthwhile when there is only one random variable, it was shown that when used in concert with a Karhunen-Lòeve (KL) representation of a spatially varying cross section, the SFEM becomes increasingly more efficient as the number of random variables increases. This is due to the fact that the number of terms in the PC expansion, hence the number of coupled SFEM equations, does not increase as rapidly as the number of terms in the quadrature tensor product. This additional cost may be offset somewhat by the use of sparse grid quadratures [89] for higher dimensions (they can require more function evaluations than a tensor product to achieve the same accuracy for smaller dimensions), a topic for future research. This is particularly important when the distribution is Gaussian because SFEM will be unstable for higher PC orders.

In multiplying media, a Newton-Krylov iteration is required to compute the SFEM solution since the presence of the k-eigenvalue makes the equations non-linear. As was shown, this iteration must be carefully initialized using SCM or Monte Carlo, and even a single Newton-Krylov iteration is far more time-consuming than an SCM initialization, which can achieve a high level of accuracy quite cheaply. In addition, the effort required to write an entirely new code to conduct the computation renders the method somewhat less attractive. In radiation transport problems, multiplying materials are frequently present, so SCM would seem to be the method of choice for general application.

Many interesting research topics remain. Multiple random variables were incorporated using a KL expansion to represent the cross section, but this method is limited since the expansion is only strictly correct when the random variables in the expansion are Gaussian. Other random processes can be represented using transforms which allow them to be represented using Gaussian random variables. This

was demonstrated for log-normal random processes, for which the transformation is obvious, but could be applied to other distributions. Given the problems associated with using Gaussian random variables, a new method for representing stochastic random processes would also be a welcome (and nontrivial) development. Another interesting case that should be examined is uncertain inputs that can be represented using independent single random variables. The output would still be a function of each of these random variables and solution would proceed in the same manner as it did when the KL expansion was utilized.

In small scale applications for independent, uncorrelated random variables, such as those explored, the use of PC expansions is efficient and effective. The advantage to using PC expansions to represent problem outputs is that those quantities can be completely characterized using the PC moments. Thus, a relatively small dataset contains all of the information necessary to construct pdfs and cdfs, define responses of specific outputs to inputs, and compute statistical moments. In short, it is capable of producing the same results as the sampling-based approaches typically employed in nuclear applications for uncertainty quantification. The disadvantage is that, in order to extract anything more than the moments of the output, it is necessary to sample the random variables involved. Thus post-processing can be quite computationally demanding, although not as demanding as conducting a Monte Carlo simulation on the entire system. Furthermore, computationally demanding analyses such as risk assessments for nuclear reactors and the Department of Energy's nuclear waste repository in Yucca Mountain can require 10s to 100s of uncertain inputs, which may in addition be correlated [90]. As the number of dimensions increases, the number of quadrature points required by SCM and the number of terms in the PC expansion increase rapidly—e.g., if there are 100 random variables and a (small) PC order of 5 is used, there are more than 96.5 million PC coefficients in the expansion! Indeed, it may be that an optimized multi-dimensional sampling method such as Latin Hypercube, which is already in widespread use for problems of this sort, may

be more efficient than SCM for large-scale applications. It would be enlightening to conduct an analysis on a real-world system of this scale.

Appendices

Appendix A

Orthogonal Polynomials and Gaussian Quadrature

Polynomial Chaos (PC) expansions, which play a key role in this research, represent random parameters as expansions in terms of orthogonal polynomials written in terms of random variables. The theory of Gaussian quadrature, which also plays a prominent part, relies heavily on orthogonal polynomials. A system of polynomials $\{Q_n(x), n \in \mathcal{N}\}$, where $\mathcal{N} = \{0, 1, 2, \ldots\}$, is orthogonal with respect to $\rho(x)$ if

$$\int_{\mathcal{S}} Q_n(x) Q_m(x) \rho(x) dx = d_n^2 \delta_{mn}, \quad n, m \in \mathcal{N}. \tag{A.1}$$

All such orthogonal polynomials on the real line satisfy the following three-term recurrence relation:

$$-x Q_n(x) = b_n Q_{n+1}(x) + \gamma_n Q_n(x) + c_n Q_{n-1}(x), \ n \geq 1 \tag{A.2}$$

where $b_n, c_n \neq 0$ and $c_n/b_{n-1} > 0$. Hypergeometric differential equations of the form

$$s(x) y'' + \tau(x) y' + \lambda y = 0 \tag{A.3}$$

have as their solutions functions of the hypergeometric type. If

$$\lambda = \lambda_n = -n\tau' - \frac{1}{2} n(n-1) s'', \tag{A.4}$$

then the solutions of Eq. A.3, $y(x) = y_n(x)$ for integer n, are polynomials of degree n which form an orthogonal set that satisfies Eq. A.1 where

$$(s(x)\rho(x))' = \tau(x)\rho(x). \tag{A.5}$$

These polynomials are known as the classical orthogonal polynomials of a continuous variable and include the Bessel, Romanovski, Jacobi, Laguerre and Hermite families of polynomials [91].

Gaussian quadrature rules approximate integrals using a finite number of function evaluations which are then multiplied by appropriate weights and summed:

$$\int_a^b w(x)f(x)dx \approx \sum_{m=1}^M w_m f(x_m) \tag{A.6}$$

where $w(x)$ is a weight function and the w_m and x_m are the quadrature weights and abscissas, respectively. The abscissas of a Gaussian quadrature of order M in the interval (a, b) with weight function $w(x)$ are simply the M roots of an orthogonal polynomial of degree M, which also lie in the interval (a, b). The appropriate set of orthogonal polynomials satisfies the relation:

$$\int_a^b w(x)p_i(x)p_j(x)dx = \delta_{ij}.$$

The weights are then given by:

$$w_m = \frac{\langle p_{M-1}, p_{M-1}\rangle}{p_{M-1}(x_m)p'_M(x_m)} \tag{A.7}$$

where

$$\langle f, g \rangle = \int_a^b w(x)f(x)g(x)dx.$$

This ensures that the integrals of the first M polynomials multiplied by the weight function will be exact. Furthermore, it can be shown that the integrals of the next $(M - 1)$ polynomials are also exact, thus a Gaussian quadrature of order M will approximate a polynomial of degree $(2M - 1)$ exactly [92].

Appendix B

Diffusion Analysis for the Karhunen-Lòeve Expansion of the Cross Section

B.1 Gaussian Random Process

B.1.1 Variance scaled as $\mathcal{O}\left(\frac{1}{\epsilon^2}\right)$

Applying the diffusion scalings given in Eq. 3.25, setting

$$v_\sigma \sim \mathcal{O}\left(\frac{1}{\epsilon^2}\right)$$

and applying the flux expansion

$$\psi(x,\mu) = \sum_{m=0}^{\infty} \epsilon^m \psi^{(m)}(x,\mu)$$

Appendix B. Diffusion Analysis for the Karhunen-Lòeve Expansion of the Cross Section

to the transport equation (Eq. 2.1) yields:

$$\mu \sum_{m=0}^{\infty} \epsilon^m \frac{\partial \psi^{(m)}}{\partial x} + \frac{1}{\epsilon}\left(\langle \tilde{\sigma} \rangle + \sqrt{\tilde{v}_\sigma}\rho(x,\omega)\right) \times$$

$$\left(\sum_{m=0}^{\infty} \epsilon^m \psi^{(m)} - \frac{1-(1-c)\epsilon^2}{2}\sum_{m=0}^{\infty}\epsilon^m \phi^{(m)}\right) = \epsilon \tilde{Q}(x,\mu). \quad \text{(B.1)}$$

where

$$\rho(x,\omega) = \sum_{k=1}^{\infty} \sqrt{\gamma_k}\varphi_k(x)\xi_k(\omega)$$

and $\gamma_k = \frac{\lambda_k}{\tilde{v}_\sigma}$ (see Eq. 3.12). Multiplying through by ϵ then yields:

$$\mu \sum_{m=0}^{\infty} \epsilon^{m+1}\frac{\partial \psi^{(m)}}{\partial x} + \sigma(x,\omega)\left(\sum_{m=0}^{\infty}\epsilon^m \psi^{(m)} - \frac{1-(1-c)\epsilon^2}{2}\sum_{m=0}^{\infty}\epsilon^m \phi^{(m)}\right) = \epsilon^2 \tilde{Q}(x,\mu)$$

$$\text{(B.2)}$$

where the stochastic cross section is written as one term,

$$\sigma(x,\omega) = \left(\langle \tilde{\sigma} \rangle + \sqrt{\tilde{v}_\sigma}\rho(x,\omega)\right),$$

since its two parts are scaled in the same way.

We now look at the equation for each order of epsilon:

$\mathcal{O}(1)$:

$$\sigma(x,\omega)\left(\psi^{(0)} - \frac{1}{2}\phi^{(0)}\right) = 0$$

$$\psi^{(0)} = \frac{1}{2}\phi^{(0)} \qquad\qquad\qquad \text{(B.3)}$$

$\mathcal{O}(\epsilon)$:

$$\mu\frac{\partial \psi^{(0)}}{\partial x} + \sigma(x,\omega)\left(\psi^{(1)} - \frac{1}{2}\phi^{(1)}\right) = 0$$

Apply Eq. B.3:

$$\frac{\mu}{2}\frac{\partial \phi^{(0)}}{\partial x} + \sigma(x,\omega)\left(\psi^{(1)} - \frac{1}{2}\phi^{(1)}\right) = 0$$

$$\psi^{(1)} = \frac{1}{2}\phi^{(1)} - \frac{\mu}{2\sigma(x,\omega)}\frac{\partial \phi^{(0)}}{\partial x} \tag{B.4}$$

$\mathcal{O}(\epsilon^2):$

$$\mu\frac{\partial \psi^{(1)}}{\partial x} + \sigma(x,\omega)\left(\psi^{(2)} - \frac{1}{2}\phi^{(2)} + \frac{1-c}{2}\phi^{(0)}\right) = \frac{\tilde{Q}}{2}$$

Apply Eq. B.4:

$$\frac{\mu}{2}\frac{\partial \phi^{(1)}}{\partial x} - \frac{\mu^2}{2\sigma(x,\omega)}\frac{\partial^2 \phi^{(0)}}{\partial x^2} + \sigma(x,\omega)\left(\psi^{(2)} - \frac{1}{2}\phi^{(2)} + \frac{1-c}{2}\phi^{(0)}\right) = \frac{\tilde{Q}}{2}$$

Integrate over μ:

$$-\frac{1}{3\sigma(x,\omega)}\frac{\partial^2 \phi^{(0)}}{\partial x^2} + (1-c)\sigma(x,\omega)\phi^{(0)} = \frac{1}{2}\int_{-1}^{1} d\mu \cdot \tilde{Q}(x,\mu) \tag{B.5}$$

So, finally, a stochastic diffusion equation is achieved:

$$-D(x,\omega)\frac{\partial^2 \phi(x)}{\partial x^2} + \sigma_a(x,\omega)\phi(x) = \frac{1}{2}\int_{-1}^{1} d\mu \cdot Q(x,\mu) \tag{B.6}$$

where $D(x,\omega) = \frac{1}{3\sigma(x,\omega)}$ and $\sigma_a(x,\omega) = (1-c)\sigma(x,\omega)$.

B.1.2   Variance scaled as $\mathcal{O}\left(\frac{1}{\epsilon}\right)$

Applying the diffusion scalings given in Eq. 3.25, setting

$$v_\sigma \sim \mathcal{O}\left(\frac{1}{\epsilon}\right)$$

and applying the flux expansion

$$\psi(x,\mu) = \sum_{m=0}^{\infty} \epsilon^{\frac{m}{2}}\psi^{(m)}(x,\mu)$$

to the transport equation (Eq. 2.1) yields:

$$\mu \sum_{m=0}^{\infty} \epsilon^{\frac{m}{2}} \frac{\partial \psi^{(m)}}{\partial x} + \left(\frac{\langle \tilde{\sigma} \rangle}{\epsilon} + \frac{\sqrt{\tilde{v}_\sigma}}{\sqrt{\epsilon}} \rho(x,\omega) \right) \times$$

$$\left(\sum_{m=0}^{\infty} \epsilon^{\frac{m}{2}} \psi^{(m)} - \frac{1 - (1-c)\epsilon^2}{2} \sum_{m=0}^{\infty} \epsilon^{\frac{m}{2}} \phi^{(m)} \right) = \epsilon \tilde{Q}(x, \mu). \quad \text{(B.7)}$$

where

$$\rho(x, \omega) = \sum_{k=1}^{\infty} \sqrt{\gamma_k} \varphi_k(x) \xi_k(\omega)$$

and $\gamma_k = \frac{\lambda_k}{\tilde{v}_\sigma}$ (see Eq. 3.12). Multiplying through by ϵ then yields:

$$\mu \sum_{m=0}^{\infty} \epsilon^{\frac{m}{2}+1} \frac{\partial \psi^{(m)}}{\partial x} + \left(\langle \tilde{\sigma} \rangle + \sqrt{\epsilon \tilde{v}_\sigma} \rho(x,\omega) \right) \times$$

$$\left(\sum_{m=0}^{\infty} \epsilon^{\frac{m}{2}} \psi^{(m)} - \frac{1 - (1-c)\epsilon^2}{2} \sum_{m=0}^{\infty} \epsilon^{\frac{m}{2}} \phi^{(m)} \right) = \epsilon^2 \tilde{Q}(x, \mu) \quad \text{(B.8)}$$

We now look at the equation for each order of epsilon:

$\mathcal{O}(\mathbf{1}):$

$$\langle \tilde{\sigma} \rangle \left(\psi^{(0)} - \frac{1}{2} \phi^{(0)} \right) = 0$$

$$\psi^{(0)} = \frac{1}{2} \phi^{(0)} \tag{B.9}$$

$\mathcal{O}(\epsilon^{\frac{1}{2}}):$

$$\langle \tilde{\sigma} \rangle \left(\psi^{(1)} - \frac{1}{2} \phi^{(1)} \right) + \sqrt{\tilde{v}_\sigma} \rho \left(\psi^{(0)} - \frac{1}{2} \phi^{(0)} \right) = 0$$

$$\psi^{(1)} = \frac{1}{2} \phi^{(1)} \tag{B.10}$$

$\mathcal{O}(\epsilon):$

$$\mu \frac{\partial \psi^{(0)}}{\partial x} + \langle \tilde{\sigma} \rangle \left(\psi^{(2)} - \frac{1}{2} \phi^{(2)} \right) + \sqrt{\tilde{v}_\sigma} \rho \left(\psi^{(1)} - \frac{1}{2} \phi^{(1)} \right) = 0$$

Apply Eqs. B.9 and B.10:

$$\mu \frac{\partial \psi^{(0)}}{\partial x} + \langle \tilde{\sigma} \rangle \left(\psi^{(2)} - \frac{1}{2} \phi^{(2)} \right) = 0$$

$$\psi^{(2)} = \frac{1}{2} \phi^{(2)} - \frac{\mu}{2 \langle \tilde{\sigma} \rangle} \frac{\partial \phi^{(0)}}{\partial x} \tag{B.11}$$

$\mathcal{O}(\epsilon^{\frac{3}{2}})$:

$$\mu \frac{\partial \psi^{(1)}}{\partial x} + \langle \tilde{\sigma} \rangle \left(\psi^{(3)} - \frac{1}{2} \phi^{(3)} \right) + \sqrt{\tilde{v}_{\sigma}} \rho \left(\psi^{(2)} - \frac{1}{2} \phi^{(2)} \right) = 0$$

Apply Eqs. B.10 and B.11:

$$\frac{\mu}{2} \frac{\partial \phi^{(1)}}{\partial x} + \langle \tilde{\sigma} \rangle \left(\psi^{(3)} - \frac{1}{2} \phi^{(3)} \right) + \sqrt{\tilde{v}_{\sigma}} \rho \left(\frac{1}{2} \phi^{(2)} - \frac{\mu}{2 \langle \tilde{\sigma} \rangle} \frac{\partial \phi^{(0)}}{\partial x} - \frac{1}{2} \phi^{(2)} \right) = 0$$

$$\psi^{(3)} = \frac{1}{2} \phi^{(3)} - \frac{\mu}{2 \langle \tilde{\sigma} \rangle} \frac{\partial \phi^{(1)}}{\partial x} + \sqrt{\tilde{v}_{\sigma}} \rho \frac{\mu}{2 \langle \tilde{\sigma} \rangle} \frac{\partial \phi^{(0)}}{\partial x}$$

$$\tag{B.12}$$

$\mathcal{O}(\epsilon^2)$:

$$\mu \frac{\partial \psi^{(2)}}{\partial x} + \langle \tilde{\sigma} \rangle \left(\psi^{(4)} - \frac{1}{2} \phi^{(4)} \right) + \sqrt{\tilde{v}_{\sigma}} \rho \left(\psi^{(3)} - \frac{1}{2} \phi^{(3)} \right) + \frac{1-c}{2} \phi^{(0)} = \frac{\tilde{Q}}{2}$$

Apply Eqs. B.11 and B.12:

$$\frac{\mu}{2} \frac{\partial \phi^{(2)}}{\partial x} - \frac{\mu^2}{2 \langle \tilde{\sigma} \rangle} \frac{\partial^2 \phi^{(0)}}{\partial x^2} + \langle \tilde{\sigma} \rangle \left(\psi^{(4)} - \frac{1}{2} \phi^{(4)} + \frac{1-c}{2} \phi^{(0)} \right)$$

$$+ \sqrt{\tilde{v}_{\sigma}} \rho \left(\frac{1}{2} \phi^{(3)} - \frac{\mu}{2 \langle \tilde{\sigma} \rangle} \frac{\partial \phi^{(1)}}{\partial x} + \sqrt{\tilde{v}_{\sigma}} \rho \frac{\mu}{2 \langle \tilde{\sigma} \rangle} \frac{\partial \phi^{(0)}}{\partial x} - \frac{1}{2} \phi^{(3)} \right) = \frac{\tilde{Q}}{2}$$

Integrate over μ:

$$-\frac{1}{3 \langle \tilde{\sigma} \rangle} \frac{\partial^2 \phi^{(0)}}{\partial x^2} + (1-c) \langle \tilde{\sigma} \rangle \phi^{(0)} = \frac{1}{2} \int_{-1}^{1} d\mu \cdot \tilde{Q}(x, \mu) \tag{B.13}$$

So, finally, an analytic diffusion equation is achieved:

$$-\langle D \rangle \frac{\partial^2 \phi(x)}{\partial x^2} + \langle \sigma_a \rangle \phi(x) = \frac{1}{2} \int_{-1}^{1} d\mu \cdot Q(x, \mu) \tag{B.14}$$

B.2   Log-Normal Random Process

We begin with the cross section scalings given in Eqs. 3.33 and 3.36, which assume $v_\sigma \sim \mathcal{O}\left(\frac{1}{\epsilon}\right)$:

$$e^{\langle w(x) \rangle} = \frac{\langle \tilde{\sigma} \rangle}{\epsilon} \left(1 - \frac{\epsilon \tilde{y}}{2} + \frac{3(\epsilon \tilde{y})^2}{8} + \mathcal{O}(\epsilon^3) \right) \tag{B.15}$$

$$e^{\sqrt{v_w}\rho(x,\omega)} = 1 + \rho\sqrt{\epsilon \tilde{y}} + \frac{\rho^2}{2}\epsilon \tilde{y} + \left(\frac{\rho^3}{6} + \frac{\rho}{4} \right)(\epsilon \tilde{y})^{\frac{3}{2}} + \left(\frac{\rho^4 - 6\rho^2}{24} \right)(\epsilon \tilde{y})^2 + \mathcal{O}(\epsilon^{\frac{5}{2}}). \tag{B.16}$$

Substituting into the transport equation (Eq. 2.1) and applying the diffusion scalings given in Eq. 3.25 and the flux expansion

$$\psi(x, \mu) = \sum_{m=0}^{\infty} \epsilon^{\frac{m}{2}} \psi^{(m)}(x, \mu)$$

yields:

$$\mu \sum_{m=0}^{\infty} \epsilon^{\frac{m}{2}} \frac{\partial \psi^{(m)}}{\partial x} + \frac{\langle \tilde{\sigma} \rangle}{\epsilon} \left(1 - \frac{\epsilon \tilde{y}}{2} + \frac{3(\epsilon \tilde{y})^2}{8} + \mathcal{O}(\epsilon^3) \right) \times$$
$$\left(1 + \rho\sqrt{\epsilon \tilde{y}} + \frac{\rho^2}{2}\epsilon \tilde{y} + \left(\frac{\rho^3}{6} + \frac{\rho}{4} \right)(\epsilon \tilde{y})^{\frac{3}{2}} + \frac{\rho^4 - 6\rho^2}{24}(\epsilon \tilde{y})^2 + \mathcal{O}(\epsilon^{\frac{5}{2}}) \right) \times$$
$$\left(\sum_{m=0}^{\infty} \epsilon^{\frac{m}{2}} \psi^{(m)} - \frac{1 - (1-c)\epsilon^2}{2} \sum_{m=0}^{\infty} \epsilon^{\frac{m}{2}} \phi^{(m)} \right) = \epsilon \tilde{Q}(x, \mu). \tag{B.17}$$

Multiplying through by ϵ then yields:

$$\mu \sum_{m=0}^{\infty} \epsilon^{\frac{m}{2}+1} \frac{\partial \psi^{(m)}}{\partial x} + \langle \tilde{\sigma} \rangle \left(1 - \frac{\epsilon \tilde{y}}{2} + \frac{3(\epsilon \tilde{y})^2}{8} + \mathcal{O}(\epsilon^3) \right) \times$$
$$\left(1 + \rho\sqrt{\epsilon \tilde{y}} + \frac{\rho^2}{2}\epsilon \tilde{y} + \left(\frac{\rho^3}{6} + \frac{\rho}{4} \right)(\epsilon \tilde{y})^{\frac{3}{2}} + \frac{\rho^4 - 6\rho^2}{24}(\epsilon \tilde{y})^2 + \mathcal{O}(\epsilon^{\frac{5}{2}}) \right) \times$$
$$\left(\sum_{m=0}^{\infty} \epsilon^{\frac{m}{2}} \psi^{(m)} - \frac{1 - (1-c)\epsilon^2}{2} \sum_{m=0}^{\infty} \epsilon^{\frac{m}{2}} \phi^{(m)} \right) = \epsilon^2 \tilde{Q}(x, \mu). \tag{B.18}$$

We now look at the equation for each order of epsilon:

Appendix B. Diffusion Analysis for the Karhunen-Lòeve Expansion of the Cross Section

$\mathcal{O}(\mathbf{1})$:

$$\langle\tilde{\sigma}\rangle\left(\psi^{(0)} - \frac{1}{2}\phi^{(0)}\right) = 0$$

$$\psi^{(0)} = \frac{1}{2}\phi^{(0)} \qquad\qquad\qquad (\text{B.19})$$

$\mathcal{O}(\epsilon^{\frac{1}{2}})$:

$$\langle\tilde{\sigma}\rangle\left[\psi^{(1)} - \frac{1}{2}\phi^{(1)} + \rho\sqrt{\tilde{y}}\left(\psi^{(0)} - \frac{1}{2}\phi^{(0)}\right)\right] = 0$$

$$\psi^{(1)} = \frac{1}{2}\phi^{(1)} \qquad\qquad\qquad (\text{B.20})$$

$\mathcal{O}(\epsilon)$:

$$\mu\frac{\partial\psi^{(0)}}{\partial x} + \langle\tilde{\sigma}\rangle\left[\psi^{(2)} - \frac{1}{2}\phi^{(2)} + \rho\sqrt{\tilde{y}}\left(\psi^{(1)} - \frac{1}{2}\phi^{(1)}\right)\right.$$

$$\left. + \frac{(\rho^2 - 1)}{2}\tilde{y}\left(\psi^{(0)} - \frac{1}{2}\phi^{(0)}\right)\right] = 0$$

Apply Eqs. B.19 and B.20:

$$\mu\frac{\partial\psi^{(0)}}{\partial x} + \langle\tilde{\sigma}\rangle\left(\psi^{(2)} - \frac{1}{2}\phi^{(2)}\right) = 0$$

$$\psi^{(2)} = \frac{1}{2}\phi^{(2)} - \frac{\mu}{2\langle\tilde{\sigma}\rangle}\frac{\partial\phi^{(0)}}{\partial x} \qquad\qquad (\text{B.21})$$

$\mathcal{O}(\epsilon^{\frac{3}{2}})$:

$$\mu\frac{\partial\psi^{(1)}}{\partial x} + \langle\tilde{\sigma}\rangle\left[\psi^{(3)} - \frac{1}{2}\phi^{(3)} + \rho\sqrt{\tilde{y}}\left(\psi^{(2)} - \frac{1}{2}\phi^{(2)}\right)\right.$$

$$\left. + \frac{(\rho^2 - 1)}{2}\tilde{y}\left(\psi^{(1)} - \frac{1}{2}\phi^{(1)}\right) + \left(\frac{\rho^3}{6} - \frac{\rho}{4}\right)\tilde{y}^{\frac{3}{2}}\left(\psi^{(0)} - \frac{1}{2}\phi^{(0)}\right)\right] = 0$$

Apply Eqs. B.19, B.20 and B.21:

$$\frac{\mu}{2}\frac{\partial\phi^{(1)}}{\partial x} + \langle\tilde{\sigma}\rangle\left(\psi^{(3)} - \frac{1}{2}\phi^{(3)}\right) - \rho\sqrt{\tilde{y}}\frac{\mu}{2}\frac{\partial\phi^{(0)}}{\partial x} = 0$$

$$\psi^{(3)} = \frac{1}{2}\phi^{(3)} - \frac{\mu}{2\langle\tilde{\sigma}\rangle}\frac{\partial\phi^{(1)}}{\partial x} + \rho\sqrt{\tilde{y}}\frac{\mu}{2\langle\tilde{\sigma}\rangle}\frac{\partial\phi^{(0)}}{\partial x} \qquad (\text{B.22})$$

$\mathcal{O}(\epsilon^2)$:

$$
\mu\frac{\partial \psi^{(2)}}{\partial x} + \langle\tilde{\sigma}\rangle\left[\psi^{(4)} - \frac{1}{2}\phi^{(4)} + \rho\sqrt{\tilde{y}}\left(\psi^{(3)} - \frac{1}{2}\phi^{(3)}\right)\right.
$$
$$
+ \frac{(\rho^2 - 1)}{2}\tilde{y}\left(\psi^{(2)} - \frac{1}{2}\phi^{(2)}\right) + \left(\frac{\rho^3}{6} - \frac{\rho}{4}\right)\tilde{y}^{\frac{3}{2}}\left(\psi^{(1)} - \frac{1}{2}\phi^{(1)}\right)
$$
$$
\left. + \left(\frac{\rho^4}{24} - \frac{\rho^2}{2} + \frac{3}{8}\right)\tilde{y}^2\left(\psi^{(0)} - \frac{1}{2}\phi^{(0)}\right) + \frac{1-c}{2}\phi^{(0)}\right] = \frac{1}{2}\tilde{Q}
$$

Apply Eqs. B.19, B.20, B.21 and B.22:

$$
\frac{\mu}{2}\frac{\partial\phi^{(2)}}{\partial x} - \frac{\mu^2}{2\langle\tilde{\sigma}\rangle}\frac{\partial^2\phi^{(0)}}{\partial x^2} + \langle\tilde{\sigma}\rangle\left[\psi^{(4)} - \frac{1}{2}\phi^{(4)}\right.
$$
$$
+ \rho\sqrt{\tilde{y}}\left(\frac{1}{2}\phi^{(3)} - \frac{\mu}{2\langle\tilde{\sigma}\rangle}\frac{\partial\phi^{(1)}}{\partial x} + \rho\sqrt{\tilde{y}}\frac{\mu}{2\langle\tilde{\sigma}\rangle}\frac{\partial\phi^{(0)}}{\partial x} - \frac{1}{2}\phi^{(3)}\right)
$$
$$
\left. + \frac{(\rho^2 - 1)}{2}\tilde{y}\left(\frac{1}{2}\phi^{(2)} - \frac{\mu}{2\langle\tilde{\sigma}\rangle}\frac{\partial\phi^{(0)}}{\partial x} - \frac{1}{2}\phi^{(2)}\right) + \frac{1-c}{2}\phi^{(0)}\right] = \frac{1}{2}\tilde{Q}
$$

Integrate over μ:

$$
-\frac{1}{3\langle\tilde{\sigma}\rangle}\frac{\partial^2\phi^{(0)}}{\partial x^2} + (1-c)\langle\tilde{\sigma}\rangle\phi^{(0)} = \frac{1}{2}\int_{-1}^{1} d\mu \cdot \tilde{Q}(x,\mu) \tag{B.23}
$$

So, finally, an analytic diffusion equation is achieved:

$$
-\langle D\rangle\frac{\partial^2\phi(x)}{\partial x^2} + \langle\sigma_a\rangle\phi(x) = \frac{1}{2}\int_{-1}^{1} d\mu \cdot Q(x,\mu) \tag{B.24}
$$

Appendix C

Derivative of F with Respect to $\psi_{p,\ell}$

$$\frac{\partial F_{P+1,k}}{\partial \psi_{p,\ell}} = \frac{\partial}{\partial \psi_{p,\ell}} \left[\sum_{i=0}^{P} \sum_{j=0}^{P} \vec{\phi_i} \vec{\phi_j} e_{ijk} - \delta_{k0} \right] \tag{C.1}$$

where $e_{ijk} = \langle \Phi_i \Phi_p \Phi_k \rangle$ and $\psi_{p,\ell}$, $1 \leq \ell \leq 2IN$, is the ℓth element of ψ_p, I and N are the number of spatial cells and quadrature angles, respectively. Expanding the dot product and eliminating those terms which do not contain the ℓth element of $\vec{\psi_i}$ and $\vec{\psi_j}$ yields:

$$\frac{\partial F_{P+1,k}}{\partial \psi_{p,\ell}} = \frac{\partial}{\partial \psi_{p,\ell}} \left[\sum_{i=0}^{P} \sum_{j=0}^{P} \sum_{q=0}^{2IN} \phi_{i,q} \phi_{j,q} e_{ijk} - \delta_{k0} \right] \tag{C.2}$$

$$= \frac{\partial}{\partial \psi_{p,\ell}} \left[\sum_{i=0}^{P} \sum_{j=0}^{P} \phi_{i,\frac{(\ell-m)}{N}} \phi_{j,\frac{(\ell-m)}{N}} e_{ijk} \right] \tag{C.3}$$

where $m = \text{mod}(\ell, N)$, $1 \leq m \leq N$, is the index of the quadrature angle corresponding to $\psi_{p,\ell}$. Now, those terms which do not contain $\psi_{p,\ell}$ are discarded and the

Appendix C. Derivative of F with Respect to $\psi_{p,\ell}$

derivative is taken:

$$
\begin{aligned}
\frac{\partial F_{P+1,k}}{\partial \psi_{p,\ell}} &= \frac{\partial}{\partial \psi_{p,\ell}} \left[\phi^2_{p,\frac{(\ell-m)}{N}} e_{ppk} + 2\phi_{p,\frac{(\ell-m)}{N}} \sum_{i \neq p} \phi_{i,\frac{(\ell-m)}{N}} e_{ijk} \right] & \text{(C.4)} \\
&= e_{ppk} \frac{\partial}{\partial \psi_{p,\ell}} \left[\left(\sum_{n=1}^{N} w_n \psi_{p,\ell-m+n} \right) \left(\sum_{n'=1}^{N} w_{n'} \psi_{p,\ell-m+n'} \right) \right] \\
&\quad + 2w_m \sum_{\substack{i=0 \\ i \neq p}}^{P} \phi_{i,\frac{(\ell-m)}{N}} e_{ipk} & \text{(C.5)} \\
&= e_{ppk} \frac{\partial}{\partial \psi_{p,\ell}} \left[2w_m \psi_{p,\ell} \sum_{\substack{n=1 \\ n \neq m}}^{N} w_n \psi_{p,\ell-m+n} + w_m^2 \psi_{p,\ell}^2 \right] \\
&\quad + 2w_m \sum_{\substack{i=0 \\ i \neq p}}^{P} \phi_{i,\frac{(\ell-m)}{N}} e_{ipk} & \text{(C.6)} \\
&= 2w_m \left[e_{ppk} \left(\sum_{\substack{n=1 \\ n \neq m}}^{N} w_n \psi_{p,\ell-m+n} + w_m \psi_{p,\ell} \right) + \sum_{\substack{i=0 \\ i \neq p}}^{P} \phi_{i,\frac{(\ell-m)}{N}} e_{ipk} \right] & \text{(C.7)} \\
&= 2w_m \left[e_{ppk} \sum_{n=1}^{N} w_n \psi_{p,\ell-m+n} + \sum_{\substack{i=0 \\ i \neq p}}^{P} \phi_{i,\frac{(\ell-m)}{N}} e_{ipk} \right]. & \text{(C.8)}
\end{aligned}
$$

But $\sum_{n=1}^{N} w_n \psi_{p,\ell-m+n} = \phi_{p,\frac{(\ell-m)}{N}}$, thus

$$
\begin{aligned}
\frac{\partial F_{P+1,k}}{\partial \psi_{p,\ell}} &= 2w_m \left[\phi_{p,\frac{(\ell-m)}{N}} e_{ppk} + \sum_{\substack{i=0 \\ i \neq p}}^{P} \phi_{i,\frac{(\ell-m)}{N}} e_{ipk} \right] & \text{(C.9)} \\
&= 2w_m \sum_{i=0}^{P} \phi_{i,\frac{(\ell-m)}{N}} e_{ipk} & \text{(C.10)}
\end{aligned}
$$

References

[1] C. Levermore, G. Pomraning, D. Sanzo, and J. Wong, "Linear transport theory in a random medium," *Journal of Mathematical Physics*, vol. 27, pp. 2526–2536, Oct. 1986.

[2] C. Levermore, J. Wong, and G. Pomraning, "Renewal theory for transport processes in binary statistical mixtures," *Journal of Mathematical Physics*, vol. 29, pp. 995–1004, Apr. 1988.

[3] D. Vanderhaegen, "Radiative transfer in statistically heterogeneous mixtures," *Journal of Quantitative Spectroscopy and Radiative Transfer*, vol. 36, pp. 557–561, Dec. 1986.

[4] D. Vanderhaegen, "Impact of a mixing structure on radiative transfer in random media," *Journal of Quantitative Spectroscopy and Radiative Transfer*, vol. 39, pp. 333–337, Apr. 1988.

[5] M. Adams, E. Larsen, and G. Pomraning, "Benchmark results for particle transport in a binary markov statistical medium," *Journal of Quantitative Spectroscopy and Radiative Transfer*, vol. 42, pp. 253–266, Oct. 1989.

[6] F. Malvagi and G. Pomraning, "Renormalized equations for linear transport in stochastic media," *Journal of Mathematical Physics*, vol. 31, pp. 892–900, Apr. 1990.

[7] F. F. Malvagi, R. Byrne, G. Pomraning, and R. Somerville, "Stochastic radiative transfer in a partially cloudy atmosphere," *Journal of the Atmospheric Sciences*, vol. 50, pp. 2146–2158, July 1993.

[8] G. Pomraning, "Statistics, renewal theory, and particle transport," *Journal of Quantitative Spectroscopy and Radiative Transfer*, vol. 42, pp. 279–293, Oct. 1989.

References

[9] G. Pomraning and R. Sanchez, "The use of renewal theory for stochastic transport," *Journal of Quantitative Spectroscopy and Radiative Transfer*, vol. 43, pp. 267–70, Apr. 1990.

[10] G. Pomraning, *Linear Kinetic Theory and Particle Transport in Stochastic Mixtures*. World Scientific, 1991.

[11] G. Pomraning, "The variance in stochastic transport problems with markovian mixing," *Journal of Quantitative Spectroscopy and Radiative Transfer*, vol. 56, pp. 629–646, Nov. 1996.

[12] D. Sahni, "Application of reactor noise techniques to neutron transport problems in a random medium," *Annals of Nuclear Energy*, vol. 16, no. 8, pp. 397–408, 1989.

[13] D. Sahni, "Equivalence of generic equation method and the phenomenological model for linear transport problems in a two-state random scattering medium," *Journal of Mathematical Physics*, vol. 30, pp. 1554–1559, July 1989.

[14] R. Sanchez, "Linear kinetic theory in stochastic media," *Journal of Mathematical Physics*, vol. 30, pp. 2498–2511, Nov. 1989.

[15] R. Sanchez and G. Pomraning, "A statistical analysis of the double heterogeneity problem," *Annals of Nuclear Energy*, vol. 18, no. 7, pp. 371–, 1991.

[16] O. Zuchuat, R. Sanchez, I. Zmijarevic, and F. Malvagi, "Transport in renewal statistical media: Benchmarking and comparison with models," *Journal of Quantitative Spectroscopy and Radiative Transfer*, vol. 51, pp. 689–722, May 1994.

[17] A. Akcasu, "Modified-levermore-pomraning equation: Its derivation and its limitations," *Annals of Nuclear Energy*, vol. 34, pp. 579–590, July 2007.

[18] E. Larsen and A. Prinja, "A new eerivation of akcasu's "mlp" equations for 1-d particle transport in stochastic media," *Annals of Nuclear Energy*, vol. 35, pp. 620–626, Apr. 2008.

[19] R. Sanchez, "A critique of the modified levermore-pomraning equations," *Annals of Nuclear Energy*, vol. 35, pp. 446–457, Mar. 2008.

[20] A. K. Prinja and G. Pomraning, "On the propagation of a charged particle beam in a random medium i: Gaussian statistics," *Transport Theory and Statistical Physics*, vol. 24, pp. 535–564, Apr. 1995.

References

[21] A. Prinja and A. Gonzalez-Aller, "Particle transport in the presence of parametric noise," *Nuclear Science and Engineering*, vol. 124, pp. 89–96, Sept. 1996.

[22] G. Pomraning and A. K. Prinja, "On the propagation of a charged particle beam in a random medium ii: Discrete binary statistics," *Transport Theory and Statistical Physics*, vol. 24, pp. 565–590, Apr. 1995.

[23] M. Selim and M. Sallah, "Transport of neutral particles in a finite continuous stochastic medium with gaussian statistics," *Transport Theory and Statistical Physics*, vol. 37, pp. 460–482, Sept. 2008.

[24] M. Selim and M. Sallah, "Neutron transport through semi-infinite continuous stochastic media using gaussian statistics," *Annals of Nuclear Energy*, vol. 35, pp. 1613–1620, Sept. 2008.

[25] A. Gandini, "A generalized perturbation method for bi-linear functionals of the real and adjoint neutron fluxes," *Journal of Nuclear Engineering*, vol. 21, pp. 755–765, Oct. 1967.

[26] J. Helton, J. Johnson, C. Sallaberry, and C. Storlie, "Survey of sampling-based methods for uncertainty and sensitivity analysis," *Reliability Engineering and System Safety*, vol. 91, pp. 1175–1209, Oct. 2006.

[27] A. Gandini, "Equivalent generalized perturbation theory (egpt)," *Annals of Nuclear Energy*, vol. 13, no. 3, pp. 109–114, 1986.

[28] M. Loève, *Probability Theory II, 4th edition*. New York: Springer-Verlag, 1977.

[29] N. Wiener, "The homogeneous chaos," *American Journal of Mathematics*, vol. 60, pp. 897–936, Oct. 1938.

[30] H. Ogura, "Orthogonal functionals of the poisson process," *IEEE Transactions on Information Theory*, vol. 18, no. 4, pp. 473–481, 1972.

[31] D. Xiu and G. Karniadakis, "The wiener-askey polynomial chaos for stochastic differential equations," *SIAM Journal on Scientific Computing*, vol. 24, no. 2, pp. 619–644, 2002.

[32] D. Xiu, *Generalized (Wiener-Askey) Polynomial Chaos*. Doctoral dissertation, Brown University, May 2004.

[33] R. Ghanem and P. Spanos, *Stochastic Finite Elements: A Spectral Approach*. New York: Springer-Verlag, 1991.

References

[34] R. Ghanem and W. Brzakala, "Stochastic finite-element analysis of soil layers with random interface," *Journal of Engineering Mechanics*, vol. 122, pp. 361–369, Apr. 1996.

[35] R. Ghanem, "Probabilistic characterization of transport in heterogeneous media," *Computer Methods in Applied Mechanics and Engineering*, vol. 158, pp. 199–220, June 1998.

[36] R. Ghanem and S. Dham, "Stochastic finite element analysis for multiphase flow in heterogeneous porous media," *Transport in Porous Media*, vol. 32, pp. 239–262, Sept. 1998.

[37] R. Ghanem, "Scales of fluctuation and the propagation of uncertainty in random porous media," *Water Resources Research*, vol. 34, pp. 2123–2136, Sept. 1998.

[38] R. Ghanem and B. Hayek, "Probabilistic modeling of flow over rough terrain," *Journal of Fluids Engineering*, vol. 124, pp. 42–50, Mar. 2002.

[39] R. Ghanem and M. Pellissetti, "Adaptive data refinement in the spectral stochastic finite element method," *Communications in Numerical Methods in Engineering*, vol. 18, pp. 141–151, Feb. 2002.

[40] R. Ghanem, "Stochastic finite elements with multiple random non-gaussian properties," *Journal of Engineering Mechanics*, vol. 125, pp. 26–40, Jan. 1999.

[41] R. Ghanem and J. Red-Horse, "Propagation of probabilistic uncertainty in complex physical systems using a stochastic finite element approach," *Physica D*, vol. 133, pp. 137–144, Sept. 1999.

[42] A. Sarkar and R. Ghanem, "Mid-frequency structural dynamics with parameter uncertainty," *Computer Methods in Applied Mechanics and Engineering*, vol. 191, pp. 5499–5513, Nov. 2002.

[43] A. Sarkar and R. Ghanem, "A substructure approach for the midfrequency vibration of stochastic systems," *Journal of the Acoustical Society of America*, vol. 113, pp. 1922–1934, Apr. 2002.

[44] R. Ghanem and A. Sarkar, "Reduced models for the medium-frequency dynamics of stochastic systems," *Journal of the Acoustical Society of America*, vol. 113, pp. 834–846, Feb. 2003.

[45] R. Ghanem, S. Masri, M. Pellissetti, and R. Wolfe, "Identification and prediction of stochastic dynamical systems in a polynomial chaos basis," *Computer Methods in Applied Mechanics and Engineering*, vol. 194, pp. 1641–1654, Apr. 2005.

References

[46] C. Soize and R. Ghanem, "Physical systems with random uncertainties: Chaos representations with arbitrary probability measure," *SIAM Journal on Scientific Computing*, vol. 26, no. 2, pp. 395–410, 2005.

[47] R. Ghanem, G. Saad, and A. Doostan, "Efficient solution of stochastic systems: Application to the embankment dam problem," *Structural Safety*, vol. 29, pp. 238–251, July 2007.

[48] C. Desceliers, C. Soize, and R. Ghanem, "Identification of chaos representations of elastic properties of random media using experimental vibration tests," *Computational Mechanics*, vol. 39, pp. 831–838, May 2007.

[49] B. Faverjon and R. Ghanem, "Stochastic inversion in acoustic scattering," *Journal of the Acoustical Society of America*, vol. 119, pp. 3577–3588, June 2006.

[50] G. Ghosh, R. Ghanem, and J. Red-Horse, "Analysis of eigenvalues and modal interaction of stochastic systems," *AIAA Journal*, vol. 43, pp. 2196–2201, Oct. 2005.

[51] R. Ghanem and G. Ghosh, "Efficient characterization of the random eigenvalue problem in a polynomial chaos decomposition," *International Journal for Numerical Methods in Engineering*, vol. 72, pp. 486–504, Mar. 2007.

[52] G. Ghosh and R. Ghanem, "Stochastic convergence acceleration through basis enrichment of polynomial chaos expansions," *International Journal for Numerical Methods in Engineering*, vol. 73, pp. 162–184, Jan. 2008.

[53] R. Ghanem, "Nonlinear gaussian spectrum of log-normal stochastic processes and variables," *Journal of Applied Mechanics*, vol. 66, pp. 964–973, Dec. 1999.

[54] S. Sakamoto and R. Ghanem, "Polynomial chaos decomposition for the simulation of non-gaussian nonstationary stochastic processes," *Journal of Engineering Mechanics*, vol. 128, pp. 190–201, Feb. 2002.

[55] S. Sakamoto and R. Ghanem, "Simulation of multi-dimensional non-gaussian non-stationary random fields," *Probabilistic Engineering Mechanics*, vol. 17, pp. 167–176, Apr. 2002.

[56] D. Xiu, D. Lucor, C. Su, and G. Karniadakis, "Stochastic modeling of flow-structure interactions using generalized polynomial chaos," *Journal of Fluids Engineering*, vol. 124, pp. 51–59, Mar. 2002.

[57] D. Xiu and G. Karniadakis, "Modeling uncertainty in flow simulations via generalized polynomial chaos," *SIAM Journal on Scientific Computing*, vol. 187, pp. 137–167, May 2003.

References

[58] D. Xiu and G. Karniadakis, "A new stochastic approach to transient heat conduction modeling with uncertainty," *International Journal of Heat and Mass Transfer*, vol. 46, pp. 4681–4693, Nov. 2003.

[59] D. Xiu and G. Karniadakis, "Modeling uncertainty in steady state diffusion problems via generalized polynomial chaos," *Computer Methods in Applied Mechanics and Engineering*, vol. 191, pp. 4927–4948, Sept. 2002.

[60] D. Xiu and D. Tartakovsky, "Numerical methods for differential equations in random domains," *SIAM Journal on Scientific Computing*, vol. 28, no. 3, pp. 1167–1185, 2006.

[61] D. Xiu and G. Karniadakis, "Supersensitivity due to uncertain boundary conditions," *International Journal for Numerical Methods in Engineering*, vol. 61, pp. 2114–2138, Nov. 2004.

[62] X. Wan, D. Xiu, and G. Karniadakis, "Stochastic solutions for the two-dimensional advection-diffusion equation," *SIAM Journal on Scientific Computing*, vol. 26, no. 2, pp. 578–590, 2004.

[63] X. Wan and G. Karniadakis, "An adaptive multi-element generalized polynomial chaos method for stochastic differential equations," *Journal of Computational Physics*, vol. 209, pp. 617–642, Nov. 2005.

[64] D. Xiu, I. Kevrekidis, and R. Ghanem, "An equation-free, multiscale approach to uncertainty quantification," *Computing in Science and Engineering*, vol. 7, pp. 16–23, May-June 2005.

[65] D. Xiu and S. Sherwin, "Parametric uncertainty analysis of pulse wave propagation in a model of a human arterial network," *Journal of Computational Physics*, vol. 226, pp. 1385–1407, Oct. 2007.

[66] A. Emery, "Some thoughts on solving the radiative transfer equation in stochastic media using polynomial chaos and wick products as applied to radiative equilibrium," *Journal of Quantitative Spectroscopy and Radiative Transfer*, vol. 93, pp. 61–77, June 2005.

[67] M. Williams, "Polynomial chaos functions and neutron diffusion," *Nuclear Science and Engineering*, vol. 155, pp. 109–118, Jan. 2007.

[68] M. Williams, "Polynomial chaos functions and stochastic differential equations," *Annals of Nuclear Energy*, vol. 33, pp. 774–785, June 2006.

References

[69] L. Mathelin, M. Hussaini, and T. Zang, "Stochastic approaches to uncertainty quantification in cfd simulations," *Numerical Algorithms*, vol. 38, no. 1-3, pp. 209–236, 2005.

[70] I. Babuska, F. Nobile, and R. Tempone, "A stochastic collocation method for elliptic partial differential equations with random input data," *SIAM Journal on Numerical Analysis*, vol. 45, no. 3, pp. 1005–1034, 2007.

[71] X. Xu, "A multiscale stochastic finite element method on elliptic problems involving uncertainties," *Computer Methods in Applied Mechanics and Engineering*, vol. 196, pp. 2723–2736, May 2007.

[72] J. Baroth, P. Bressolette, C. Chauviere, and M. Fogli, "An efficient sfe method using lagrange polynomials: Application to nonlinear mechanical problems with uncertain parameters," *Computer Methods in Applied Mechanics and Engineering*, vol. 4196, pp. 4419–4429, Sept. 2007.

[73] G. Blatman and B. Sudret, "Sparse polynomial chaos expansions and adaptive stochastic finite elements using a regression approach," *Comptes Rendus Mecanique*, vol. 336, pp. 518–523, June 2008.

[74] J. Foo and Z. Y. G. Karniadakis, "Stochastic simulation of riser-sections with uncertain measured pressure loads and/or uncertain material properties," *Journal of Engineering Mechanics*, vol. 196, pp. 4250–4271, Sept. 2007.

[75] B. Ganis, H. Klie, M. Wheeler, T. Wildey, I. Yotov, and D. Zhang, "Stochastic collocation and mixed finite elements for flow in porous media," *Computer Methods in Applied Mechanics and Engineering*, vol. 197, pp. 3547–3559, Aug. 2008.

[76] J. Ko, D. Lucor, and P. Sagaut, "Sensitivity of two-dimensional spatially developing mixing layers with respect to uncertain inflow conditions," *Physics of Fluids*, vol. 20, no. 20, 2008.

[77] D. Lucor, C. Enaux, H. Jourdren, and P. Sagaut, "Stochastic design optimization: Application to reacting flows," *Computer Methods in Applied Mechanics and Engineering*, vol. 196, pp. 5047–5062, Nov. 2007.

[78] D. Xiu and J. Hesthaven, "High-order collocation methods for differential equations with random inputs," *SIAM Journal on Scientific Computing*, vol. 27, no. 3, pp. 1118–1139, 2005.

References

[79] B. Ganapathysubramanian and N. Zabaras, "Modeling diffusion in random heterogeneous media: Data-driven models, stochastic collocation and the variational multiscale method," *Journal of Computational Physics*, vol. 226, pp. 326–353, Sept. 2007.

[80] B. Ganapathysubramanian and N. Zabaras, "A seamless approach towards stochastic modeling: Sparse grid collocation and data driven input models," *Finite Elements in Analysis and Design*, vol. 44, pp. 298–320, Mar. 2008.

[81] G. Bell and S. Glasstone, *Nuclear Reactor Theory*. New York: Van Nostrand Reinhold Company, 1970.

[82] E. Lewis and W. Miller, *Computational Methods of Neutron Transport*. Lagrange Park, IL: American Nuclear Society, Inc., 1993.

[83] J. Warsa, T. Wareing, J. Morel, and J. McGhee, "Krylov subspace iterations for k-eigenvalue calculations," *Nuclear Science and Engineering*, vol. 147, pp. 26–42, May 2004.

[84] R. Koekoek and R. Swarttouw, "The askey-scheme of hypergeometric orthogonal polynomials and its q-analogue," Tech. Rep. 94-05, TU Delft, Delft, The Netherlands, 1994.

[85] E. Fichtl, J. Warsa, and A. Prinja, "Krylov iterative methods and synthetic acceleration for transport in binary statistical media," in *Joint International Meeting on Mathematics and Computation and Supercomputing in Nuclear Applications*, (Monterey, CA), American Nuclear Society, April 15-19 2007.

[86] E. Larsen, "Unconditionally stable diffusion-synthetic acceleration methods for the slab geometry discrete ordinates equations 1: Theory," *Nuclear Science and Engineering*, vol. 82, no. 1, pp. 47–63, 1982.

[87] L. Lorence, J. Morel, and E. Larsen, "An s_2 synthetic acceleration scheme for the one-dimensional s_n equations with linear discontinuous spatial differencing," *Nuclear Science and Engineering*, vol. 101, pp. 341–351, Apr. 1989.

[88] A. Sood, R. Forster, and D. Parsons, "Analytical benchmark test set for criticality code verification," *Progress in Nuclear Energy*, vol. 42, no. 1, pp. 55–106, 2003.

[89] S. Smolyak, "Quadrature and interpolation formulas for tensor products of certain classes of functions," *Soviet Mathematics Doklady*, vol. 4, pp. 240–243, 1963.

References

[90] C. Sallaberry, J. Helton, and S. Hora, "Extension of latin hypercube samples with correlated variables," *Reliability Engineering and System Safety*, vol. 93, pp. 1047–1059, July 2008.

[91] W. Schoutens, *Stochastic Processes and Orthogonal Polynomials.* New York: Springer-Verlag, 2000.

[92] W. Press, S. Teukolsky, and W. V. B. Flannery, *Numerical Recipes in Fortran C: The Art of Scientific Computing.* Cambridge, U.K.: Cambridge University Press, 1992.